

# Biologically Inspired Wing Tip Geometry Optimization

By

Andrea Marinelli

A Thesis

Submitted to the Faculty

of the

WORCESTER POLYTECHNIC INSTITUTE

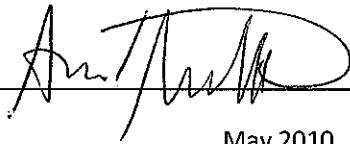
in partial fulfillment of the requirements of the

Degree of Master of Science

in

Mechanical Engineering

by

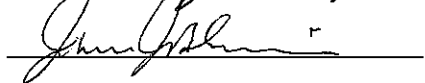


May 2010

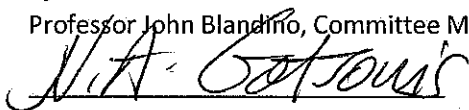
APPROVED:



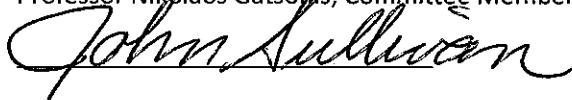
Professor David J. Olinger, Thesis Advisor



Professor John Blandino, Committee Member



Professor Nikolaos Gatsos, Committee Member



Professor John Sullivan, Graduate Committee Representative

## ABSTRACT

Wingtip vortices are an important problem in aerodynamic and hydrodynamic engineering because of their contribution to induced drag, tip cavitation, and wake turbulence. These effects decrease equipment efficiency and lifespan, which increases application costs. Biology provides an inspiring solution to this problem in avian flight through the spreading of primary feathers. Previous studies have shown increased lift to drag ratio and efficiency of wings and propeller blades through modified wingtip geometry. The goal of this project is to optimize the tip geometry (primary feather angle) of a test wing for minimal tip vortex strength using genetic algorithms to mimic natural design evolution. Ultrasonic transducers are used to measure the wing tip vortex circulation in wind tunnel tests for each candidate design. Although neither angle of attack series converged completely, there was partial convergence in each. Due to the fluctuations in the low angle of attack tests, the parent selection algorithm was altered for the high angle of attack series, which resulted in improved convergence trends. A genetic algorithm that used uniform crossover breeding, a 20% mutation rate, and roulette wheel parent selection methods was used to generate an improved tip geometry at a low angle of attack of  $6^\circ$  and a freestream velocity of 15.25 m/s over the course of 17 generations. This improved design consisted of three key features, a staggered leading edge, a drastic mid-section vertical separation, and an upswept trailing edge. A second algorithm, which employed uniform crossover, a 20% mutation rate, and an elitist selection roulette parent selection, provided an improved tip geometry for a  $12^\circ$  angle of attack at a freestream velocity of 11.5 m/s. This improved design consisted of three key features, a downswept leading edge, a drastic mid-section vertical separation, and an upturned trailing edge. Both results showed that the wing tip vortex strength can be reduced by approximately 20% by manipulating tip geometry and that the trailing edge traits produce the most prominent effects on vortex strength.

## ACKNOWLEDGEMENTS

The completion of this project was only possible through the contributions of the following people. First and foremost, I would like to thank my advisor Prof. David Olinger for his development of, involvement in, and mentorship throughout this project. His experience in using genetic algorithms to develop aerodynamic designs was an essential component of this project's realization.

I would like to thank Sarah Taylor and Andrew Day for providing significant insight into the creation and application of genetic algorithms to aerodynamics problems. Particularly, I appreciate the genetic algorithm codes provided, which I was able to adapt to the present work.

For the fabrication of the test wing, I would like to thank Neil Whitehouse and Russ Morin. Neil provided ample assistance in the manufacturing of parts, instruction in machine use, and assembly advice. Russ provided extremely timely fabrication of all rapid prototyped parts.

I would also like to thank Barbara Edilberti, Gloria Boudreau, Barbara Fuhrman, Pamela St. Louis, Tracey Coetzee, and the rest of Mechanical Engineering Department at Worcester Polytechnic Institute. The support I have received from the faculty and staff over the years has been critical to my growth as a student and a person.

Finally, I would like to thank my friend and family for their patience and encouragement of all of my academic endeavors.

# TABLE OF CONTENTS

<b>LIST OF FIGURES.....</b>	<b>V</b>
<b>LIST OF TABLES .....</b>	<b>VII</b>
<b>NOMENCLATURE .....</b>	<b>VIII</b>
<b>1. INTRODUCTION.....</b>	<b>1</b>
1.1 BACKGROUND .....	1
1.2 LITERATURE REVIEW .....	5
1.2.1 <i>Computer Simulations of Evolution</i> .....	5
1.2.2 <i>Biologically Inspired design</i> .....	12
1.2.3 <i>Vorticity Measurement Techniques</i> .....	17
1.3 OBJECTIVES & OVERVIEW.....	20
<b>2. EXPERIMENTAL METHODS .....</b>	<b>22</b>
2.1 WIND TUNNEL.....	22
2.2 TEST WING DESIGN .....	22
2.3 CIRCULATION MEASUREMENT .....	26
2.3.1 <i>Wind Tunnel Setup</i> .....	27
2.3.2 <i>Circulation Function Derivation</i> .....	28
2.3.3 <i>Wing Tunnel Circulation Calibration Measurements</i> .....	30
2.3.4 <i>Circulation Measurement Repeatability</i> .....	32
2.4 GENETIC ALGORITHM .....	33
2.5 TEST PROCEDURE .....	35
<b>3. RESULTS .....</b>	<b>37</b>
3.1 LOW ANGLE OF ATTACK SERIES .....	37
3.1.1 <i>Early Generations</i> .....	41
3.1.2 <i>Middle Generations</i> .....	43
3.1.3 <i>Final Generations</i> .....	45
3.1.4 <i>Discussion of Low AoA Results</i> .....	47
3.2 HIGH ANGLE OF ATTACK SERIES .....	51
3.2.1 <i>Early Generations</i> .....	56
3.2.2 <i>Middle Generations</i> .....	58
3.2.3 <i>Final Generations</i> .....	61
3.2.4 <i>Discussion of High AoA Results</i> .....	64
3.3 COMPARISON OF LOW AND HIGH ANGLE OF ATTACK RESULTS .....	68
<b>4. CONCLUSIONS.....</b>	<b>69</b>
<b>5. FUTURE WORK.....</b>	<b>71</b>
<b>REFERENCES.....</b>	<b>73</b>
<b>APPENDICES.....</b>	<b>75</b>
APPENDIX A: ANGLE SENSOR CALIBRATION .....	75

APPENDIX B: ANGLE SENSOR VIRTUAL INSTRUMENT .....	83
APPENDIX C: PRELIMINARY VELOCITY TEST .....	84
APPENDIX D: CIRCULATION FORMULA DERIVATION .....	86
APPENDIX E: GENETIC ALGORITHM CODES .....	89
<i>Initial Population Code</i> .....	89
<i>Selection Roulette Code</i> .....	90
<i>Genetic Algorithm Code</i> .....	91
<i>Elitist Roulette Code</i> .....	92
<i>Elitist Genetic Algorithm Code</i> .....	93
APPENDIX F: LOW AoA GENERATION DATA .....	94
<i>Generation #1</i> .....	94
<i>Generation #2</i> .....	97
<i>Generation #3</i> .....	98
<i>Generation #4</i> .....	99
<i>Generation #5</i> .....	100
<i>Generation #6</i> .....	101
<i>Generation #7</i> .....	102
<i>Generation #8</i> .....	103
<i>Generation #9</i> .....	104
<i>Generation #10</i> .....	105
<i>Generation #11</i> .....	106
<i>Generation #12</i> .....	107
<i>Generation #13</i> .....	108
<i>Generation #14</i> .....	109
<i>Generation #15</i> .....	110
<i>Generation #16</i> .....	111
<i>Generation #17</i> .....	112
APPENDIX G: HIGH AoA GENERATION DATA .....	113
<i>Generation #1</i> .....	113
<i>Generation #2</i> .....	116
<i>Generation #3</i> .....	117
<i>Generation #4</i> .....	118
<i>Generation #5</i> .....	119
<i>Generation #6</i> .....	120
<i>Generation #7</i> .....	121
<i>Generation #8</i> .....	122
<i>Generation #9</i> .....	123
<i>Generation #10</i> .....	124
<i>Generation #11</i> .....	125
<i>Generation #12</i> .....	126

# LIST OF FIGURES

FIGURE 1: FORMATION OF TIP VORTICES [1] .....	1
FIGURE 2: INDUCED DRAG [2].....	2
FIGURE 3: PROPELLER BLADE CAVITATION FROM REF [4].....	2
FIGURE 4: HARRIS HAWK WITH SLOTTED WINGTIPS FROM REF [7].....	3
FIGURE 5: GENETIC ALGORITHM FLOWCHART .....	7
FIGURE 6: SAMPLE SELECTION ROULETTE WHEEL.....	9
FIGURE 7: SINGLE POINT CROSSOVER.....	10
FIGURE 8: MULTI-POINT CROSSOVER .....	10
FIGURE 9: SILK FLAP ADDED TO NACA 4412 (TOP) AND RESULTING CHANGE IN CRITICAL AoA (BOTTOM) FROM REF [26] .....	13
FIGURE 10: BANNASCH TEST WING EVOLUTION FROM REF [26] .....	16
FIGURE 11: PROPELLER WITH TIP FIN FROM REF [5].....	17
FIGURE 12: ULTRASONIC TRANSDUCER SCHEMATIC FROM REF [29].....	19
FIGURE 13: TEST WING ASSEMBLY DRAWING .....	23
FIGURE 14: TEST WING.....	24
FIGURE 15: ANGLE MEASUREMENT AND LOCKING SYSTEM.....	25
FIGURE 16: XGM868 FLOWMETER .....	27
FIGURE 17: WIND TUNNEL TEST SET UP.....	28
FIGURE 18: CIRCULATION MEASUREMENT DIAGRAM.....	29
FIGURE 19: WIND TUNNEL CALIBRATION DATA FOR LOW AoA.....	31
FIGURE 20: WIND TUNNEL CALIBRATION DATA FOR HIGH AoA .....	32
FIGURE 21: CIRCULATION REPEATABILITY DATA.....	33
FIGURE 22: GENETIC ALGORITHM FLOWCHART APPLIED TO CURRENT WORK .....	34
FIGURE 23: LOW AoA CIRCULATION DATA .....	38
FIGURE 24: INDIVIDUAL 1 -1 1 -1 4 -2 0 4 .....	40
FIGURE 25: INDIVIDUAL 1 -1 1 -1 4 -2 0 4 CONFIGURATION .....	41
FIGURE 26: INDIVIDUAL -4 2 4 1 4 0 4 4.....	42
FIGURE 27: INDIVIDUAL 4 0 0 2 -2 2 -1 3.....	42
FIGURE 28: INDIVIDUAL 4 4 1 -4 3 0 -2 -4 .....	42
FIGURE 29: INDIVIDUAL -4 2 4 1 4 3 4 4.....	43
FIGURE 30: INDIVIDUAL 3 -1 -2 -1 4 -2 0 4 .....	43
FIGURE 31: INDIVIDUAL 3 -1 -2 -1 -2 3 0 4 .....	44
FIGURE 32: INDIVIDUAL 1 -1 1 -1 4 -2 0 4 .....	44
FIGURE 33: INDIVIDUAL 3 0 -2 2 -2 2 -1 4 .....	45
FIGURE 34: INDIVIDUAL 3 1 0 3 -2 -1 0 4.....	45
FIGURE 35: INDIVIDUAL 1 0 -2 2 4 -2 0 4.....	46
FIGURE 36: PROMINENT CONFIGURATION (1 -1 1 -1 4 -2 0 4).....	48
FIGURE 37: WINGLET DESIGNED BY STEVE WILLITS FROM REF [33] .....	49
FIGURE 38: STANDARD WINGLET FLOW VISUALIZATION FROM REF [34] .....	50
FIGURE 39: INDIVIDUAL 1 -1 1 -1 -1 -2 0 4 CONFIGURATION .....	51
FIGURE 40: INDIVIDUAL 0 0 0 0 0 0 0 .....	52
FIGURE 41: HIGH AoA CIRCULATION DATA.....	53
FIGURE 42: INDIVIDUAL -2 -4 -4 1 -4 4 1 3 .....	54
FIGURE 43: INDIVIDUAL -2 -4 -4 1 -4 4 1 3 CONFIGURATION .....	55

FIGURE 44: INDIVIDUAL 3 -2 -3 4 -4 3 4 4 .....	56
FIGURE 45: INDIVIDUAL 0 -3 0 4 -3 4 2 3.....	57
FIGURE 46: INDIVIDUAL 4 3 -2 2 -3 -3 -4 -4 .....	57
FIGURE 47: INDIVIDUAL -2 -4 1 -3 -4 4 1 3 .....	58
FIGURE 48: INDIVIDUAL -2 -4 -4 1 -4 4 1 3 .....	58
FIGURE 49: INDIVIDUAL -2 -3 1 -3 2 4 3 3 .....	59
FIGURE 50: INDIVIDUAL -2 -4 -4 1 -4 -2 -1 3 .....	60
FIGURE 51: INDIVIDUAL -2 -2 -4 1 -4 -2 -3 3 .....	60
FIGURE 52: INDIVIDUAL -2 -4 -4 -1 -4 0 1 3 .....	60
FIGURE 53: INDIVIDUAL -2 -4 -4 1 -4 4 2 3 .....	61
FIGURE 54: INDIVIDUAL -2 -4 -4 1 -4 4 3 3 .....	62
FIGURE 55: INDIVIDUAL -2 -4 -4 1 -4 4 1 3 CONFIGURATION .....	64
FIGURE 56: INDIVIDUAL -2 -4 -4 1 -4 4 2 3 CONFIGURATION .....	65
FIGURE 57: INDIVIDUAL -2 -4 -4 1 -4 4 3 3 CONFIGURATION .....	66
FIGURE 58: BIOLOGICALLY INSPIRED TIP GEOMETRY FROM REF [36] .....	67
FIGURE 59: FLOW OVER DOWNSWEPT FEATHERS .....	67
FIGURE 60: ANGLE SENSOR CALIBRATION SET-UP.....	75
FIGURE 61: POTENTIOMETER CALIBRATION FRONT PANEL .....	76
FIGURE 62: POTENTIOMETER CALIBRATION BLOCK DIAGRAM .....	77
FIGURE 63: FEATHER 1 ANGLE SENSOR CALIBRATION DATA .....	78
FIGURE 64: FEATHER 2 ANGLE SENSOR CALIBRATION .....	78
FIGURE 65: FEATHER 3 ANGLE SENSOR CALIBRATION .....	79
FIGURE 66: FEATHER 4 ANGLE SENSOR CALIBRATION .....	79
FIGURE 67: FEATHER 5 CALIBRATION DATA.....	80
FIGURE 68: FEATHER 6 CALIBRATION DATA.....	80
FIGURE 69: FEATHER 7 CALIBRATION DATA.....	81
FIGURE 70: FEATHER 8 CALIBRATION DATA.....	81
FIGURE 71: ANGLE SENSOR FRONT PANEL .....	83
FIGURE 72: ANGLE SENSOR BLOCK DIAGRAM .....	83
FIGURE 73: VELOCITY TEST SCHEMATIC .....	84
FIGURE 74: VELOCITY TEST DATA .....	85

# LIST OF TABLES

TABLE 1: SAMPLE POPULATION FITNESS .....	8
TABLE 2: LOW AoA GENERATION #18.....	46
TABLE 3: HIGH AoA GENERATION #12 .....	62
TABLE 4: POTENTIOMETER CALIBRATION DATA .....	82
TABLE 5: GENERATION #1 DATA.....	94
TABLE 6: GENERATION #2 DATA.....	97
TABLE 7: GENERATION #3 DATA.....	98
TABLE 8: GENERATION #4 DATA.....	99
TABLE 9: GENERATION #5 DATA.....	100
TABLE 10: GENERATION #6 DATA.....	101
TABLE 11: GENERATION #7 DATA.....	102
TABLE 12: GENERATION #8 DATA.....	103
TABLE 13: GENERATION #9 DATA.....	104
TABLE 14: GENERATION #10 DATA.....	105
TABLE 15: GENERATION #11 DATA.....	106
TABLE 16: GENERATION #12 DATA.....	107
TABLE 17: GENERATION #13 DATA.....	108
TABLE 18: GENERATION #14 DATA.....	109
TABLE 19: GENERATION #15 DATA.....	110
TABLE 20: GENERATION #16 DATA.....	111
TABLE 21: GENERATION #17 DATA.....	112
TABLE 22: GENERATION #1 DATA.....	113
TABLE 23: GENERATION #2 DATA.....	116
TABLE 24: GENERATION #3 DATA.....	117
TABLE 25: GENERATION #4 DATA.....	118
TABLE 26: GENERATION #6 DATA.....	120
TABLE 27: GENERATION #7 DATA.....	121
TABLE 28: GENERATION #8 DATA.....	122
TABLE 29: GENERATION # DATA.....	123
TABLE 30: GENERATION #10 DATA.....	124
TABLE 31: GENERATION #11 DATA.....	125
TABLE 32: GENERATION #12 DATA.....	126



## NOMENCLATURE

$a$	= distance to vortex core
$AR$	= aspect ratio
$b$	= span length
$c$	= chord length
$c$	= speed of sound
$C_d$	= coefficient of drag
$C_l$	= coefficient of lift
$D_i$	= induced drag
$F_i$	= individual fitness value
$j$	= number of individuals
$k$	= gene label
$L$	= lift force
$P$	= path length
$R$	= percent of total fitness value
$r$	= radius
$t$	= thickness
$U_0$	= freestream velocity
$v$	= velocity
$V_\infty$	= freestream velocity
$W$	= downwash velocity
$x$	= location along chord length
$z$	= distance behind trailing edge
$\alpha$	= angle of attack
$\Delta t$	= time difference
$\theta_F$	= feather angle
$\Gamma$	= circulation

# 1. INTRODUCTION

## 1.1 Background

Wing tip vortices are an unavoidable and troublesome byproduct of lift. For example, the wing of an aircraft is designed so that the pressure below the wing will be greater than the pressure above it. This is what provides lift and allows the plane to fly. However, this pressure difference causes the air at the tip of the wing to spill over from the bottom to the top of the wing creating a trailing vortex [1,2,3] (see Figure 1).

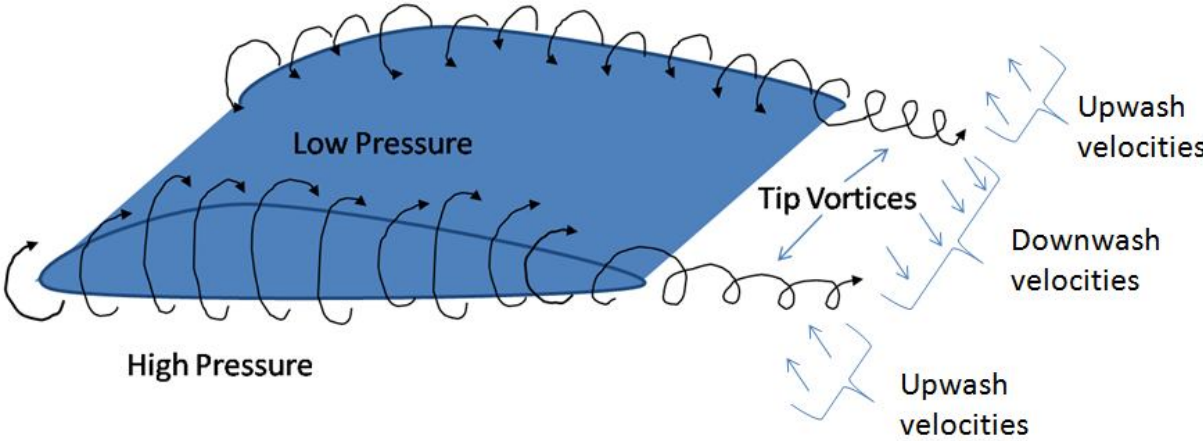


Figure 1: Formation of Tip Vortices [1]

These vortices reduce the efficiency of the wing or propeller blade. The presence of the vortex creates an imposed downwash velocity ( $w$ ) as shown in Figure 2. This downwash velocity changes the effective local freestream velocity and lift vectors (see Figure 2). This adds a component of force in the backward direction called induced drag ( $D_i$ ) (see Figure 2). This force results in energy loss and inefficiency [1,2,3].

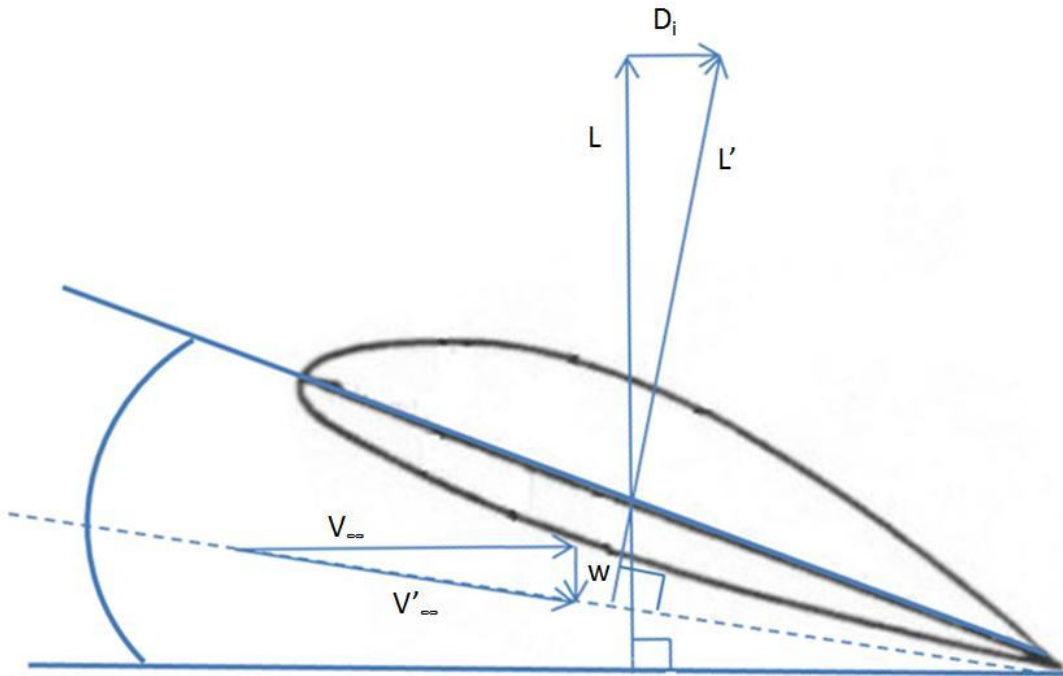


Figure 2: Induced Drag [2]

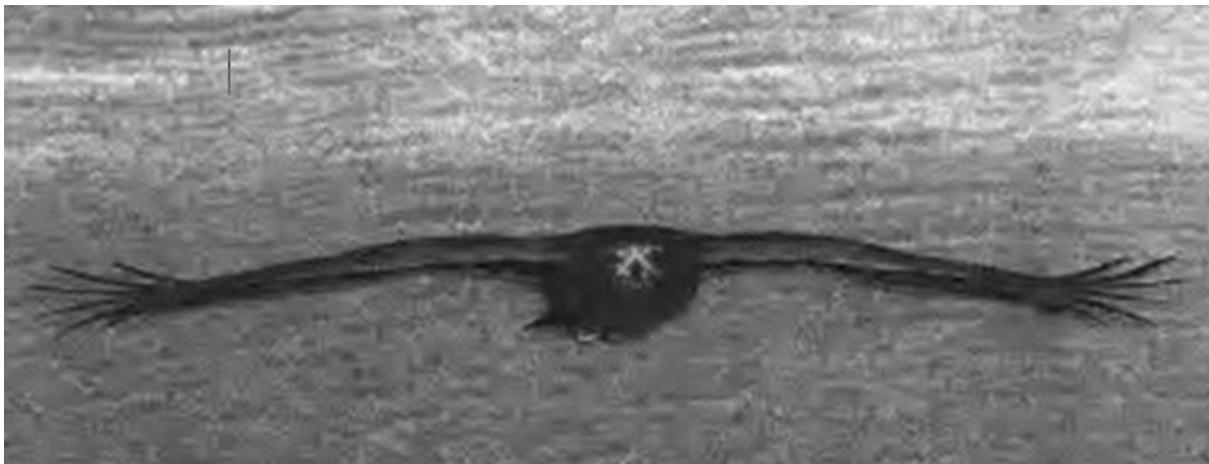
In underwater applications, tip cavitations are an effect caused by tip vortices formed on propeller blades in water. At the center of the vortex, there is an area of very low pressure. This low pressure creates bubbles in the vortex core (see Figure 3) [4]. The cavitations can create noise and erode propeller blades. This erosion reduces the lifespan of the equipment [5].



Figure 3: Propeller Blade Cavitation from Ref [4]

In addition to the inefficiency they cause, tip vortices are the main contributor to hazardous wake turbulence [6]. The vortices create a large gradient of downwash to upwash velocities behind the wing as shown in Figure 1. As another aircraft passes through this gradient, the plane will have a tendency to roll or, in extreme cases, structural failure can occur [1].

Although these vortices are an unavoidable effect of lift, if their strength is minimized, the problems associated with them could also be minimized. There are two ways in which birds, in nature, combat the problem of wing tip vortices. Birds that fly primarily over the sea tend to have long narrow wings with pointed tips. While this is effective in birds, it is not realistic for propellers or small aspect ratio wings. Birds that soar over land tend to have smaller aspect ratios, which gives them the ability to maneuver more easily through the more varied wind patterns that occur due to the varying surface temperatures and geological formations. In order to compensate for this smaller wingspan, many of these birds have developed primary feathers at their wingtips that spread horizontally and vertically (see Figure 4). [7]



**Figure 4: Harris Hawk with Slotted Wingtips from Ref [7]**

The shorter wingspans of gliding land birds have evolved with many of the same motivations used in aerodynamic designs, namely aerodynamic efficiency (high lift to drag ratio), maneuverability, and

weight considerations. It follows that the wing tips that have evolved in nature should then be considered in mechanical design, which is an example of the use of biomimetics.

In the field of biomimetics, scientists attempt to mimic the systems and materials found in nature for engineering and scientific applications [8]. Many every day products have been inspired by nature as well. For instance, Velcro® was invented by George de Mestral based on the way cocklebur persistently attached to his dog's fur when they went for walks [8, 9]. Similarly, products like anti-slip shoes and paints have been inspired by naturally occurring characteristics [8].

However, a key concept of biomimetics is that it is often more beneficial to understand that creating an exact replica of a mechanism engineered by nature is often not as beneficial as the process by which that mechanism evolved [9]. Characteristics of mechanisms currently existing in nature have come to exist through years of evolution driven by the need to survive. Competition for resources puts a limiting constraint on that survival. Evidence of nature's failed designs can be seen in the fossils of extinct species [8]. While natural evolution takes place over millions of years, man can learn from this optimization process and try to use that knowledge to mimic its results.

This theory can apply to many different areas of engineering including information processing for electronics companies, tissue engineering for biomedical purposes, and polymer synthesis for chemists [8]. The particular area of interest for the present work is in the field of aerodynamics. As mentioned previously, bird flight exhibits particularly important characteristics. The concept of biomimetics has often been applied specifically to Micro Aerial Vehicle (MAV) design.

MAVs are a subcategory of unmanned air vehicles (UAVs). They have a largest linear dimension of no greater than 6 inches. The aircraft's small size allows for inexpensive system cost and a high level of portability. The purpose of these crafts is to maneuver within a close range of a target area without being detected and provide surveillance information. In order to fulfill this objective, MAVs must be

capable of sharp turns near buildings, handling turbulent winds up to 25 mph, and performing repeated climbs to an altitude of 350 feet. In addition to the performance requirements, the system needs a simple control system so that minimal training is required for its operators. [10]

Biomimetics has already had a significant effect on MAV design. Through observations of nature, engineers and scientists have been inspired to investigate flapping motion wings [11], membrane wing shape morphing [12], and improved planform shape [13, 14]. The intent of the present work is to extend the reach of biomimetics influence on MAVs (as well as propeller blades) to modified wingtip geometry.

## **1.2 Literature Review**

In order to evaluate the usefulness of avian inspired wingtips to aerodynamic designs, it is necessary to review previous studies regarding previous optimizations based in nature, research specifically related to avian wingtips, and techniques that can be used to measure the effect of those wingtips on the trailing vortex strength.

### **1.2.1 Computer Simulations of Evolution**

Charles Darwin theorized that variations exist within species, a lack of resources causes competition between those species, and that variations that favor the survival of the species are more likely to be preserved. He referred to this process as natural selection or, as phrased by Herbert Spencer [15], survival of the fittest. This provides some explanation as to how species found in nature develop certain characteristics. Further, given a fairly constant environment, evolution can lead to convergence of these characteristics [15].

For decades scientists have been attempting to mimic optimization through evolution with computer simulation. An early example of this was a technique called *evolutionary* operation, which was advocated by G.E.P. Box and colleagues in the late 1950's [16]. In this technique, a manufacturing

plant is treated as a species which evolves based on the votes of members of a technical committee. Although this process has been applied effectively to many manufacturing processes, it was never used as an independent computer simulation. In the same time period, Friedberg created a computer program that could choose instructions based on their stored history of success [16]. This gave the program the ability to choose, given a moderate pool of options, the most efficient program. Friedberg did not specifically claim that this program was designed to mimic natural evolution, but it was observed to do so and inspired further work in the area.

Since that time the method called *artificial life*, which is related to the work of Barricelli, also in the late 1950's, has been studied by many, including Conrad (1970,1981,1985), Pattee(1970), and Rizki(1985) [16]. This process is a simulation of a hierarchic ecosystem in which the population is given different traits, and the evolutionary behaviors due to reproduction and mutation rules are observed. In the mid 1960's, Rechenberg, Schwefel, and Bienert generated an algorithm called *evolutionary strategy* to optimize fluid mechanics problems and later extended its application to general function optimization [16]. In *evolutionary strategy*, each part of the trial solution is considered a trait of the species, not as individual genes along a chromosome. More detail on these computer simulations as well as others can be found in Fogel [16].

*Genetic Algorithms* are the most popular type of evolutionary computation and are particularly useful in optimization problems [17, 18]. The method was first formally discussed by Fraser in 1957, Bremermann (1962), and many of Holland's students at the University of Michigan (1967 to 1973) [16]. This process is similar to *evolutionary strategy*, but in this algorithm, each individual (or design candidate) in the population is represented by a "chromosome" that contains a string of genes. Each gene is represented by a number, which represents a specific individual trait [16,17,13]. For instance, in the present work, each chromosome is a sequence of 8 feathers. The numerical value of a gene

determines the feather orientation. The full procedure involved in completing a genetic algorithm can be seen in Figure 5.

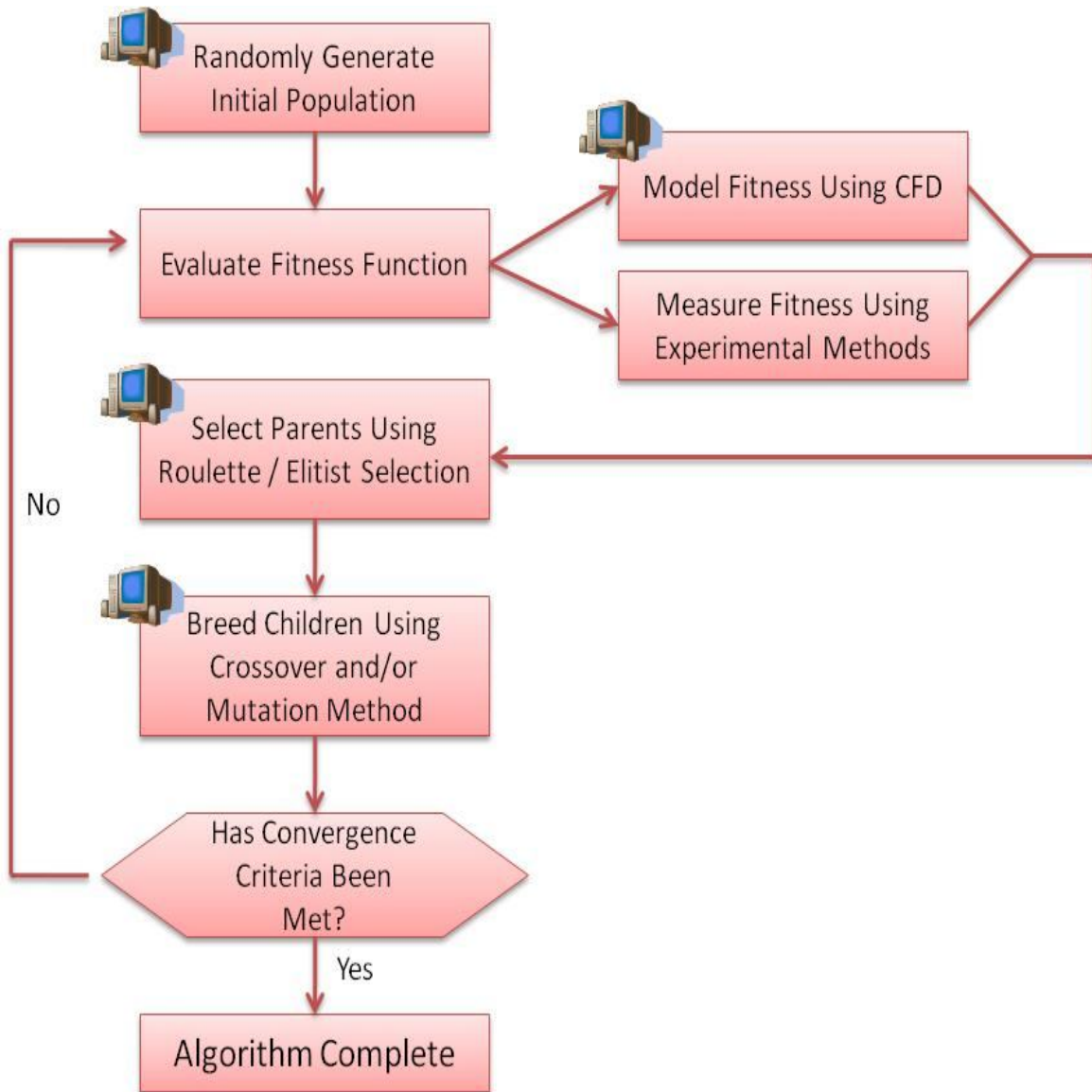


Figure 5: Genetic Algorithm Flowchart

A random number generator can be used to assign numerical values to genes of the chromosome to define each individual (candidate design) in the population. This process is repeated to create a sufficiently large initial population with  $j$  individuals, which should be at least two or three times standard population size, which will be used for all generations after the first [19].



Next, each individual in the population is evaluated using a fitness function, which is directly related to the success level of the individual. This fitness value can be calculated based on an optimization criterion that is found either computationally or experimentally. In the present work, the tip geometry is optimized for minimal circulation. Therefore, to create a fitness function that is proportional to performance, the inverse of circulation is taken to be the fitness value. The circulation value associated with each individual is measured experimentally in a wind tunnel. Once each individual is assigned a fitness function, parents are selected based on their individual fitness value.

The next step of the algorithm is parent selection. The most common form of parent selection is *roulette wheel selection* [16, 13, 14]. In this method, the fitness value of each individual ( $F_i$ ) is divided by the sum of the fitness values of the entire population. Each individual is then assigned a portion ( $R$ ) of an assumed roulette wheel, as shown in equation (1). Therefore, the individual with a greater fitness value will have a higher probability of being selected as a parent. For example, Table 1 shows a list of individuals in a population and their respective fitness values. Figure 6 shows the roulette wheel for parent selection for this population.

$$R = \frac{F_i}{\sum_{i=1}^J F_i} \quad (1)$$

**Table 1: Sample Population Fitness**

Individual	Chromosome	Fitness Value ( $F_i$ )	% of Total (R)
1	22101102	17	12.1
2	21001022	58	41.1
3	01220111	6	4.3
4	10012011	36	25.5
5	11021220	24	17.0

Total		141	100
-------	--	-----	-----

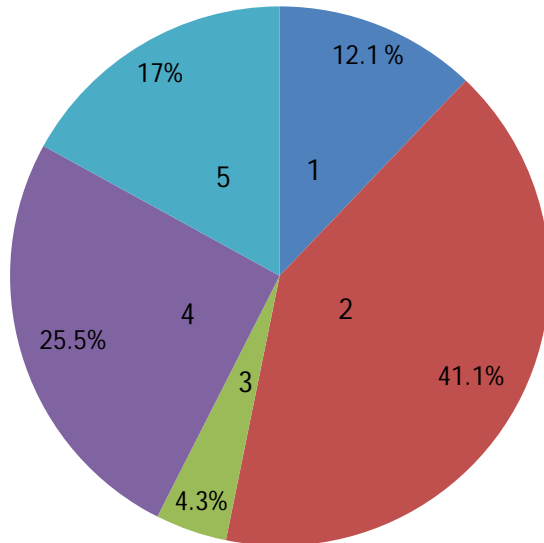


**Figure 6: Sample Selection Roulette Wheel**

Elitist strategy can be used in addition to the roulette wheel method of selection. In this method, the two individuals with the highest R values are automatically selected to be parents of the next generation [15,17,13,14]. This guarantees the survival of the best designs. The remaining parents in a population can then be selected using the roulette wheel selection method.

Once the parent individuals have been selected, they are used to breed new individuals for the following generation (see Figure 5). The general population size must be sufficiently large to allow for the optimal solution to be found without requiring excessive testing. The total solution space ( $n = 9^8$  in our work) for the problem must be calculated. Then, the general population size must be at least the size  $j = \log_2(n)$ . In order to pair parents effectively, the population size should also be a multiple of 4 ( $j=28$  in our work).

There are two common methods of breeding individuals to make up these populations, crossover (sexual) reproduction and mutation (asexual). There are multiple methods of crossover breeding. The simplest method is single point crossover. In this method, a single point along the chromosome is selected. The genes before this point are taken from the first parent and combined with those after that point of the second parent to create the first offspring. The second offspring is created from the opposite process (see Figure 7). The same process can be used in multipoint crossover, a method (see Figure 8).



Figure 7: Single Point Crossover

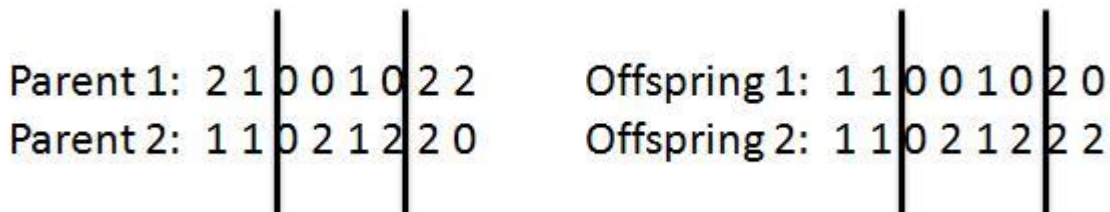


Figure 8: Multi-Point Crossover

Although single-point crossover was originally thought to keep blocks of good code together, resulting in improved offspring, a study by Syswerda showed that uniform crossover showed better results with less computational effort [16]. For this reason, this breeding method was selected for the current work. In the uniform crossover method, for each gene in the string, a parent is randomly selected and the gene from that parent is used in the offspring [13,14].

The other breeding method often used in genetic algorithms is mutation. This can be applied in addition to crossover or independently (asexual reproduction). In each case, a probability of mutation is assigned uniformly to each gene in the chromosome of each individual in the population. For this work, a 20% mutation rate was used in conjunction with the uniform crossover method.

Most genetic algorithms used in design optimization use crossover breeding techniques with mutation; however, there is some debate over the importance of sexual reproduction in evolution. Some theories suggest that sexual reproduction allows for greater mixability (the ability to combine well with variety of other traits), while asexual reproduction increases the mean fitness of the population [19]. This theory suggests that in sexual reproduction, genes that are more compatible with a greater variety of neighboring genes are passed on, while in asexual reproduction it is more likely that the best individual genes are passed on. The study completed by Livnat et al [19] did not make any conclusions on the importance of sexual reproduction in optimization, but it did suggest that it improved the evolvability of the individual and that asexual reproduction led to a higher mean fitness in their study. It is also important to note that mutation was not used in the Livnat study [19].

In the current work, a genetic algorithm was used to evolve the tip geometry of test wing to optimize for minimum circulation. An initial population size of 84 individuals was tested followed by numerous generations of 28 individuals. Parents were selected from each previous population using the *roulette wheel selection* method and, in some cases, *elitist selection*. The parents then bred children using uniform crossover with a 20 % mutation rate applied to each gene. Cloning (e.g. allowing identical parents to mate to create identical children) was used in this algorithm as it is a common characteristic of breeding used in genetic algorithms [20,21].

### 1.2.2 Biologically Inspired design

In nature, evolution has taken place over a large expanse of time and place. Over the course of this immense experiment, many designs have been developed, tested, and improved over time. For this reason, particularly in the case of complicated fluid dynamics adaptations, designs found in biology can be of great inspiration and use to engineers. In some cases, computational simulations of evolution are used, while others simply apply characteristics observed in nature to engineering designs.

Genetic algorithms have successfully applied to many different areas within engineering. For instance, in civil engineering, genetic algorithms have been used to optimize truss design for minimum weight and number of cross-section types [22]. In controls engineering, genetic algorithms have been used for multiple applications such as design of aerospace control systems, non-linear system identification, and mix-mode scheduling [23]. Genetic algorithms have also been used in biology to simulate protein folding by optimizing for minimum energy level conformations [24]. These applications were successful for multiple reasons. First for the truss and non-linear system applications, the algorithms were an improvement over conventional methods because they were capable of optimizing for multiple criteria. The mixed-mode scheduling and protein folding applications were optimization problems which had not been able to be solved using brute force searches. In the case of protein folding, it has been suggested that the success of genetic algorithms is due to their ability to mimic the folding pathway instead of a random search [24]. Although genetic algorithms have successfully been applied to many areas of science and engineering, due to the content of the current work, this section will focus on previous studies that use biologically inspired design in the fields of aerodynamic and fluid dynamic applications.

As flow separation on wings is an important phenomenon, much work has been done to combat this problem. Studies by W. Liebe [25], R. Bannasch [28], the group of Dietrich Bechert [29], and others

have investigated the interaction of the light feathers, or coverts, on bird wings with flow separation [28]. Bannasch was able to simulate these feathers with a silk apparatus that, as shown by flow visualization data, responded to the reverse flow above the wing and found that these feathers did act as a brake to stop the spread of flow separation. This adaption increased the critical angle of attack of the test wing from  $18^\circ$  to more than  $40^\circ$ . Although this improvement was under the conditions of low Reynolds numbers, with more investigation, this finding could bring about improvements in aircraft design. [28]

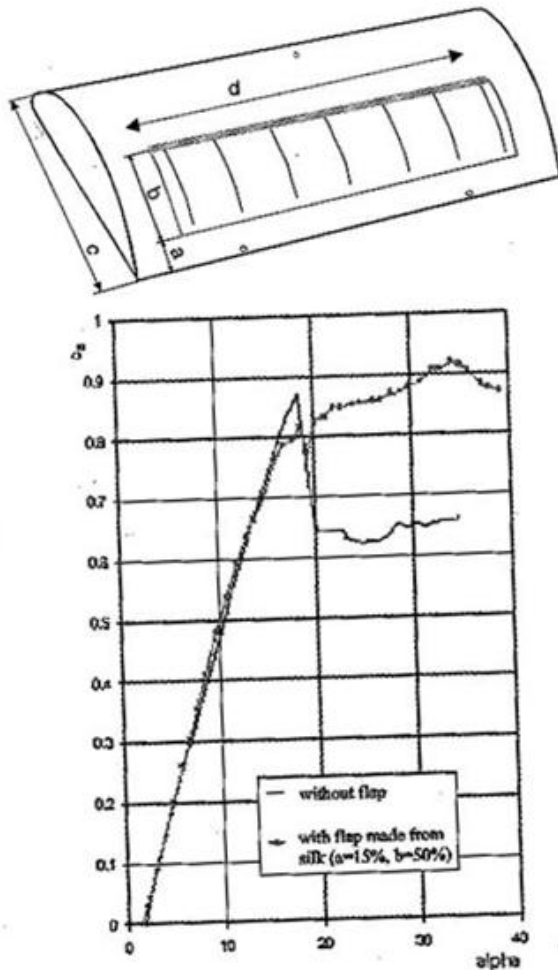


Figure 9: Silk Flap Added to NACA 4412 (top) and resulting change in critical AoA (bottom) from Ref [28]

In a previous study conducted by A. Day [13], observations of bird wings led to the exploration of the relationship between lift to drag ratio and wing planform. In this study, genetic algorithms were used to breed different species of a Micro Aerial Vehicle (MAV) wings. In this particular algorithm, uniform crossover breeding and a mutation rate of 20% were used. The work was continued by S. Taylor [14], which led to an MAV wing planform with an optimized lift to drag ratio. It is also of note that although the best design did share common attributes with some found in nature, it was unique. This best planform was a completely new design, which shows the importance of using a genetic algorithm. While testing a few planforms that have been observed in nature or are expected to meet the desired specifications can be beneficial, using a genetic algorithm allowed for the discovery of an optimal planform that had not previously been considered.

Similarly, in a study by Oyama et al [18], a genetic algorithm was used to optimize lift to drag ratio of a transonic wing design. In this case, the airfoil cross-section shape was the variable instead of the wing planform. A mutation rate of 10% and blended crossover breeding were used in this study. The wing designed through this method has fully attached flow and reduced pressure and wave drag. These positive characteristics as well as its resemblance to advanced wing designs show the ability of a genetic algorithm to optimize design. This same idea can be applied to many other areas of aerodynamic design including using wingtip geometry to decrease wingtip vortex strength.

Tucker [6] investigates the effect of a variety of wingtips on the aerodynamic forces on a base wing. Tucker measured the lift and drag of a base with a Clark Y tip, an actual Harris Hawk feathered tip, and a balsa wood feathered tip. He concludes that feathered wing tips, including the artificial set, are able to decrease induced drag because of their exposure to upwash. Flow visualization data collected in the study suggests that this decrease in induced drag is related to the changes in the wingtip vortex. In agreement with wingtip theory, this data shows that the vertical and horizontal slots between the

feathers allow for the spreading of the wingtip vortex, which decreases its harmful effects. These findings show that wingtip vortices are affected by wingtip geometry. Therefore, the next step is to manipulate the tip geometry to create an optimal design.

There have been many attempts to recreate the performance improvements provided by nature using simple winglets on glider planes. It has been found that simple winglets do provide a decrease in induced drag [26, 27]. While this decrease can also be achieved by adding to the wingspan, for applications with limited span [26], such as the propeller blades and MAVs of interest to this study, winglets are a valid option. However, simple winglets provide only a small increase in efficiency, which make them only beneficial in cases where all other options have been exhausted [27]. For this reason simple winglets are only a preliminary solution to the problem of induced drag. Further investigation regarding wingtip geometry may lead to a more significant decrease in wingtip vortex strength.

Some preliminary work on applying biomimetics to wing tip geometry has been completed by M. Stache [28]. In this study, the *evolutionary strategy* method was used to optimize the lift to drag ratio of a test wing with five wingtip feathers (see Figure 10), each of which was connected to the base wing with a lead joint allowing for attachment angle variation. The results show that this optimization improved the lift to drag ratio by 11% in contrast with a planar wing of the same area and span. Stache then continued to manipulate this design for further use in more practical applications. This research prompts continued interest in this area.

The optimization performed in this study is based on lift to drag ratio. Figure 10 also shows that, for a fixed angle of attack, the drag is decreased, while the lift stays constant. This shows that induced drag, and hence vortex strength, is affected by the wing tip geometry, which provides a motivation for the present work. In the current study, optimizing for minimum vortex strength will address the problem of induced drag as well as the other issues associated with wingtip vortices. Figure 10 also



shows that reduction in drag is more significant in some angle of attack (AoA) regimes compared to others. As a result, the AoA will be varied in our study.

As mentioned by Bannasch, the work of Stache could also be applied to other engineering designs [28]. By adapting this research to apply more particularly to propeller blades, a different optimized geometry may occur.

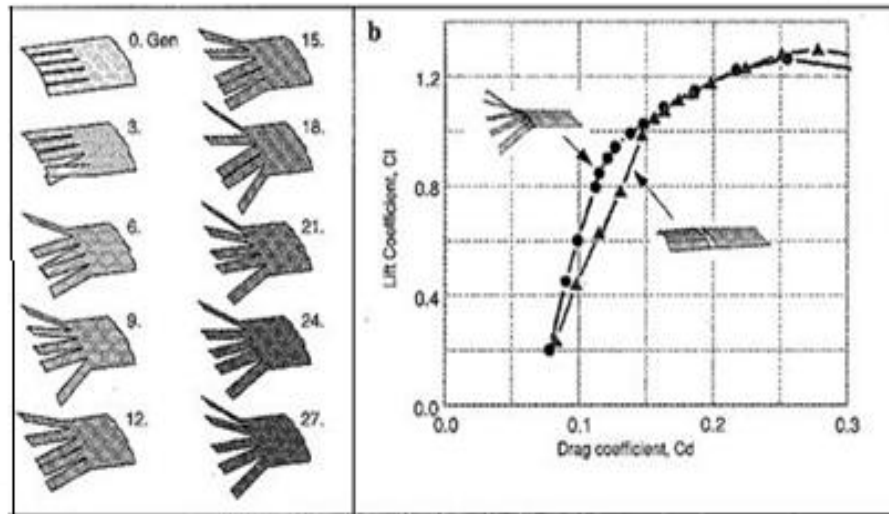


Figure 10: Bannasch Test Wing Evolution from Ref [28]

As wingtip vortices are a significant problem facing propeller blade design and lifespan, some work in the area has been conducted. S. Lunin [5] presents the benefits attained with the addition of a single simple tip fin (see Figure 11), similar to winglets found on aircraft, to the end of propeller blades. In his research, he found that a 10% improvement in propulsion efficiency could be obtained with this change in propeller geometry. With further research into more complex tip fin geometry, the tip vorticity could be further decreased. With this decrease, efficiency as well as the propeller lifespan would increase.



Figure 11: Propeller with Tip Fin from Ref [5]

### 1.2.3 Vorticity Measurement Techniques

In order to optimize the wingtip geometry for minimal vorticity, a method of measuring the circulation behind each wing design has to be selected. Some of the possible techniques are hot-wire anemometry, vane-type vorticity meters, laser-doppler anemometry, conducting fluid measurements, and acoustic methods. Each of these methods is evaluated using the following criteria.

- Ability to measure global vorticity
- Application to wind tunnel test set-up
- Ease of use
- Accuracy

The first requirement listed above eliminated some of the common techniques. Hot-wire anemometry is method that uses a probe at a single location consisting of a whetstone bridge with configured hot wire legs. The probe then reads a galvanometric voltage, which varies with changes in velocity of the flow. In addition to the fragile nature of hot-wire probes and their tendency to interfere

with flow characteristics, this method was ruled out due to its inability to measure the global circulation of a fluid flow field.

Vane-type vorticity meters measure the vorticity of the flow directly. The apparatus consists of thin bladed propeller with no angle of attack, which is also only capable of measuring circulation at a point [30], not globally.

Although some more advanced methods provide added benefits, they still have some limitations. For instance, laser-doppler anemometry uses very small, neutrally buoyant, particles to reflect laser light as they move in a fluid. The rotation rate is then sensed by an optical system of high accuracy. However, this method is limited to use in liquid flows, which is not conducive to a wind tunnel test.

Particle-image velocimetry (PIV), a laser-base technique that measures fluid velocity components on a two dimensional laser sheet, could also be used to measure circulation by integrating velocity or vorticity fields. However, PIV systems are complex and expensive.

The vorticity in an electrically conductive fluid flow can also be measured using the relationship between the potential of the electric field, the electric field intensity, and the vorticity vector. This method requires no calibration, but can again only measure vorticity at a point and requires a strong magnetic field to do so [30]

Ultrasound can be used to measure the global strength of a vortex [31]. The total circulation of a vortex is related to the tangential velocity and radius of the vortex as a function of position. The speed of a sound wave is the component of the local flow velocity in the direction of the sound wave path added to the local speed of sound, which is the basis of this technique. In order to account for the variance in local speed of sound, two signals can be transmitted in opposite directions perpendicular to

the vortex axis (see Figure 12). This velocity can then be related to the tangential velocity. The particular relationship and equations used in this study can be found in Section 2.3.2.

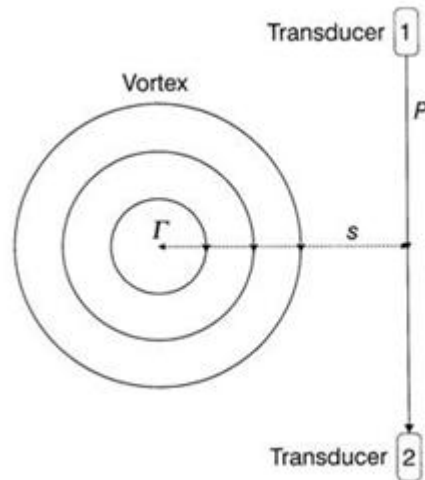


Figure 12: Ultrasonic Transducer Schematic from Ref [31]

The ultrasound method can also be applied to a closed loop acoustic path. In this version of the technique, acoustic reflectors are used to direct the sound waves in closed path encompassing the total vortex. This technique was verified by Johari & Durgin through an experiment in which they measured the circulation around delta wing vortices in air and free surface vortices in water [31]. The benefit of using this technique is that it does not require the speed of sound or vortex core location to calculate the circulation. This method is limited in that it is only valid at speeds where the flow velocity component along the ultrasound path is significantly smaller than that of the speed of sound.

Ultrasonic circulation measurement has been shown to be accurate in similar previous experiments. In 1990, H. Purutyan [32] used the ultrasonic technique to measure the circulation around a plunging airfoil. However, because of the unique set up of his experiment, his results were unconfirmed. In 1997, K. Desabrais [33] used an ultrasonic flowmeter closed signal path to measure the circulation around an airfoil as well as the distribution of the wingtip vortex behind the airfoil. He used the circulation around the airfoil to calculate the lift and confirmed his results using the Kutta Joukowski

theorem. The wingtip vortex circulation measurements were also confirmed, in this case, by Digital Particle Image Velocimetry (DPIV) data.

The ultrasonic method was selected for the present work because it has the ability to measure the global circulation, it can be used in a wind tunnel, there is no calibration necessary, and it does not interfere with the flow characteristics. Because the present work only requires the comparison of relative vortex strengths between designs, the straight path version of the ultrasonic method was used. In this case, the absolute circulation does not need to be known, so approximate values can be used for speed of sound and vortex core location, so the added complexity of a close path transducer set up is not necessary. More detail on the application of the ultrasonic method in the present experiments will be given in Section 2.3.

### **1.3 Objectives & Overview**

The overall purpose of this research is to study the effect of wingtip geometry (feather angle) on wingtip vortex strength. In order to do this, the following specific objectives needed to be accomplished:

- Create a test wing apparatus in which manipulation of the wingtip feather angles takes place from outside the wind tunnel test section without disturbing the freestream flow. Such a design will result in reduced testing time.
- Apply genetic algorithms to the test wing at high and low angles of attack to guide evolution of the tip geometry for each case. Performing two optimization runs will allow for the comparison of the effects of tip geometry at two angles of attack as well as of the results gained by two distinct initial populations.

- Using the genetic algorithms, determine a wing tip geometry that minimizes wingtip vortex strength. Optimized tip geometries will result in reduced induced drag, and also serve as a starting point for future design modifications.

Obtaining these objectives will provide a basis for new, more efficient and longer-lasting propeller blade and MAV wing designs.

The following sections include the development and description of the final test wing design, the experimental set-up, test procedure, data collection and analysis methods in Section 2. Results using the genetic algorithms applied to flow over a low aspect ratio wing at low and high angles of attack are presented in Section 3. Conclusions are drawn from those results in Section 4. Section 5 contains specific suggestions of how the topic of the present work can be continued in future research.

## **2. EXPERIMENTAL METHODS**

### **2.1 Wind Tunnel**

All of the following tests were performed in the WPI closed circuit wind tunnel located in Higgins Laboratory on the WPI campus. The wind tunnel is capable of test section freestream velocities of approximately 0 to 55 m/s. All tests were conducted at air speeds lower than 16 m/s, for which the tunnel has a turbulence level of less than .73%. The test section has a cross sectional area of .61 m by .61 and a length of 2.4 m and a contraction ratio of 6:1. The tunnel has a built in heat exchanger and temperature control panel, which was used to maintain the test section flow temperature at 69°F.

### **2.2 Test Wing Design**

A test wing was specifically designed for the purpose of this study. The wing needed to have a variable feather geometry resembling bird wings found in nature that could also apply to a propeller blade. Due to the large number of tests run as a part of this research, the mechanism was created so that the feather angles could be modified and measured without removing the wing from the wind tunnel.

The test wing was designed to mimic characteristics seen in bird wings and apply them to propeller blade design. Therefore, a 5.5" x 5.5" test wing was created to have a half aspect ratio of one, as shown in Figure 14. Gliding birds, such as a Harris Hawk, which display the vertical spreading of the primary feathers, were observed to have wings whose primary feather lengths were 25 to 35 percent of the wing half span length [34]. Therefore, the test wing has feather lengths which are 30% of the wing half span length. The wing consists of eight primary feathers in order to increase the possible geometries and decrease the chance of excessive interference. According to Bannasch [28], too many winglets will result in enough interference to increase the friction drag and eventually block the flow through the array. Each of the feathers has a tapered thickness ranging from 0.25" at the base to 0.125"

at the tip. Although flow interaction of the blunt feathers with the freestream flow provides a reason to further reduce feather thickness, other factors including manufacturing design constraints and possible vibrations issues dictated that the feather thickness could not be further reduced. The base wing consists of a hollow sheet metal rectangular casing, which is enclosed by a plastic curved piece on both the leading and trailing edge to make the wing more aerodynamic. As shown in Figure 13, the final test wing is a flat plate airfoil, with a chord length  $C = 5.25''$ , a half span length of  $b = 5.25''$ , and a thickness  $t = 0.5''$ .

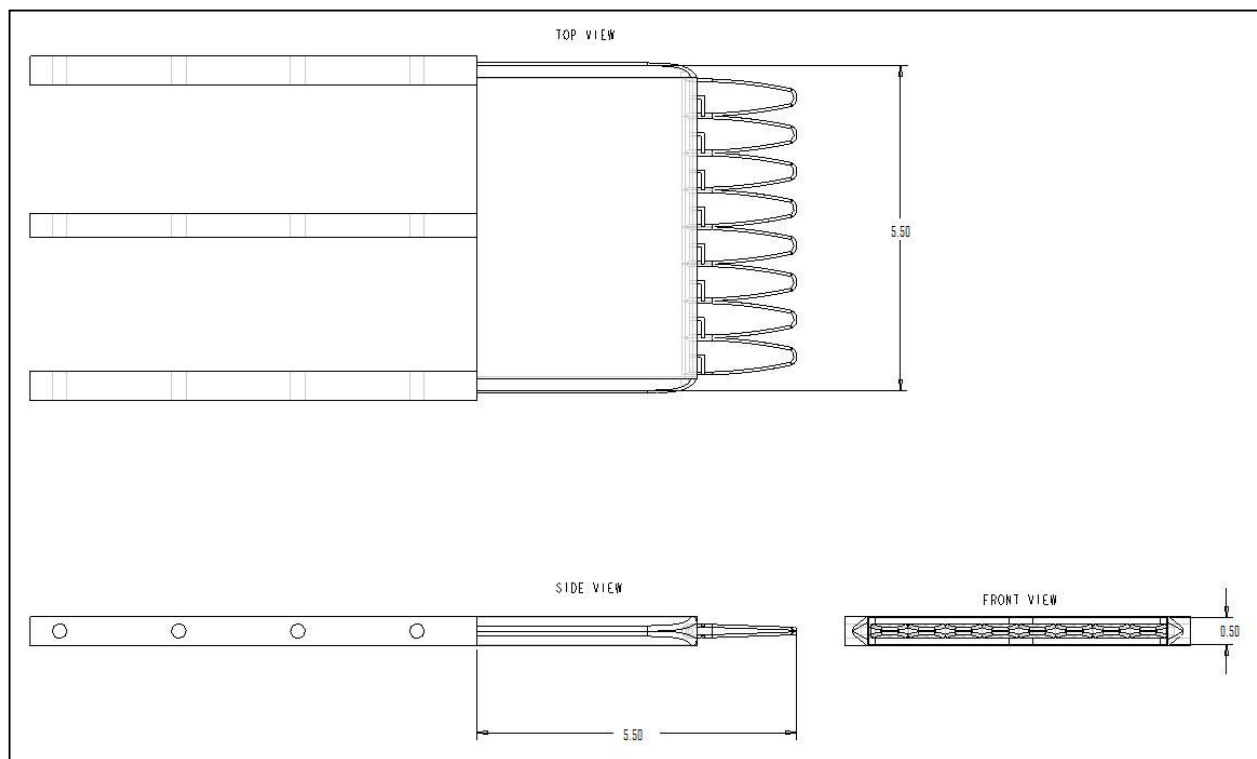


**Figure 13: Test Wing Assembly Drawing**

As the genetic algorithm may continue for many generations and each generation contains many individuals, each of which must have the fitness function measured, the experiment is most efficient if the feather angles are manipulated and measured without removing the test wing from the wind tunnel. To achieve this, each feather is attached to a steel rod that sits outside the wind tunnel, by



two pieces of fishing line that run through the hollow base of the test wing. These two lines control the position of the upper and lower side of the feather. Each steel rod has the same diameter as the base of the attached feather, which means that when the rod is turned, it creates an equivalent change in the feather angle (see Figure 14). This allows the angle of rotation of the rod to be measured instead of the actual feather rotation, which takes place inside the wind tunnel.

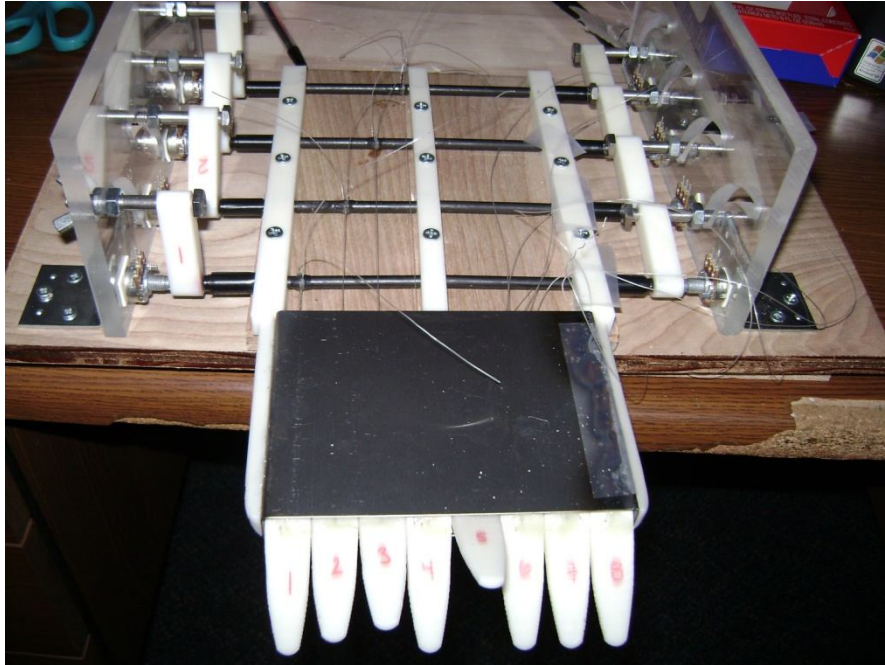


**Figure 14: Test Wing**

The use of genetic algorithms requires that each gene number corresponds to a distinct feather angle. Therefore, the angle of the feather must be measured accurately. To achieve this, each steel rod was connected to a Model P160KN-0QD15B1K rotary potentiometer, which was then adhered to a panel. As the steel rod was turned, the rod end turned at the same rate.



**Figure 15: Angle Measurement and locking System**

A LabView program was used to calibrate each potentiometer before the series of tests were run. The virtual instrument then recorded the relative voltage for a number of manually measured feather angles and exported the data to an excel file. The data was then plotted and a linear regression was used to relate the relative voltage to the feather angle. The details of this calibration can be found in Appendix A.

Once this calibration was completed and the slope and intercept recorded for each feather, another LabView virtual instrument was used to measure the angle of the each feather during the following tests. In this program, the feather number can be selected from a drop down menu. Through this selection, the appropriate slope and intercept found in the calibration are applied. The DAQ system can then read the relative voltage and display the angle of the feather on the front panel of the VI (see Appendix B).

In order to measure the fitness function of each individual accurately, the feather angles of that individual had to be appropriately set and then locked in place so that the desired angles would be maintained throughout the data collection. To do this, a perpendicular extension was added to each rod. A cap screw was inserted to this extension and ran through an arced track. On the other side of this track, a wing nut was used to lock the cap screw attached rod in place. The extension system allowed for increased torque, which prevented slippage (see Figure 15).

### **2.3 Circulation Measurement**

A GE Sensing XGM868 Flowmeter (see Figure 16) with T9 ultrasonic transducers and a STPRE preamplifier were used to measure the circulation of the wingtip vortex behind each wing design. The flowmeter has an infrared control panel and LCD display. It can output the difference in signal transit time. The flowmeter has two measurement modes: skan and skan/measure. The former uses minimal signal processing and has a 52 nanosecond resolution while the latter has increased signal processing and a higher resolution of 15 nanoseconds. However, the additional signal processing slows the response time, so this mode can only be used to measure slow velocities. The functionality and accuracy of the flowmeter were verified with a velocity test (see Appendix C).

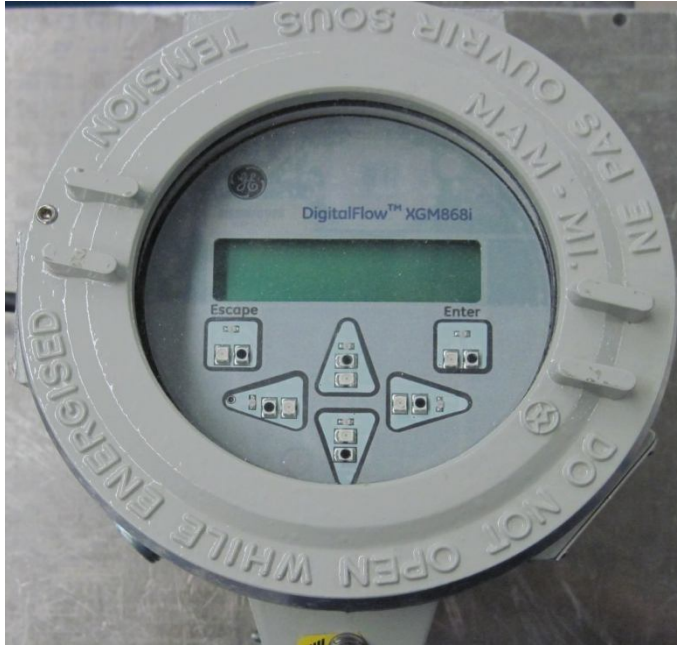


Figure 16: XGM868 Flowmeter

### 2.3.1 Wind Tunnel Setup

To measure the circulation behind the test wing, the wing was placed in the wind tunnel through a side port at a specified angle of attack. The transducers were then placed 2.67 chord lengths (distance  $z$ ) behind the test wing trailing edge through port holes in the top and bottom of the tunnel. This location was in the range between the path locations used by Purutyán [32] and Desabrais [33]. The acoustic path between the two transducers was located 1.4 chord lengths (distance  $a$ ) in the spanwise direction from the center of the wingtip vortex, which is assumed to be located at the wingtip (see Figure 17 and Figure 18). According to the vortex distribution data collected by Desabrais, the transducer path should encompass the area within a radius of 1 chord length from the tip of the wing to ensure measurement of the total vortex strength [33].

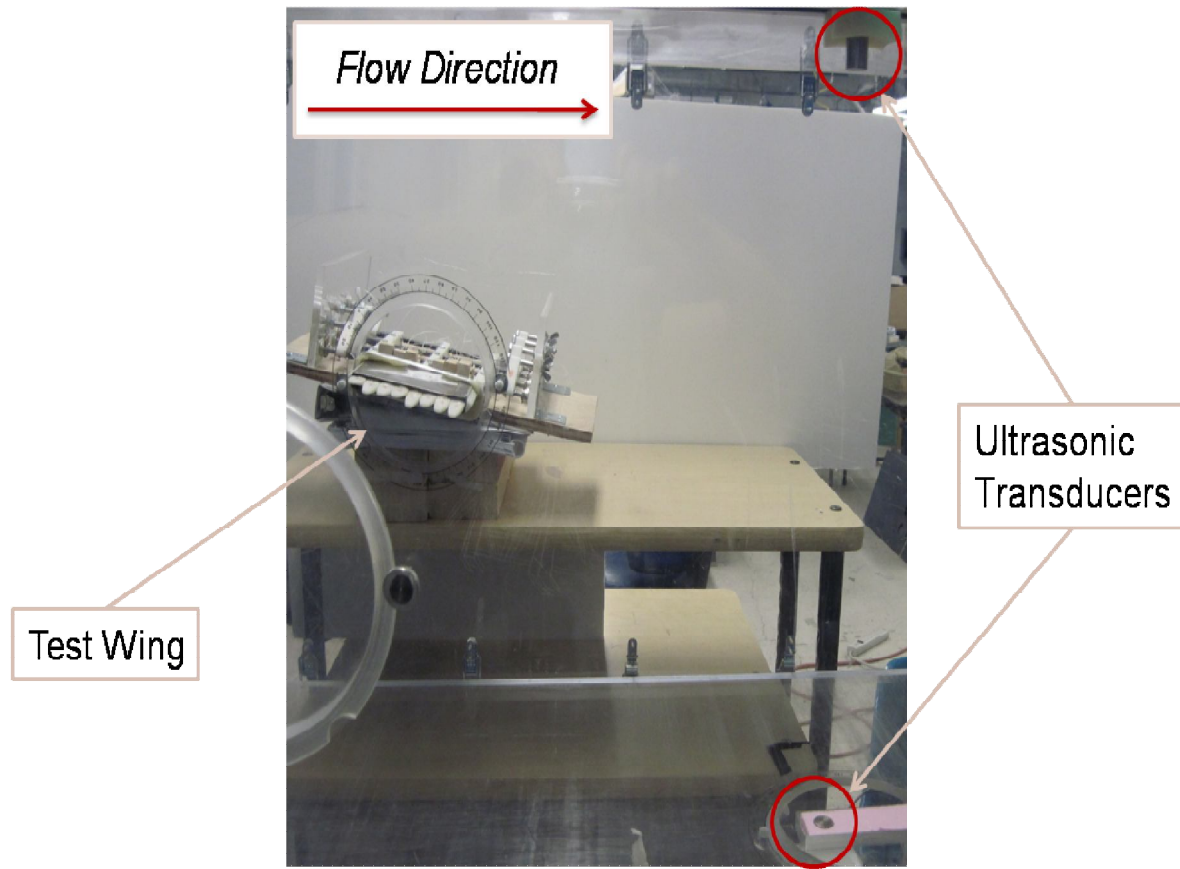


Figure 17: Wind Tunnel Test Set Up

### 2.3.2 Circulation Function Derivation

In order to calculate the circulation of the wing tip vortex trailing behind the test wing, the difference in signal transit time for an ultrasonic pulse traveling between the two transducers needs to be related to the total circulation using only known variables. A diagram of the test set up and dimensions is shown in Figure 18.

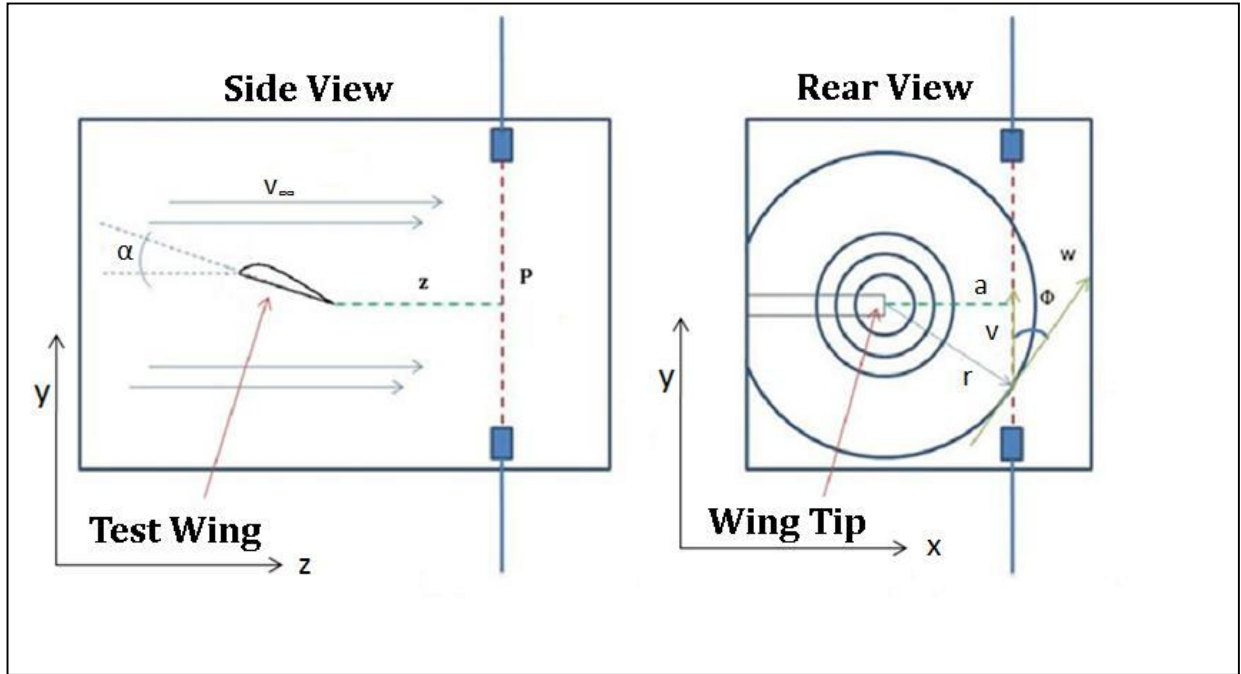


Figure 18: Circulation Measurement Diagram

For a vortex,

$$w = \frac{\Gamma}{2\pi r(y)} \quad (2)$$

As seen in Figure 18,  $v$  is the component of  $w$  along the transducer path,

$$v = w \cos \phi \quad (3)$$

$$v(a, y) = w(r(y)) \frac{a}{\sqrt{a^2 + y^2}} \quad (4)$$

Inserting equation (2) into equation (4),

$$v = \frac{\Gamma a}{2\pi(a^2 + y^2)} \quad (5)$$

Solving for velocity of transducer signals,

$$\frac{dy}{dt_{dwn}} = c - v \quad (6)$$

$$\frac{dy}{dt_{up}} = c + v \quad (7)$$

Integrating equations (6) and (7) and substituting equation (5) for  $v$  gives the following equations:

$$t_{up} = \int_{-P/2}^{P/2} \frac{1}{c + \frac{\Gamma a}{2\pi(a^2 + y^2)}} dy \quad (8)$$

$$t_{down} = \int_{-P/2}^{P/2} \frac{1}{c - \frac{\Gamma a}{2\pi(a^2 + y^2)}} dy \quad (9)$$

By evaluating these integrals and subtracting equation (8) from equation (9), the relationship shown in equation (10) is derived. The path length, distance between the transducer path and vortex core, and temperature of the air in the wind tunnel are known. The speed of sound during each test can be calculated from the measured temperature of air in the wind tunnel test section. The full derivation can be seen in Appendix D.

$$\Gamma = \frac{\Delta t \pi c^2}{2 \tan^{-1}\left(\frac{P}{2a}\right)} \quad (10)$$

### 2.3.3 Wing Tunnel Circulation Calibration Measurements

In order to account for any effects that the wind tunnel walls and ultrasonic transducer positioning may have had on the circulation of the flow through the tunnel, measurements were taken without the test wing in the tunnel. During this test, 20 data points of the  $\Delta t$  between the signal transit times was measured for a range of velocities between 0 and 20 m/s. Above the speed of 20 m/s the drift of the ultrasound signal became significant, and consistent data could not be recorded. The data from these measurements are shown in Figure 19 and Figure 20 with error bars representing one standard deviation.

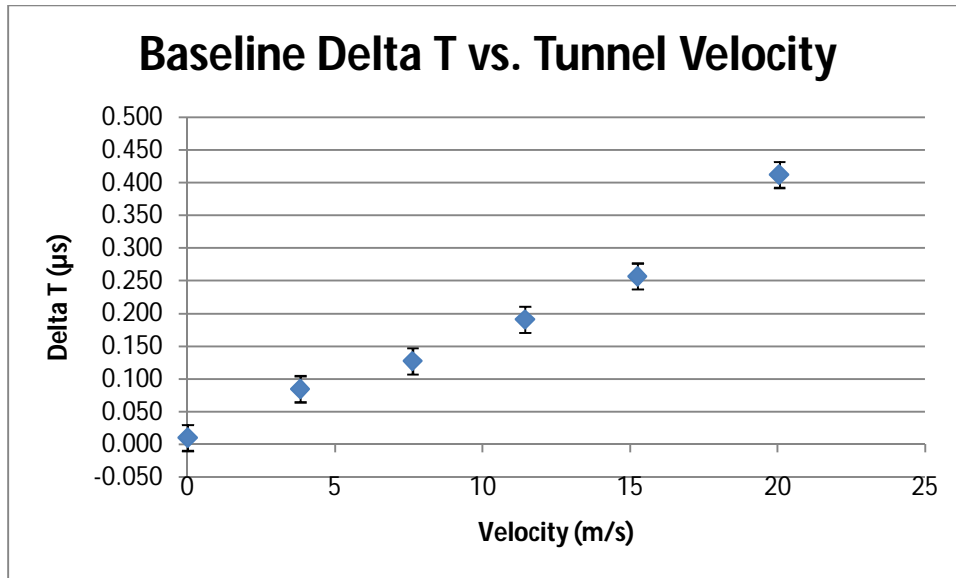


Figure 19: Wind Tunnel Calibration Data for Low AoA

In order to create stronger vortices without creating significant signal drift, a velocity of approximately 15 m/s was used for the low angle of attack series of tests. Therefore, a  $\Delta t$  of .257  $\mu\text{s}$  was subtracted from all transit time test data before it was used to calculate the circulation for a given individual. The adjusted circulation calculated was a result only of the test wing's presence in the tunnel.

The wind tunnel was then recalibrated before the high angle of attack series of tests. In this case, the signal drift became a more significant obstacle, and calibration data could only be collected for speeds up to 11.5 m/s, as shown in Figure 20. Therefore, all of the high angle of attack tests were conducted with a freestream velocity of 11.5 m/s, and a  $\Delta t$  of .149  $\mu\text{s}$  was subtracted from the delta t data prior to calculating the respective circulation values.



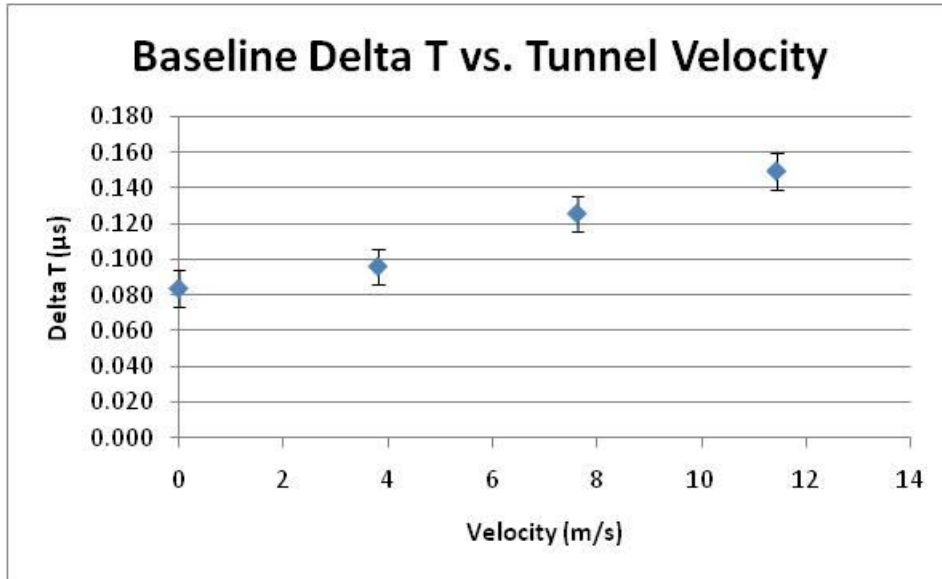


Figure 20: Wind Tunnel Calibration Data for High AoA

### 2.3.4 Circulation Measurement Repeatability

In order to determine the error in the circulation measurements, repeatability data was collected. Twelve circulation data points of a test wing were taken at  $69^\circ$  to  $70^\circ$  over the course of 3 days at a variety times during the day. As the circulation calculation does account for temperature, one trial data point was taken while the tunnel was at a temperature of  $79^\circ$ . The data points collected are shown with the resulting 95% confidence interval in Figure 21.

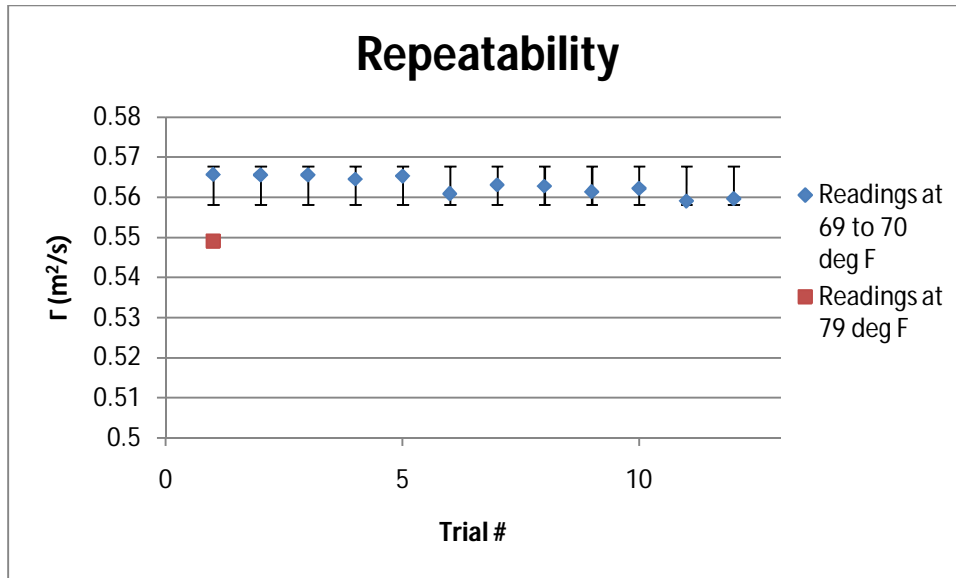


Figure 21: Circulation Repeatability Data

Figure 21 shows that although temperature should be accounted for in the calculation of the circulation, data taken when the tunnel is in the process of cooling fall significantly out of the 95%. From the constant temperature data, the standard deviation was found to be approximately .002  $\mu$ s. Therefore the 95% confidence interval is shown as  $\pm$ .004  $\mu$ s.

## 2.4 Genetic Algorithm

The genetic algorithm used in these experiments is computed using three MatLab programs. These programs are modified versions of those used in previous studies by Day [13] and Taylor [14] and can be found in Appendix E. These codes were able to randomly generate an initial population, read the fitness functions for each individual of a user specified generation out of a file "Population.xls", select parents using the roulette wheel selection method, place those parents into the next generation, create two children per two parent pair using multipoint crossover, and apply random mutations to those children.

In order to use these programs, the population sizes, chromosome characteristics, and mutation rates need to be set to the desired values. For this experiment, each feather could be set to  $\pm 20^\circ$  with

$\pm 1^\circ$  of accuracy. So, each gene in the chromosome will represent a position of between  $20^\circ$  and  $-20^\circ$  in  $5^\circ$  increments. This means that the chromosome is eight genes long and each gene can be represented by a number from  $-4 \leq k \leq 4$  representing one fifth of its feather angle, as shown in equation (11). Following the population sizing guidelines mentioned previously, this gives an initial population size of  $j=84$  individuals and a general population size of  $j=28$  individuals. A mutation rate of 20% was used following other studies [13,14]. Figure 22 outlines the steps of the genetic algorithm as applied specifically to the present work.

$$\theta_F = 5k \tag{11}$$

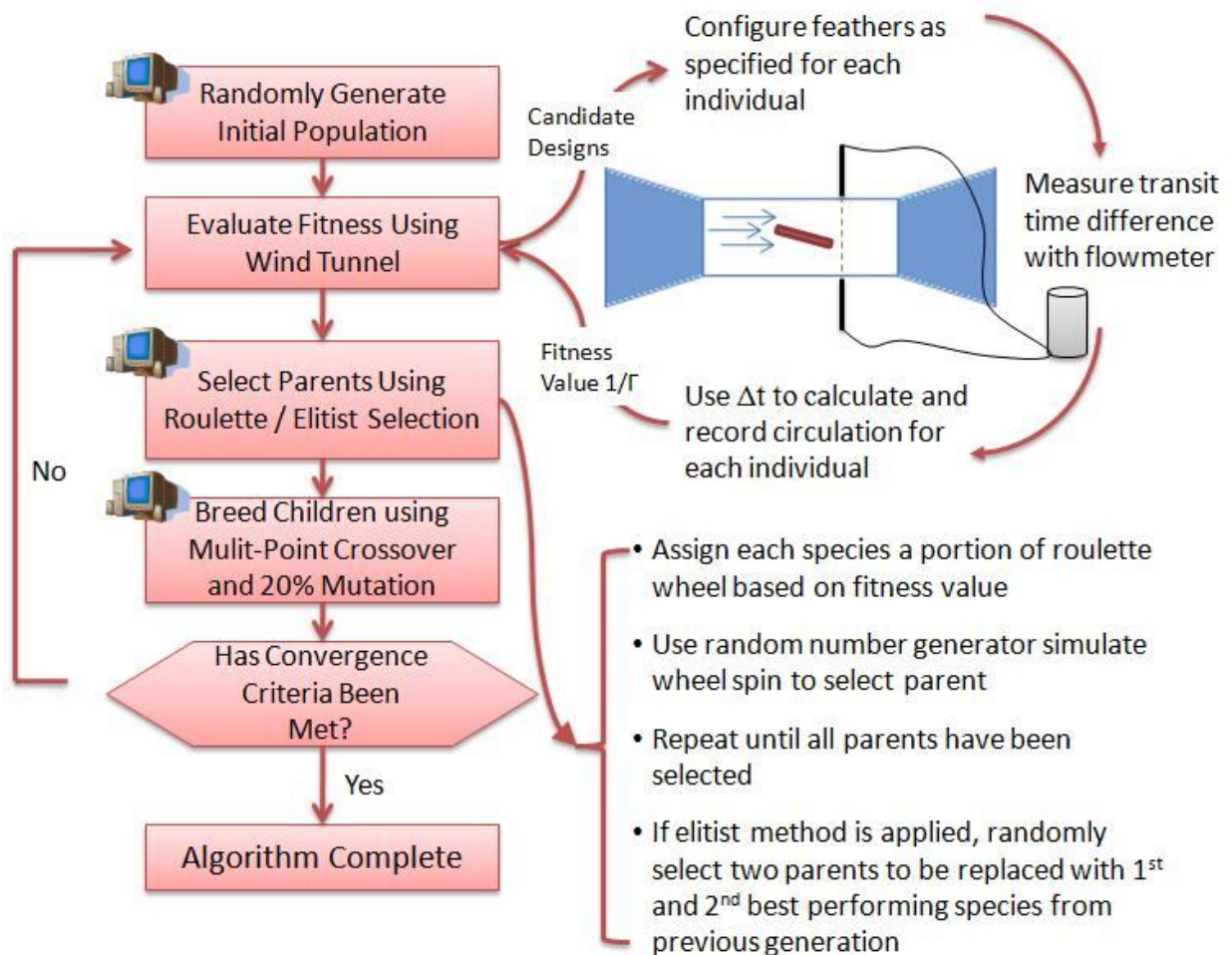


Figure 22: Genetic Algorithm Flowchart Applied to Current Work

For the first series of tests, the traditional roulette wheel style parent selection described in Section 1.2.1 was used. Cloning was allowed in this algorithm is a common characteristic of breeding used in genetic algorithms [20,21]. The inverse of the circulation measured for each individual was taken, which gave a traditional fitness value proportional to performance level. Then, the minimum value of those inverse circulation values was subtracted from each to create the fitness function. By subtracting the minimum value, the fitness functions became more distinct while only eliminating the worst design from the parent selection.

Due to the slow convergence rate of the first series of tests, the original selection roulette code was modified and an elitist parent selection was implemented in addition to the selection roulette as discussed in Section 1.2.1. In this case, the same fitness function was used. In order to keep the random pairing of parents intact, all 28 parents were selected using the roulette selection. Then 2 parents were randomly replaced with the first and second best performing design from the previous generation. These adapted codes can be seen in Appendix E.

## **2.5 Test Procedure**

The following steps were taken before each series of tests, low and high angle of attack. First, the tunnel calibration measurements discussed in Section 2.3.3 were taken so that the adjusted circulation data to follow could be calculated. Then, the test wing was inserted into the tunnel through a custom port with a cutout approximately the size of the wing. In order to block any air flow in and out of the tunnel, foam was placed in all gaps between the port and the wing surface. Foam was also placed above and below the plastic tip feathers to prevent flow through the test wing casing. Wood blocks were added to the opening of the casing external to the tunnel for additional flow blockage. A pitot probe was then used to check for any flow streams entering the tunnel through the wing port.

At the start of each new generation, or each day if testing occurred over the course of multiple days, a number of preparation steps were required. Based on the information gained through the repeatability testing discussed in Section 2.3.4, the steady state temperature condition of the tunnel was found to be important. Therefore, the tunnel was run at the test velocity of 15.25 m/s for a length of time to allow the temperature read out to reach 69° and remain there for a half hour before testing began. The angle of attack of the test wing was then verified to be the correct value, 6° for low angle of attack and 12° for high angle of attack using a digital inclinometer.

For each individual, the LabView Angle Sensor program discussed in Section 2.2 was used to measure and set the angle of each feather. For each feather, the lever arm attached to the potentiometer was moved in its track until the readout of the LabView program showed the desired feather angle within  $\pm 0.1^\circ$ . Then, the wing-nut was tightened to lock the feather into position while the readout remained at the desired value.

The circulation data for each individual was collected with the XGM868 flowmeter. The Skan/Measure mode was used due to the low tangential velocity component of the vortex. For each individual, twenty sequential  $\Delta t$  data points were recorded. The adjusted circulation values were then calculated and averaged as discussed in Section 2.3.

### 3. RESULTS

There were two separate evolutionary series run as a part of this experiment. In the first series, the genetic algorithm was applied to the test wing at a low angle of attack of  $6^\circ$  in a flow with a velocity of approximately 15 m/s. In the second series, the angle of attack was set to a high angle of  $12^\circ$  to provide comparable data for a varied flight condition. Due to the calibration difficulties discussed in Section 2.3.3, the freestream test velocity was reduced to 11.5 m/s. The data collected during these series of tests are examined in the following sections.

#### 3.1 Low Angle of Attack Series

The first series of tests was for a low angle of attack of  $6^\circ$ . This optimization was truncated after 17 generations due to its lack of progress towards a single optimum design. Figure 23 shows the progression of the minimum, maximum, average, and paternal average over the course of the 17 generations. Due to some unexpected fluctuations in circulation measurements of identical designs over different generations, during the latter part of the test series a baseline measurement, all feathers at  $0^\circ$ , was taken at the start of each generation (see Figure 23).

The error bars on the average circulation data series represent one standard deviation, which was calculated using the data in Section 2.3.4. This repeatability error applies to each series in Figure 23, but was removed from all but one series to improve the data clarity.

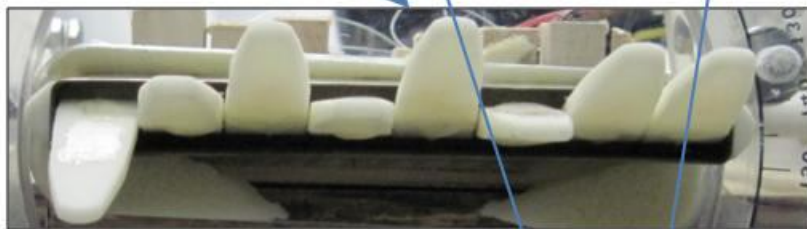
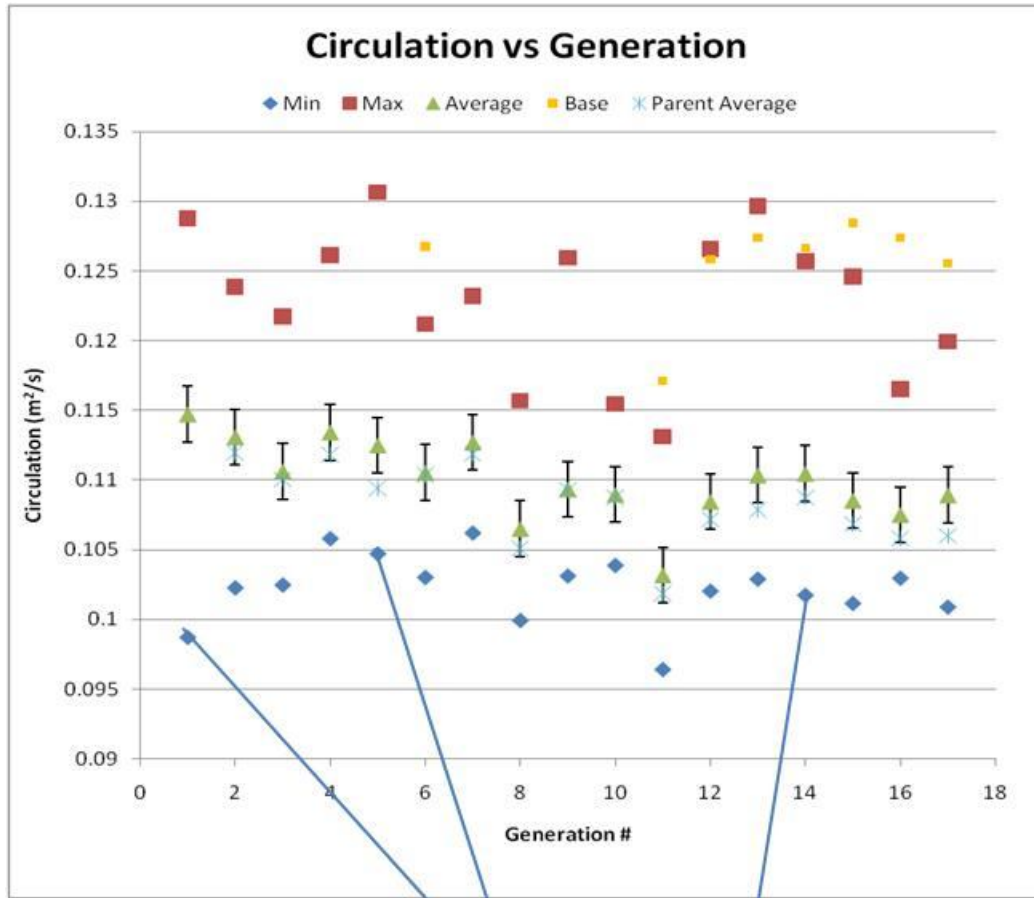


Figure 23: Low AoA Circulation Data

The wing images in the lower portion of Figure 23 provide a brief description of the evolution of the wing generated by the genetic algorithm over the course of the 17 generation test series. Even as early as the first generation, it is clear that an upturned trailing edge feather provides improved performance. Then, in the fifth generation, a specific trailing edge configuration evolved that would remain the dominant configuration throughout the duration of testing. Once the trailing edge pattern had evolved, a staggered angle leading edge geometry was generated in the 14<sup>th</sup> generation. This final design would achieve the highest fitness in each of the following three generations.

As expected, Figure 23 shows that the average circulation per generation decreases slightly over the course of the 17 generations. The parent average shows a similar trend. This average is a more accurate representation of the progression of the design over the generations as it does not include data points affected by mutations. This shows that as the generations evolve, they tend towards traits that create weaker tip vortices, which displays the effectiveness of the genetic algorithm. However, the minimum data series does not show the expected downward trend.

The maximum value series fluctuates greatly over the course of the 17 generations. This can be explained by the mutations incorporated into the genetic algorithm. An otherwise well-performing design could be greatly affected by a mutation. For instance, it was established that the geometry of the trailing edge is of particular importance. By generation 7, all designs with a negative angle at feather 8 were completely eradicated. After that point, a negative angle at feather 8 occurred only through mutation. All designs containing that mutation performed, at most, in the bottom 25<sup>th</sup> percentile of the generation.

The minimum value varied more than expected throughout the progression of the test series. There are a few factors that may have contributed to this outcome. First of all, the best design of the first generation failed to perform as well in subsequent generations. This led to an apparent step back



in the evolution of the geometry between generations 1 and 2. However, the increase in circulation was actually due to a difference in circulation values for two identical tip geometries. Second, there were a few similar cases of fluctuation in circulation readings of identical tip geometries over the course of the 17 generations. In particular, generation 8 and generation 11 stand out as being shifted downward in regards to all of the series trends. This is confirmed in the case of generation 11, where the baseline reading was taken and was significantly lower than typical generations. Because of these unexpected fluctuations, beginning at generation 11, a base reading of the geometry with all feathers positioned at  $0^\circ$  was recorded to provide a baseline comparison for the minimum data points. This was used to show which decreases in circulation were due to modified tip geometry opposed to test conditions.

Due to the small differences between the circulation measurements of similar individuals, the algorithm was terminated after generation 17. At this point, the generation had not converged to a single design, but a 20% decrease in vortex strength had been obtained. The most prominent design can be seen in Figure 24 and Figure 25. Although the genetic algorithm did not lead to complete convergence, 3 out of 8 traits (feather orientations) converged, and 5 out of 8 traits converged among 80% of the population. The progression of this convergence is detailed in the following sections.



Figure 24: Individual 1 -1 1 -1 4 -2 0 4

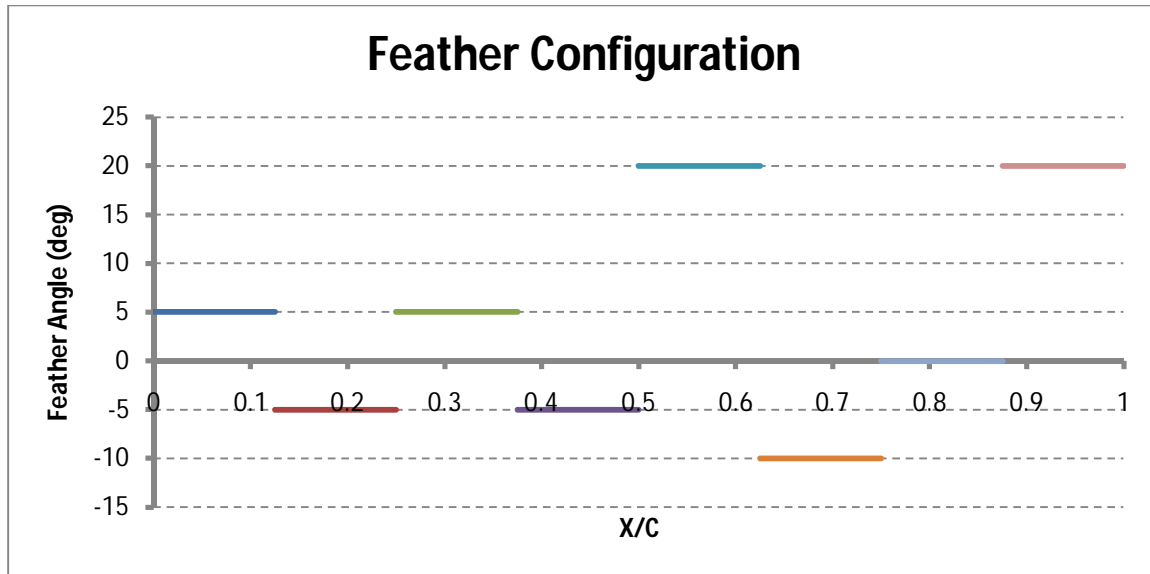


Figure 25: Individual 1 -1 1 -1 4 -2 0 4 Configuration

### 3.1.1 Early Generations

The first generation contained a variety of tip geometries with circulation values ranging from 0.099 to 0.129  $\text{m}^2/\text{s}$ . The best performing individuals were -4 2 4 1 4 0 4 4 and 4 0 0 2 -2 2 -1 3 with vortex strengths of 0.098704 and 0.102846  $\text{m}^2/\text{s}$ , respectively. Images of these individuals can be found in Figure 26 and Figure 27. Note that these individuals share the common trait of a high angle trailing edge feather. The poorest performing wing was individual 4 4 1 -4 3 0 -2 -4 with a vortex strength of 0.129  $\text{m}^2/\text{s}$  and a trailing edge feather position of  $-20^\circ$  (see Figure 28). The importance of the trailing edge feather trait can be seen in the full generation data set (see Table 5 in Appendix F). In generation one, all of the individuals in the lowest performing 42% of the generation had a trailing edge feather with a negative angle trait, and all of the individuals in the top 29% of the generation had positive angle traits at the trailing edge feather.



Figure 26: Individual -4 2 4 1 4 0 4 4

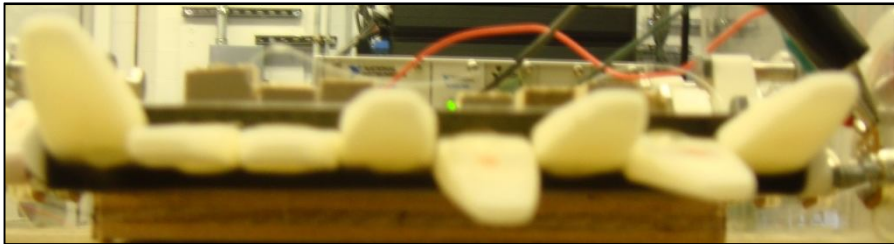


Figure 27: Individual 4 0 0 2 -2 2 -1 3

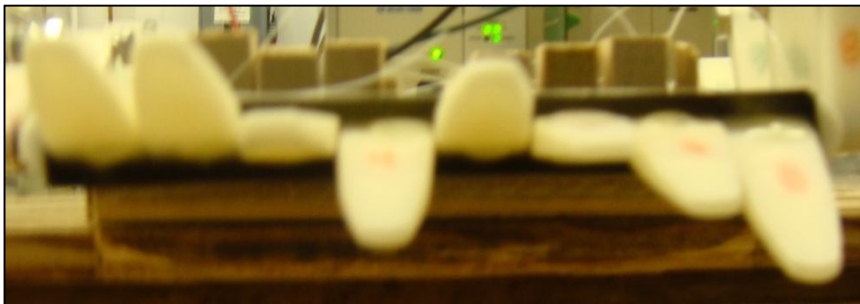


Figure 28: Individual 4 4 1 -4 3 0 -2 -4

In the second generation (see Table 6), the performances of the first and second best designs in the first generation were not attained. Although these were still among the best designs, they did not reach their previously low circulation values. A new individual (-4 2 4 1 4 3 4 4, see Figure 29) was bred in generation two, which became the best performing individual and remained so through generation three (see Table 7) . However, even with its high performance, this individual was not selected as a parent in the fourth generation (see Table 8).

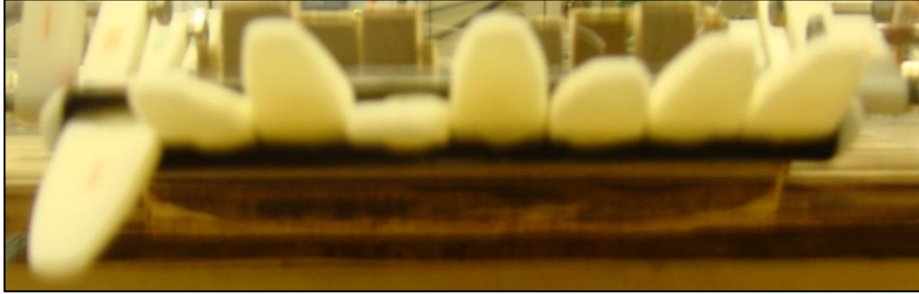


Figure 29: Individual -4 2 4 1 4 3 4 4

In the fourth generation, the new individual 3 -1 -2 -1 4 -2 0 4 (see Figure 30) was bred and became the best performing individual of the generation. Although the previous best individual was no longer present, the second best individual 4 0 0 2 -2 2 -1 3, which previously attained similarly low circulation values, was present in this generation. This shows that although the best performing individual in the fourth generation did not have the lowest circulation value of all of the previous tests, it was likely the best performing individual. This individual became more prominent and remained the best performing candidate design in the fifth generation (see Table 9).

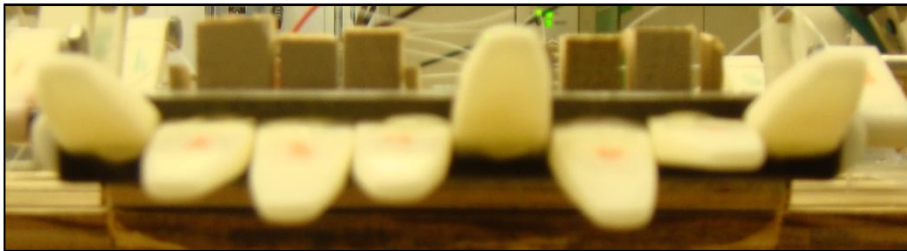


Figure 30: Individual 3 -1 -2 -1 4 -2 0 4

### 3.1.2 Middle Generations

In generation six (see Table 8), individual 3 -1 -2 -1 4 -2 0 4 was out-performed slightly by a similar candidate design, individual 3 -1 -2 -1 -2 3 0 4 (see Figure 31). However, the difference between the circulation measurements was only  $0.000097 \text{ m}^2/\text{s}$ , which is much smaller than the standard

deviation of .002. Individual 3 -1 -2 -1 -2 3 0 4 was not selected as a parent for generation seven (see Table 11), so it is unclear which individual was truly superior.

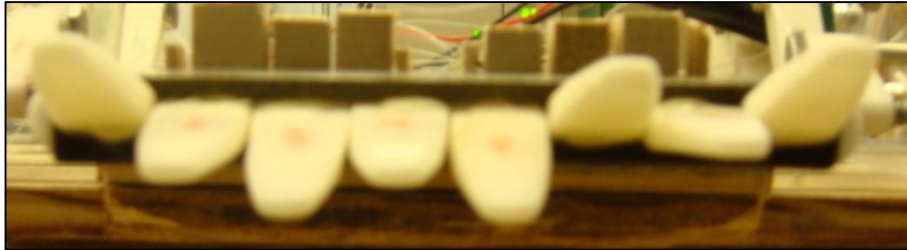


Figure 31: Individual 3 -1 -2 -1 -2 3 0 4

In generation seven, individual 3 -1 -2 -1 4 -2 0 4 was again outperformed slightly by a new candidate design, individual 1 -1 1 -1 4 -2 0 4 (see Figure 32). The improvement was only marginal at  $0.0003 \text{ m}^2/\text{s}$ , which is again much smaller than the standard deviation. In this case, both of these individuals were selected as parents for generation eight (see Table 12).



Figure 32: Individual 1 -1 1 -1 4 -2 0 4

In generation eight, both of these individuals were outperformed by the new individual 3 0 -2 2 -2 2 -1 4 (see Figure 33). This was by a more significant margin of  $0.0011 \text{ m}^2/\text{s}$ . However, this individual was not selected as a parent for generation nine (see Table 13).



Figure 33: Individual 3 0 -2 2 -2 2 -1 4

Generation nine brought the new individual 3 1 0 3 -2 -1 0 4 (see Figure 34). Although this individual remained one of the top designs, it was narrowly outperformed by the best design of generation seven 1 -1 1 -1 4 -2 0 4. After this point, a few other similar best geometries were also eliminated as they either were not selected as parents or failed to uphold their previously low circulation values. Although there were some fluctuation in the best design, it is important to note the similar trailing edge geometries between all of these individuals.



Figure 34: Individual 3 1 0 3 -2 -1 0 4

### 3.1.3 Final Generations

By generation ten (see Table 14), the best performing candidate design was once again individual 1 -1 1 -1 4 -2 0 4 followed closely by the best performer of generation nine, individual 3 1 0 3 -2 -1 0 4. From generation ten through the remainder of the series of tests, all of the best performing individual contained the identical trailing edge geometry of 4 -2 0 4.

In generation thirteen (see Table 17), the new design 1 0 -2 2 4 -2 0 4 (see Figure 35) was created and became the best performing individual. As this was only by the slim margin of 0.00042

m<sup>2</sup>/s, in the subsequent generations, the previously best geometry of 1 -1 1 -1 4 -2 0 4 regained its status as the best performing design and maintained that status throughout the remainder of the generations.

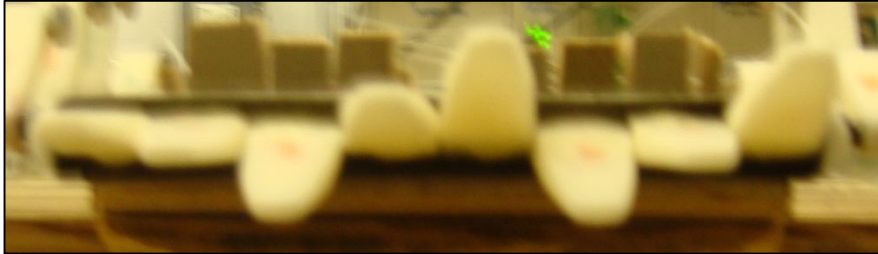


Figure 35: Individual 1 0 -2 2 4 -2 0 4

Although generation seventeen (see Table 21 in Appendix F) did not converge to this individual, this was most likely due to the small separation between the fitness functions of this individual and other similar individuals. The measurements taken for generation seventeen were used to generate an eighteenth generation. Although measurements were not taken for the individuals of this generation, it does illustrate the partial convergence at this point as shown below in Table 2.

Table 2: Low AoA Generation #18

Chromosome #	Configuration Number							
	Feather 1	Feather 2	Feather 3	Feather 4	Feather 5	Feather 6	Feather 7	Feather 8
1	1	-1	-4	-1	4	-2	0	4
2	3	-1	1	-1	4	-2	0	4
3	1	-1	0	-1	4	-3	0	4
4	-2	-1	1	-1	4	-1	0	4
5	1	-1	1	-1	4	-2	0	4
6	1	-1	1	-1	4	-2	0	4
7	3	-1	1	-1	4	-2	0	4
8	3	-1	1	-1	4	-2	0	4
9	3	3	1	-1	4	-2	0	4
10	1	-1	-4	-1	4	-2	0	4
11	3	-1	0	-1	2	-3	0	4
12	3	3	1	-1	4	-2	0	4

13	3	-1	1	-1	4	-2	0	4
14	3	-1	1	-1	4	-2	0	4
15	3	-1	1	-1	4	-2	0	3
16	3	-1	-1	-1	4	-2	0	4
17	1	-1	2	-1	4	-3	0	-1
18	1	0	0	4	4	-1	0	4
19	1	-1	1	-1	1	-2	0	-2
20	1	-1	1	-3	4	-2	0	4
21	3	-1	2	-1	4	-2	-1	4
22	3	-1	0	-1	4	-2	-3	4
23	1	-2	1	-1	4	-2	0	4
24	3	3	-4	-1	4	-2	0	4
25	3	3	0	4	4	-2	0	0
26	3	3	1	-1	4	-3	0	4
27	3	-1	-3	-1	4	-2	0	4
28	3	-1	1	-1	4	0	0	4

Table 2 shows that although the algorithm did not reach complete convergence (a parent population consisting of identical individuals), among the fourteen parents selected from generation seventeen to progress to generation eighteen, there was some convergence. Feathers four, seven, and eight reached complete convergence. Feather five reached almost complete convergence, with only one parent out of the fourteen having a differing feather angle. While having only a 79% convergence to the feather angle of the dominant individual, feather six was almost completely converged in that all of the differing feather angles were only 5° from the converged value of -10°. This partial convergence as well as the slow overall evolution of the wing means that it is likely that small angle changes do not create significant changes in vortex strength depending on the feather position along the chord line.

### 3.1.4 Discussion of Low AoA Results

The most prominent design at the end of the low angle of attack series of tests (individual 1 -1 1 -1 4 -2 0 4) has many specific characteristics that are most likely linked to its successful performance. The leading edge consists of small feather angles (5°) with alternating positive and negative directions.



There is a large split between the feather angles in the mid-section (between feathers 4 and 5). This is followed by an upswept trailing edge from feather 6 to feather 8. Each of these characteristics can be linked to aerodynamic theory. Although the time constraints of this project did not allow for flow visualization to be completed, the following section discusses some possible explanations for the performance improvements achieved by this tip geometry.

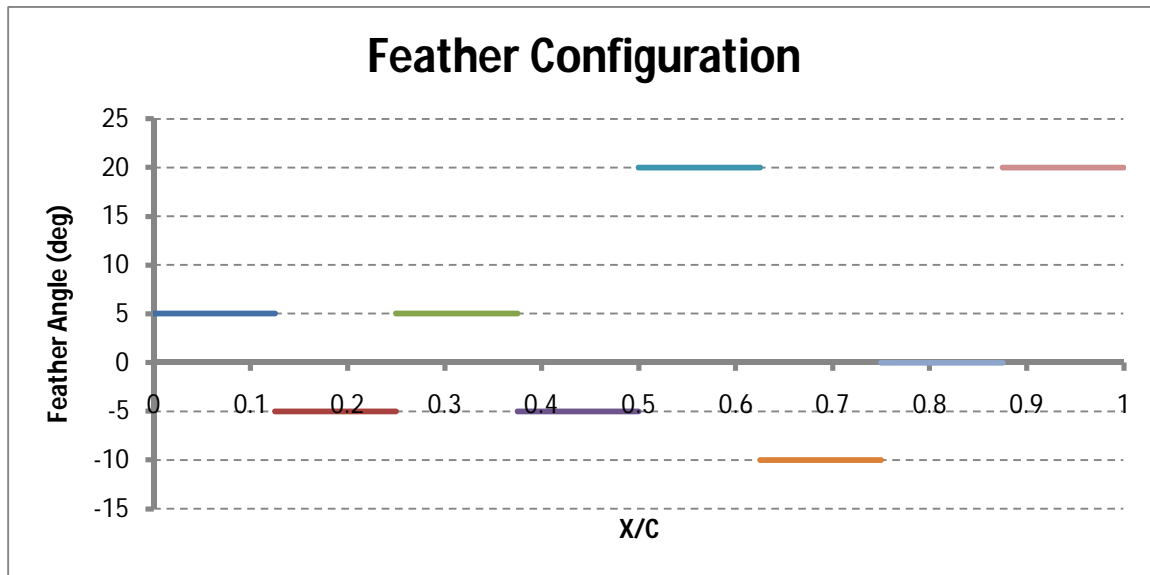


Figure 36: Prominent Configuration (1 -1 1 -1 4 -2 0 4)

The trailing edge geometry appears to have the most prominent effect on vortex strength due to the early elimination of downward angles in this region and the early convergence of all parent designs to a single feather angle at feather 8. This is consistent with theory in that the trailing edge is the location of the vortex formation. This region consists primarily of upswept tip geometry similar to the classical single winglet (see Figure 37). The classical winglet design is effective because although the vortex is not eliminated, it is weakened as well as displaced [26,27, 37].



Figure 37: Winglet Designed by Steve Willits from Ref [35]

Figure 38 shows a flow visualization experiment comparing MAV tip vortices with and without winglets. These images confirm the classical theory in that the vortex is more diffuse in image with the winglet (right). It is also shown that the vortex core location is elevated by the winglet. This displacement moves the airflow so that it has less of an effect on the MAV wing aerodynamics. This is likely the cause of the decrease in vortex strength created by the upswept trailing edge of individual 1 -1 1-1 4 -2 0 4.

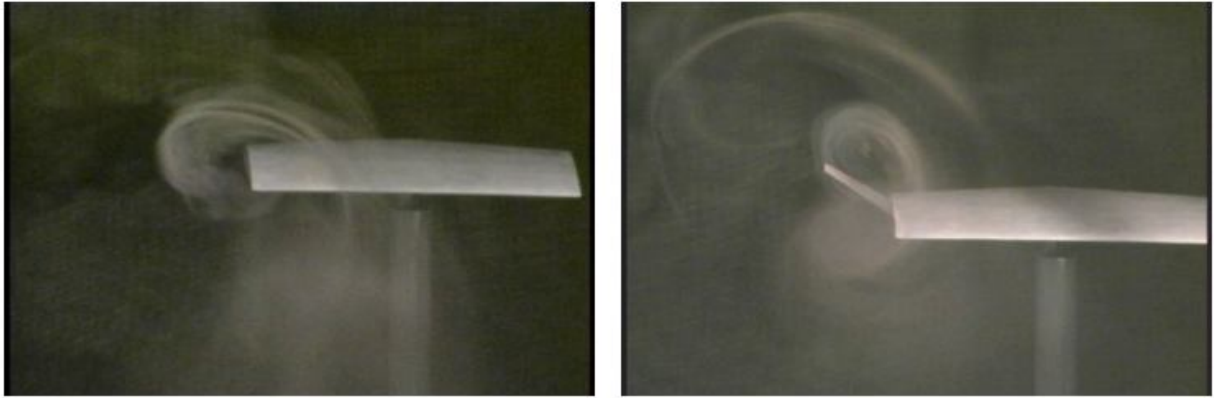


Figure 38: Standard Winglet Flow Visualization from Ref [36]

The leading edge feathers have only slight alternating feather angles of the smallest increment allowable in this experiment ( $\pm 5^\circ$ ). This alternating pattern supports the theory that spreading the tip vortices leads to decreased global circulation and, therefore, decreased induced drag. Vertical and horizontal spreading of feathers has been shown to spread the vortex [7]. It then follows that, although the feather configuration angles on the leading edge are small, the alternating pattern creates ample vertical spreading, which results in vortex spreading and a decrease in global circulation.

The large split in feather angles mid-wing is not distinctly reminiscent of either traditional winglet design or bird wings. However, due to the fact that there were similar designs that were outperformed by this individual, it is clear that the split does serve some purpose. For instance, in generation 16, individual 1 -1 1 -1 -1 -2 0 4 (see Figure 39) had a circulation value of  $.107317 \text{ m}^2/\text{s}$  in comparison to that of the prominent individual (1 -1 1 -1 4 -2 0 4), which was  $.102972 \text{ m}^2/\text{s}$ . The only difference between these two designs is feather 5, which means that the high feather angle at this point has a significant effect on the circulation associated with individual 1 -1 1 -1 4 -2 0 4. The split may play a similar, but more dramatic, role as the small separations between the leading edge feathers. It is possible that the split is present to further diffuse the vortex.

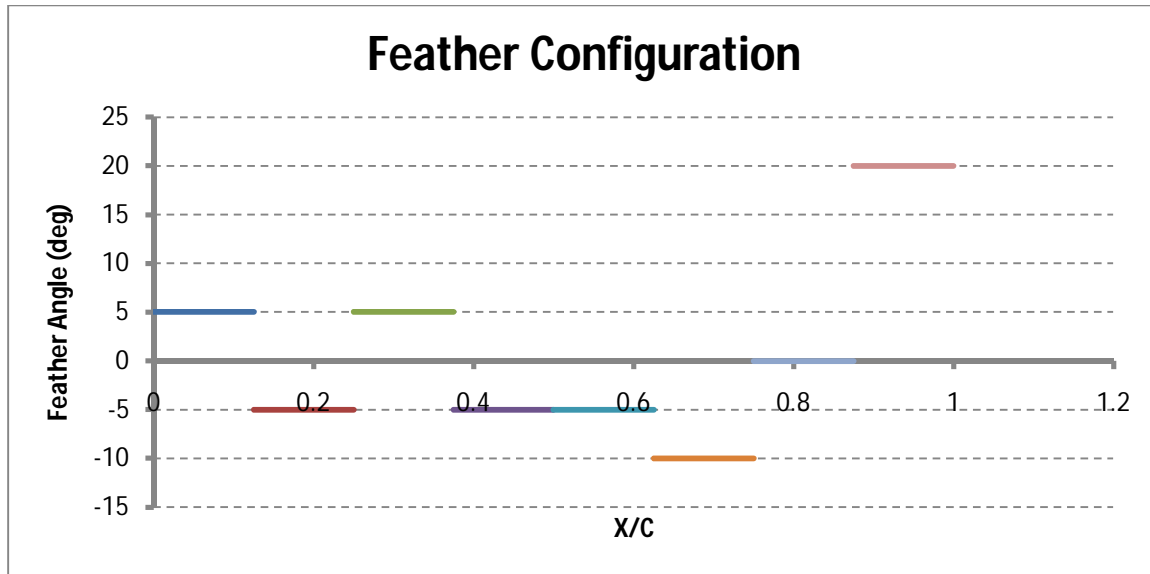


Figure 39: Individual 1 -1 1 -1 -1 -2 0 4 Configuration

In the case of this test series, seventeen generations of testing were completed in order to establish the dominant design. This required a total of 532 designs to be measured. In comparison, the entire solutions space consisted of  $8^9$  differing designs. This means that using the genetic algorithm allowed only 0.0004% of the solution space to be tested.

### 3.2 High Angle of Attack Series

A second series of tests was completed in order to explore the effects of increased angle of attack on vortex strength. For this series of tests, the angle of attack was set to  $12^\circ$  for each circulation measurement. As previously discussed, due to inconsistent readings at a velocity of 15.25 m/s, the freestream velocity was decreased to 11.5 m/s. Because of the fluctuations in circulation measurements of identical individuals during different generations encountered during the low angle of attack series of tests, a baseline reading of the wing with all feathers at  $0^\circ$  (see Figure 40) was taken at the start of each generation of tests. Data was only collected at times when the baseline reading remained in the range of the expected repeatability error. This allowed for a more accurate comparison of generational

statistics. The parent selection method was also modified to an elitist method as discussed in Section 2.4 to speed convergence.

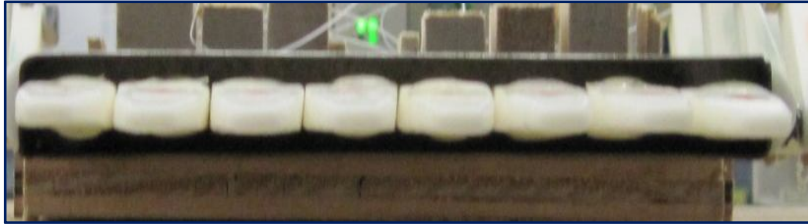


Figure 40: Individual 0000000

For this series of tests, the progression of the minimum, maximum, average, and paternal average over the course of 12 generations is shown in Figure 41. In this series of tests, each of the data values shown in Figure 41 follows the expected downward trend in circulation value. As in the low angle of attack plot, one standard deviation of error, as established in Section 2.3.4, is shown on the average value series. This error applies to all data points, but is shown on one series for clarity.

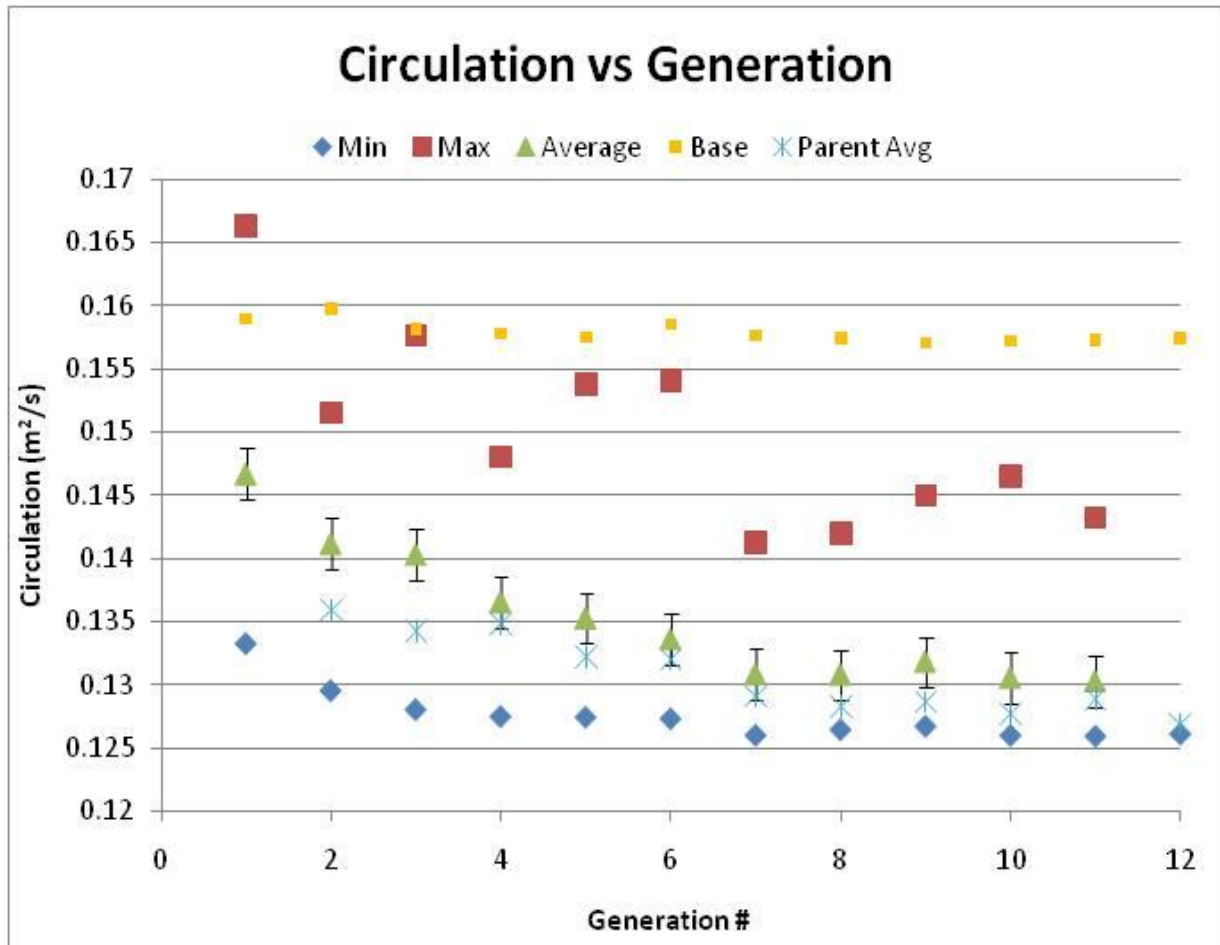


Figure 41: High AoA Circulation Data

The downward trend is particularly clear in the case of the progression of average circulation by generation. The average value decreases consistently over the course of the first 7 generations. At that point the average plateaus for the remainder of the series of tests. The downward trend represents the increasing fitness of the generation as a whole over time. This is important because although there are mutations, the average value shows that as a group, the designs are evolving towards better performance. At the point of plateau (generation 7), there is little room for improvement, and the mutations keep the average value from converging with the minimum value.

The maximum value series decreases over time overall, but it does contain large fluctuations throughout the generations. This is explained by the effect of mutations on otherwise well performing

species. Even after a system has reached complete convergence, there will be random mutations that are capable of creating maximum circulation values that vary greatly from that of the best performing design.

The paternal average decreases consistently for the first 8 generations and then fluctuates slightly while remaining very close to the minimum value for the last 4 generations. The parent average has a trend similar to that of the average. This is to be expected as the parents represent half of the individuals in the generation, and the other half of the individuals shares many common traits with the parents with the exception of mutations and differences in circulation resulting from recombination of parental traits.

The minimum value decreases significantly over the first 3 generations before settling at a constant value given by the same design for the last 9 generations. This design (individual -2 -4 -4 1 -4 4 1 3) was the most prominent individual of generation 12 as well as the best performing throughout the entirety of testing and can be seen in Figure 42 and Figure 43. This design provided a decrease of approximately 20% from the baseline circulation of the wing with each feather at position of 0°. This is the same decrease produced by the best performing design in the low angle of attack series of tests.

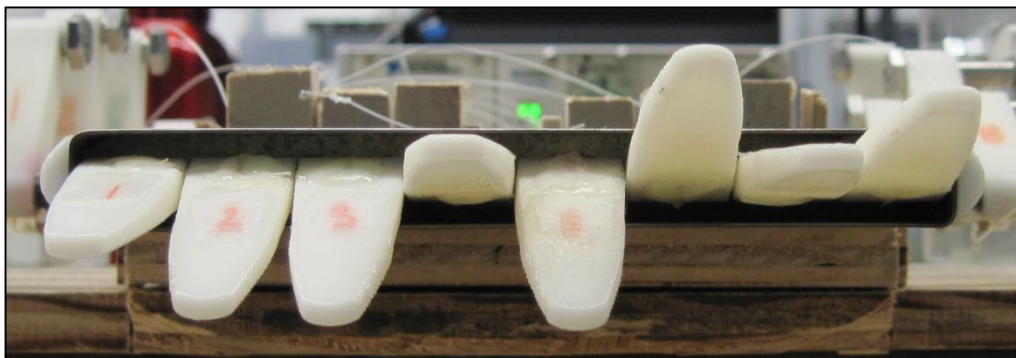


Figure 42: Individual -2 -4 -4 1 -4 4 1 3

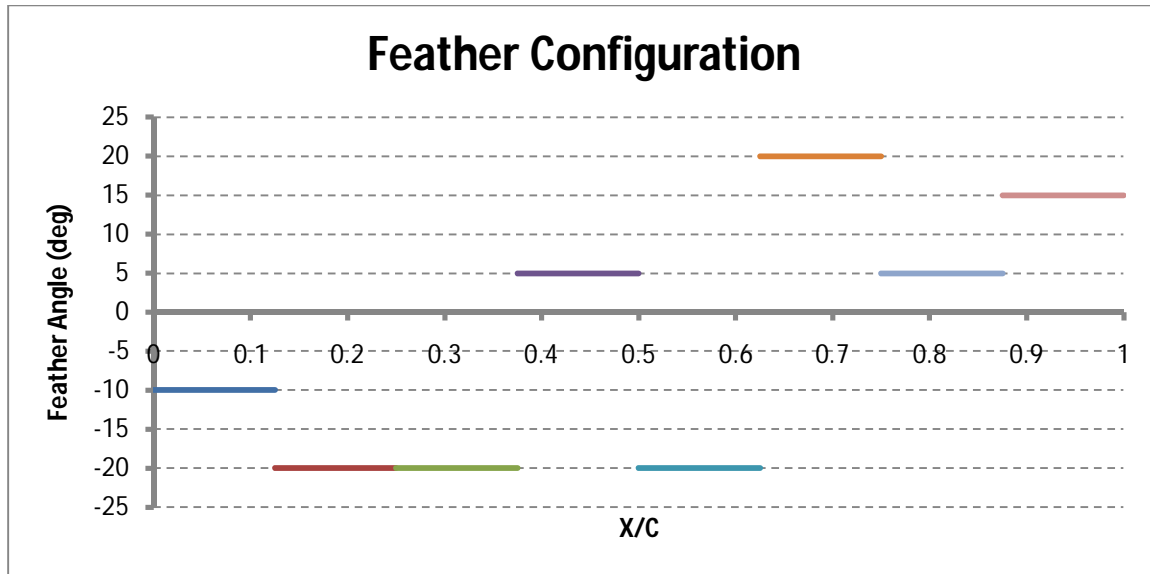


Figure 43: Individual -2 -4 -4 1 -4 4 1 3 Configuration

There are a few differences between the low and high angle of attack series that may account for the more predictable trends in the high angle of attack tests. Firstly, the baseline remained consistent as shown by the horizontal “Base” data set in Figure 41. This allowed for cleaner visual trends with reduced fluctuations due to flowmeter output throughout the rest of the data sets and direct comparison of data points throughout the 12 generations. Secondly, in this set of tests, an elitist selection method was used in conjunction with the traditional roulette wheel selection method, which ensured that the 2 best performing individuals from each generation were selected as parents for the next generation. This eliminated the increases in the minimum value data series trend due to elimination of candidate individuals.

Because the high angle of attack test exhibited more predictable trends, convergence was more distinct. By the 12<sup>th</sup> generation, the 78.5% of the parent population had converged to the best performing design (individual 2 -4 -4 1 -4 4 1 3). The entire population converged to 6 of the 8 feather positions of the final design. Due to the very similar circulation values of other individuals selected as



parents, complete convergence was unlikely, so the test was truncated here. Further details of the progression and termination of this convergence is detailed in the following sections.

### 3.2.1 Early Generations

In the first generation, there was a wide range of circulation values produced by the 84 randomly generated individuals (see Table 22). This was the only generation in which there were designs that performed worse than the base wing (individual 0 0 0 0 0 0 0). Among these designs, the best performing designs were individual 3 -2 -3 4 -4 3 4 4 and individual 0 -3 0 4 -3 4 2 3 (see Figure 44 and Figure 45) with circulation values of 0.133 m<sup>2</sup>/s. The worst performing design was individual 4 3 -2 2 -3 -3 -4 -4 with a circulation value of 0.166 m<sup>2</sup>/s (see Figure 46). Although this was early in the series of tests, it illustrated that the trailing edge is a key characteristic and that a downturned feather reduces performance value. This is supported by the fact that in the first generation, all of the designs in the top 29<sup>th</sup> performance percentile had an upturned feather 8, while all those in the bottom 14<sup>th</sup> percentile have a downturned feather 8.



Figure 44: Individual 3 -2 -3 4 -4 3 4 4

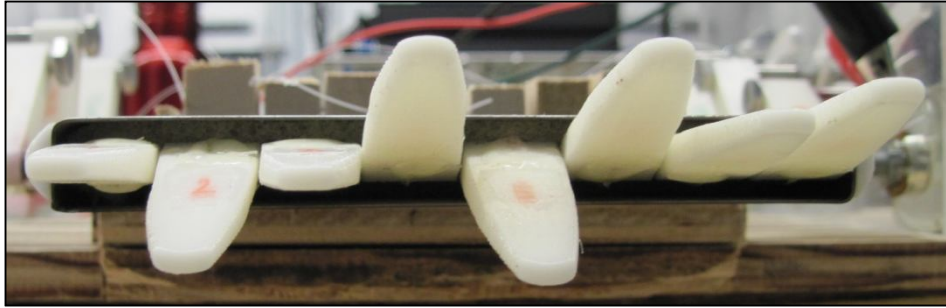


Figure 45: Individual 0 -3 0 4 -3 4 2 3

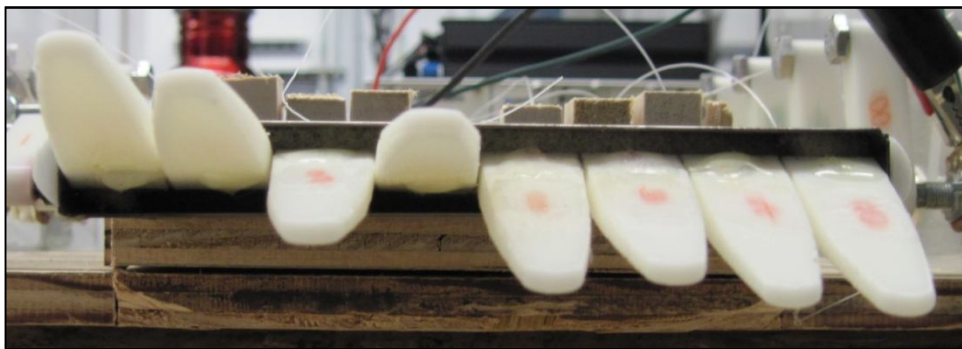


Figure 46: Individual 4 3 -2 2 -3 -3 -4 -4

In the second generation (see Table 23), individual 3 -2 -3 4 -4 3 4 4 remained the top performing species. This design performed slightly better than in the previous generation. However, a number of designs were bred that outperformed the second best design of the previous generation (individual 0 -3 0 4 -3 4 2 3). The second best design then became individual -2 -4 1 -3 -4 4 1 3 (see Figure 47).

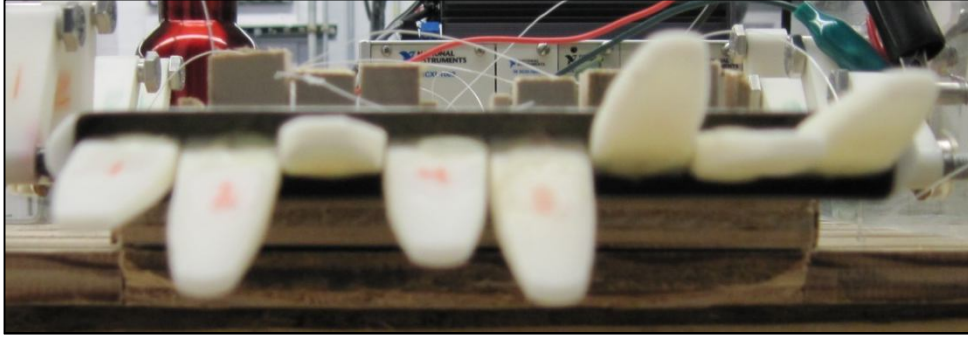


Figure 47: Individual -2 -4 1 -3 -4 4 1 3

The third generation brought a new best performing design, individual -2 -4 -4 1 -4 4 1 3 (see Figure 48), which had many traits in common with the second best design in generation 2. The secondary design from generation 2 (individual -2 -4 1 -3 -4 4 1 3) remained the second best performing species of generation 3, while also becoming a more prominent design accounting for 10% of the entire generation (see Table 24).

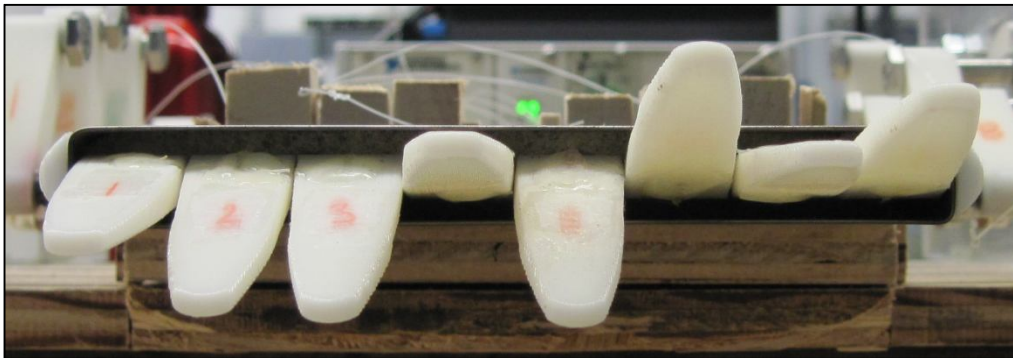


Figure 48: Individual -2 -4 -4 1 -4 4 1 3

### 3.2.2 Middle Generations

In generations 4 and 5, the two best performing designs remained the same as those from generation 3. However, they both grew in number. Because, at this point, there were multiple individuals with the configuration -2 -4 -4 1 -4 4 1 3, which consistently outperformed all other designs,

this design now held the two top ranking positions in the generation. This guaranteed it two places in the following generations.

By the 6<sup>th</sup> generation, the top seven performing individuals were all identical to individual -2 -4 -4 1 -4 4 1 3. Breeding new individuals was still providing some progress. A new design, individual -2 -3 1 -3 2 4 3 3, became the second best design (see Figure 49). However, no new individuals were able to outperform the prominent individual. This would remain true through all of the remaining generations.

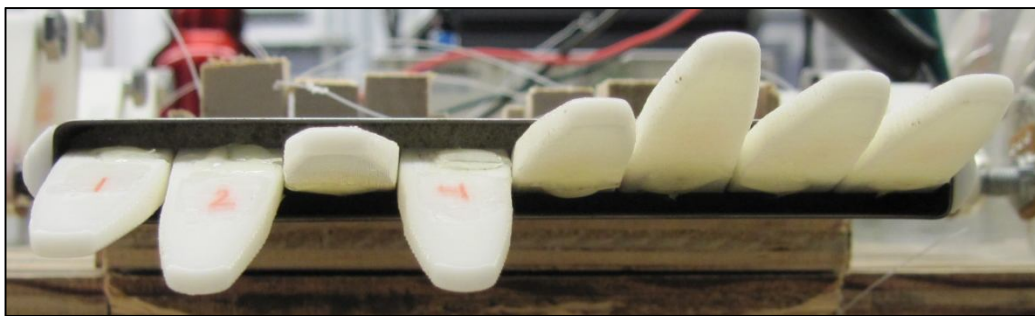


**Figure 49: Individual -2 -3 1 -3 2 4 3 3**

Although by the 7<sup>th</sup> generation, the best performing design remained constant, new improved designs were still being bred. For instance in the 7<sup>th</sup> generation (see Table 27), there were three individuals that performed within the range of circulation values collected for the many duplicate best performing individuals. These three designs (individuals -2 -4 -4 1 -4 -2 -1 3, -2 -2 -4 1 -4 -2 -3 3, and -2 -4 -4 -1 -4 0 1 3) are shown in Figure 50, Figure 51, and Figure 52, respectively. Although these individuals do not change the best performing design, introducing better performing individuals to the generation increases its overall fitness and improves the chance for better future pairing.

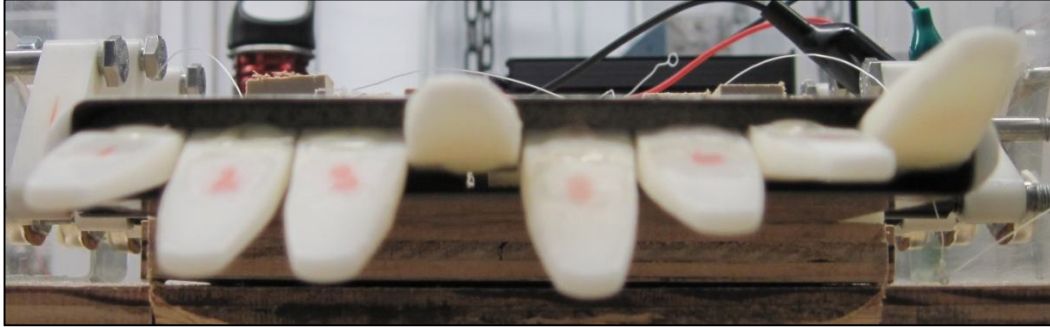


Figure 50: Individual -2 -4 -4 1 -4 -2 -1 3

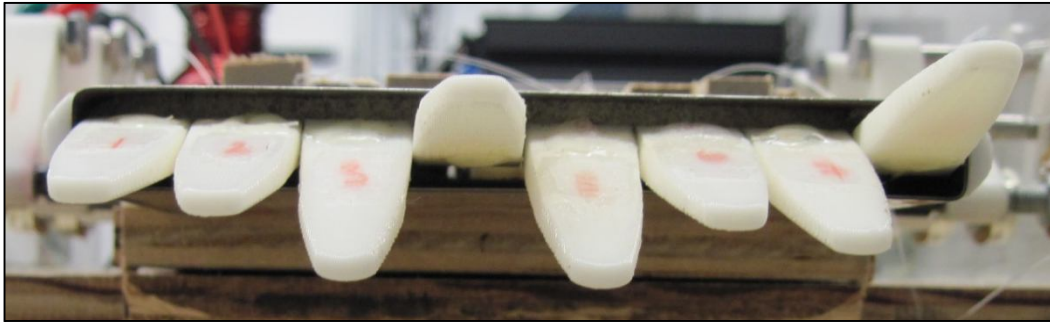


Figure 51: Individual -2 -2 -4 1 -4 -2 -3 3

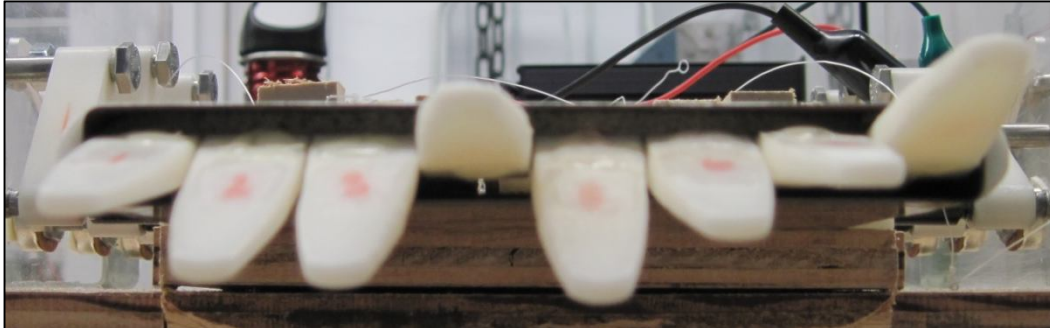


Figure 52: Individual -2 -4 -4 -1 -4 0 1 3

At this point, the progress of the algorithm came in the form of improving the average fitness of the entire population and the parents selected from each of those generations. By generation 7, the average circulation value of the generation was 10% lower than the average circulation value of

generation 1. As illustrated by Figure 41, this decrease was obtained consistently over the course of the 7 generations.

### 3.2.3 Final Generations

As discussed in the previous section, the design associated with the minimum circulation value did not change for the remainder of the 12 generations. However, there were new comparable designs that were bred in the later generations. Some designs of note are individual -2 -4 -4 1 -4 4 2 3 and individual -2 -4 -4 1 -4 4 3 3 (see Figure 53 and Figure 54). These designs were the only individuals in generations 8 through 12 to perform in the top 25 % of the generation besides the previously established best performing individual. It is important to note how similar these designs are to individual -2 -4 -4 1 -4 4 1 3. The only difference is a slight variation in the position of feather 7. The circulation values were well within the range of error, so it is unclear whether there is any significant difference between these similar designs.

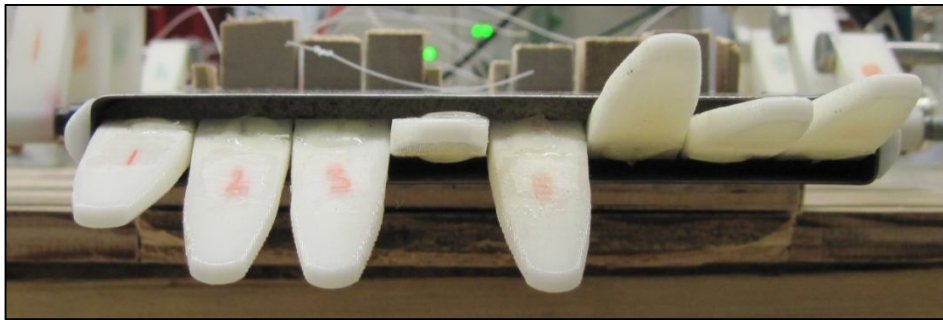


Figure 53: Individual -2 -4 -4 1 -4 4 2 3

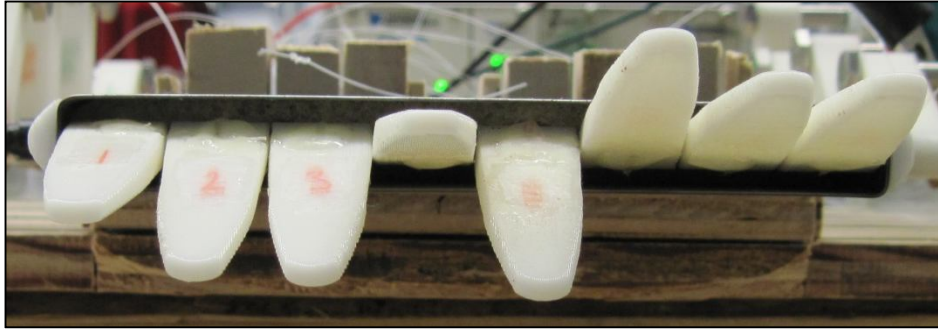


Figure 54: Individual -2 -4 -4 1 -4 4 3 3

In generations 8 through 12, the averages and paternal averages reached a plateau similar to that of the already established minimum value. This was the first trend that suggested that the algorithm was reaching convergence. Although more than half of the parents selected at this point were identical to the best performing individual, this only represented partial convergence. By generation 10, over 70% of the parent population had converged to the best performing individual. However, in order to ensure convergence, the algorithm was continued to allow the mutation function ample time to avoid a local optimum.

By the 12<sup>th</sup> generation, the selected parents had met multiple convergence criteria. Because of the effects of mutation, only the parents were examined for convergence. At this point, 79% of the parents selected were identical to individual -2 -4 -4 1 -4 4 1 3. The remaining individuals were very similar and shared 6 of 8 feather positions with the dominant individual (see Table 3).

Table 3: High AoA Generation #12

Chromosome #	Configuration Number							
	Feather 1	Feather 2	Feather 3	Feather 4	Feather 5	Feather 6	Feather 7	Feather 8
1	-2	-4	-4	1	-4	4	1	3
2	-2	-4	-4	1	-4	4	3	3
3	-2	-4	-4	1	-4	4	1	3
4	-2	-4	-4	1	-4	4	1	3
5	-2	-4	-4	1	-4	4	1	3

6	-2	-4	-4	1	-4	4	1	3
7	-2	-4	-4	1	-4	-1	3	3
8	-2	-4	-4	1	-4	4	1	3
9	-2	-4	-4	1	-4	4	1	3
10	-2	-4	-4	1	-4	4	1	3
11	-2	-4	-4	1	-4	4	2	3
12	-2	-4	-4	1	-4	4	1	3
13	-2	-4	-4	1	-4	4	1	3
14	-2	-4	-4	1	-4	4	1	3
15	4	-4	-4	1	-4	4	-3	3
16	-3	-4	-4	1	-4	4	3	3
17	-2	-4	-4	1	4	4	1	3
18	-3	3	-4	1	4	4	1	3
19	-2	-4	-4	1	-4	4	1	3
20	-2	-4	-4	1	-4	4	1	3
21	-2	-4	-4	1	4	1	3	3
22	-2	-4	-4	1	4	-1	0	3
23	-2	-4	-4	1	-4	4	-4	3
24	-2	3	-4	-1	-4	-1	1	3
25	-2	-4	-4	1	-4	4	3	3
26	-2	-4	-4	1	-4	4	1	3
27	-2	-4	-4	1	-4	4	1	3
28	-2	-4	-4	1	-4	4	1	3

The second convergence criterion was the proximity of the paternal average to the minimum value. The average circulation of the parents of the 12<sup>th</sup> generation was 0.127 m<sup>2</sup>/s. The individual minimum value for this generation was 0.126 m<sup>2</sup>/s. Given the repeatability error of ±0.004, which was established in Section 2.3.4, the paternal average value was well within the error range of the minimum value. This shows that, although the selected parent population did not completely converge to the dominant feather configuration, the circulation value did converge. Therefore, the remaining individuals were so similar to the dominant individual that their respective circulation values were not distinct enough to be eliminated from the population. Consequently, it is unlikely that further convergence would be attained through continued testing.



### 3.2.4 Discussion of High AoA Results

As discussed in the previous sections, the best performing design generated by the genetic algorithm at the high angle of attack of  $12^\circ$  and the decreased velocity of 11.5 m/s was individual -2 -4 -4 1 -4 4 1 3. As shown in Figure 55, this design consists of downswept leading edge, a staggered mid-section including a large vertical spread between feathers 5 and 6, and an upturned trailing edge. Due to the timescale of the present work, flow visualization was not available to provide definitive explanations for why these traits are beneficial, but some theory is offered as a possible explanation in the following section.

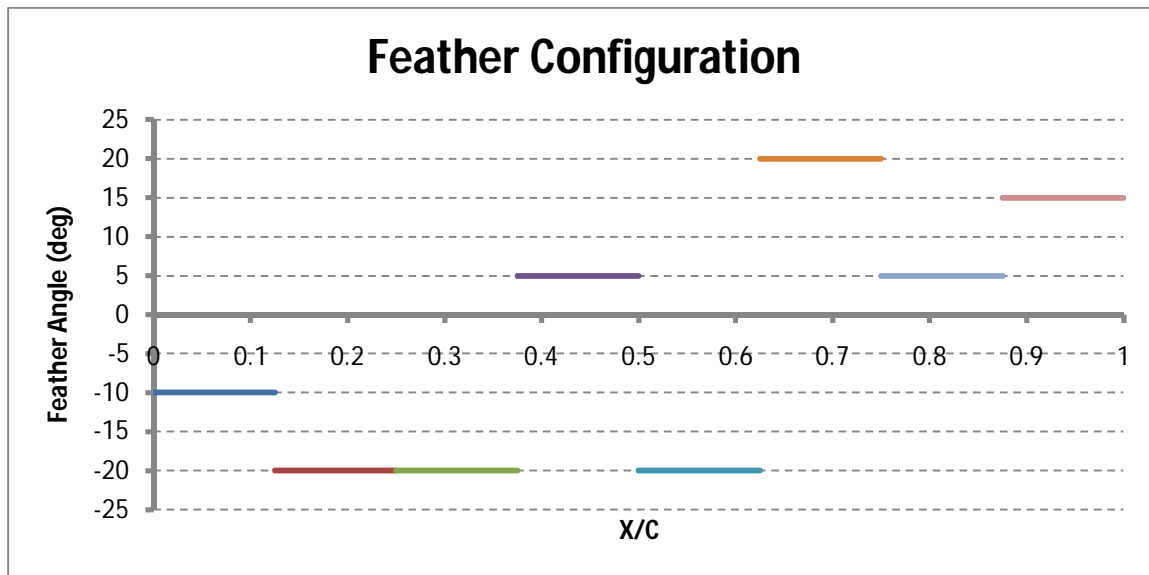


Figure 55: Individual -2 -4 -4 1 -4 4 1 3 Configuration

The trailing edge proved to be a key component in the high angle of attack series of tests as well as the previously discussed low angle of attack series, which is to be expected as it is the location of the vortex formation. Similarly, downturned trailing edge feathers on an otherwise successful design were shown to decrease the fitness of the individual. The particular configuration seemed to be less important than the overall high feather angle. This is established by the existence of similar geometries (individual -2 -4 -4 1 -4 4 2 3 and individual -2 -4 -4 1 -4 4 3 3) with similar fitness in the final generations

as shown in Figure 56 and Figure 57. As shown in this example, a small difference in feather angle does not provide a significant difference in circulation. For this reason it is likely that the intervals of angle settings every 5° was sufficient resolution. The upturned trailing edge feathers present in all of these designs is similar to that of the trailing edge in the dominant design from the low angle of attack series of tests and the traditional winglet discussed in Section 3.1.4. Consequently the same theory of a displaced and diffused vortex at the tip of the trailing edge can be used to explain this feature.

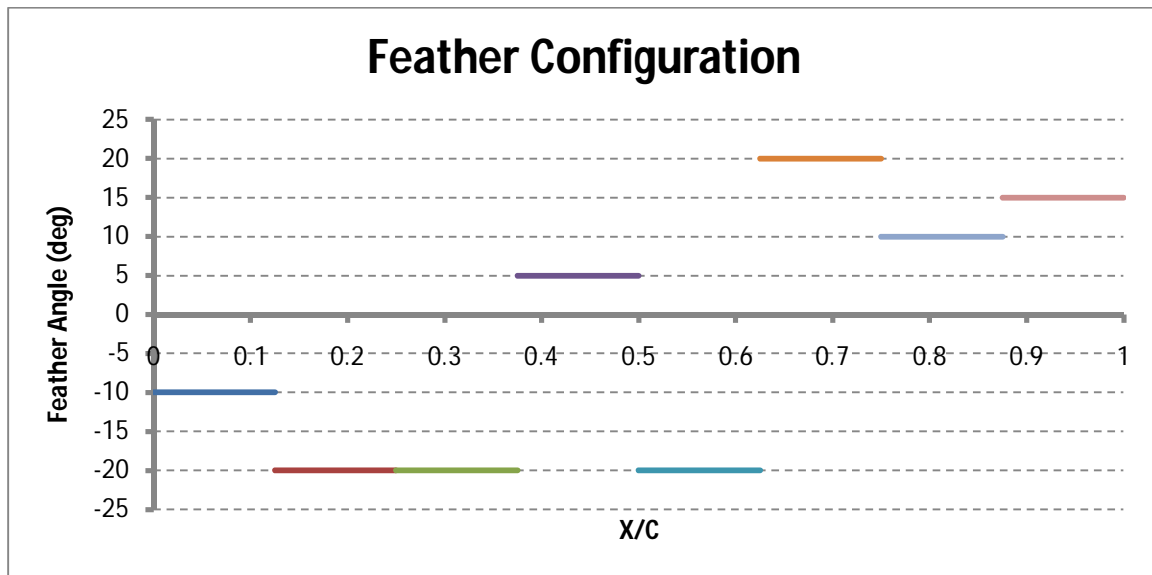


Figure 56: Individual -2 -4 -4 1 -4 4 2 3 Configuration

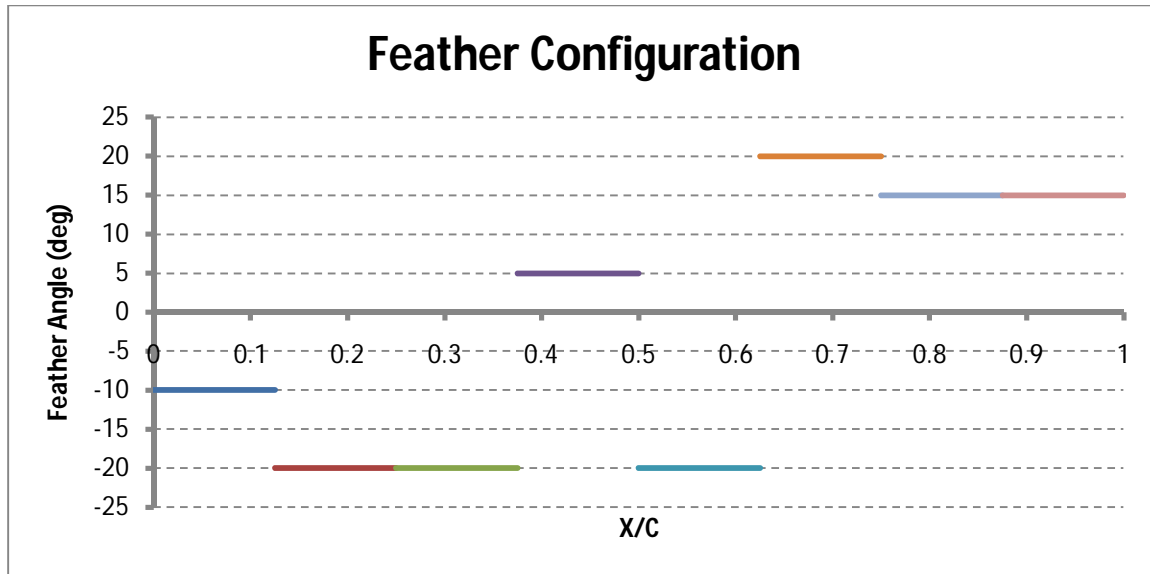


Figure 57: Individual -2 -4 -4 1 -4 4 3 3 Configuration

The downswept leading edge differs from the alternating feather configuration developed by the low angle of attack genetic algorithm. However, this downsweep is similar to the geometry established by M. Stache, as shown in Figure 58. The theoretical explanation for the performance of this design is the following. At the trailing edge of each feather, there is a downwash velocity inboard of the feather wingtip from the vortex associated with that feather tip. The next feather location, which has a more negative angle, results in the tip of the second feather being further inboard (towards the wing root) than the tip of the first feather. The upwash velocity outboard of the second feather counteracts the downwash velocity from the first feather thus decreasing the strength of each vortex (see Figure 59).

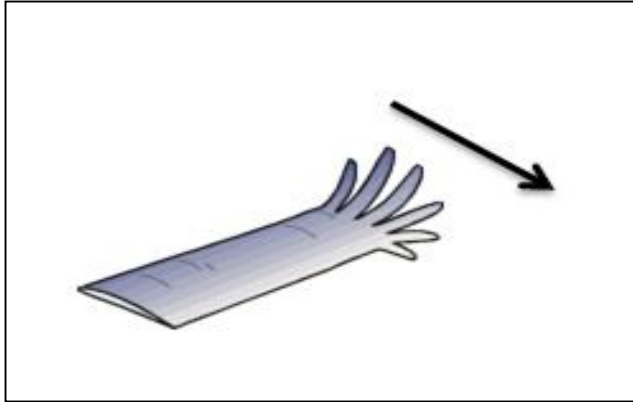


Figure 58: Biologically Inspired Tip Geometry from Ref [38]

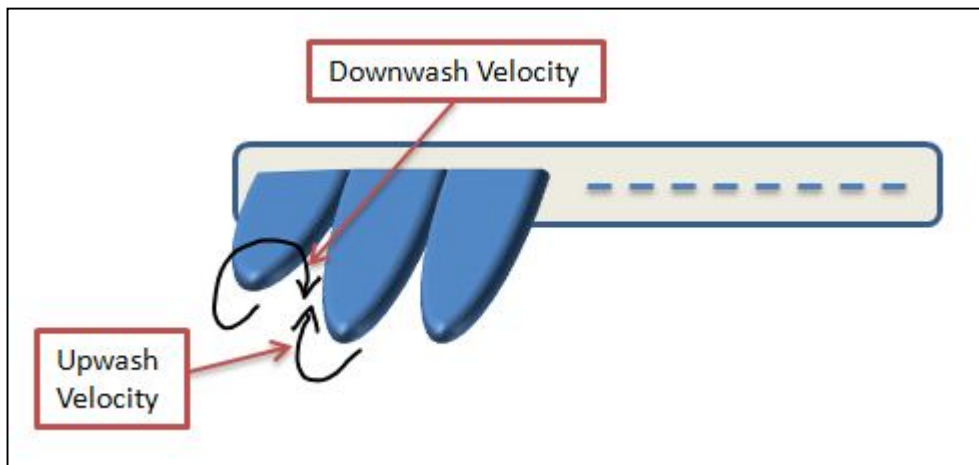


Figure 59: Flow Over Downswept Feathers

The final distinctive characteristic of individual -2 -4 -4 1 -4 4 1 3 is the large vertical separation between feathers 5 and 6. This separation is slightly closer to the trailing edge than the separation on the individual generated by the low angle of attack genetic algorithm. In each case, there is the possibility that this separation further diffuses the vortex, which decreases the global circulation value. While this is not definitive, the presence of this characteristic in both algorithms, which had differing initial populations, angles of attack, and freestream velocities, demonstrates its benefit to the performance of the wing.

In the case of this test series, twelve generations of testing were completed in order to establish the dominant design. This required a total of 364 designs to be measured. In comparison, the entire solutions space consisted of  $8^9$  differing designs. This means that using the genetic algorithm allowed only 0.0003% of the solution space to be tested.

### **3.3 Comparison of Low and High Angle of Attack Results**

As discussed in the previous sections, there were many similarities between the tip geometries developed by the low and high angle of attack genetic algorithm series. The trailing edge and mid-section separation characteristics appeared in both dominant designs. This element of repeatability increases the likelihood that these are optimum characteristics. Both of these designs were able to produce a wingtip vortex circulation that was 20% less than that of a flat wing. The equal decrease for differing angles of attack is likely due to the small aspect ratio of the test wing, which allows the wing to resist stall. It is also important to note the many differences between the two test runs such as initial population, parent selection, angle of attack, and velocity. The similar results attained for such distinct tests suggest that a single optimum design may exist for a MAV wing or propeller blade that will significantly reduce vortex strength over many flow regimes.

## 4. CONCLUSIONS

The following is a summary of the key results discussed in Section 3.

- A test wing with an aspect ratio applicable to that of a MAV or propeller blade with a variable tip geometry was designed and constructed for the purpose of implementing a genetic algorithm to find a tip geometry with minimal tip vortex strength.
- A genetic algorithm that used uniform crossover breeding, a 20% mutation rate, and roulette wheel parent selection method was used to generate an improved tip geometry at a low angle of attack of  $6^\circ$  and a freestream velocity of 15.25 m/s over the course of 17 generations. This improved design consisted of three key features, a staggered leading edge, a large mid-section vertical separation, and an upswept trailing edge.
- A second algorithm, which employed uniform crossover, a 20% mutation rate, and an elitist selection roulette parent selection, provided an improved tip geometry for a  $12^\circ$  angle of attack at a freestream velocity of 11.5 m/s. This best performing design consisted of three key features, a downswept leading edge, a large mid-section vertical separation, and an upturned trailing edge.
- The convergence of the high angle of attack algorithm showed that the use of elitist selection can be used to speed convergence when the fitness values are similar for the majority of the overall population.
- Through the use of the genetic algorithms, the testing required to find the dominant individual was reduced to 0.0003% and 0.0004% of the number of tests required to evaluate the entire solution space for the low and high angle of attack test series, respectively.

- In both cases, the trailing edge geometry developed more quickly than the remainder of the tip geometry. This signifies that the trailing edge has the most prominent effect on the wing tip vortex.
- Although flow visualization was not performed in this research. Traditional aerodynamic theory supports the improved performance of the designs generated by the genetic algorithms.
- In each set of tests, the genetic algorithm was capable of producing a tip geometry that decreased vortex strength by 20% in comparison to the same wing with a flat tip geometry. This shows that the tip geometry has an equal effect on wings at both high and low angles of attack. This may be due to the low aspect ratio of the test wing and its consequent resistance to stall.
- The similarities between the designs generated by each algorithm and the circulation reductions they provide suggest that a single tip geometry may provide a significant improvement in the efficiency of a MAV wing or propeller blade over a range of flow regimes by reducing the associated wingtip vortex strength.

## 5. FUTURE WORK

Although the research completed in the present work provided useful information on how to improve the tip geometry of MAV wings and propeller blades, there are still many unknowns regarding this problem. The following section discusses further work that can be used to confirm the improved geometries, apply these results to practical applications, and to improve the present experiment.

In order to confirm the best performing geometries obtained in this work, the experiment should be repeated with differing initial populations. In particular, in the low angle of attack case, where convergence was not met, it is important to verify that the geometry obtained is a global minimum as opposed to a local minimum circulation design. Performing these experiments with varied parent selection methods, selection roulette with and without elitist methods employed, would help to confirm the fitness of the geometries as well as testing the theory that using an the elitist method can speed convergence and its ability to find a global optimum.

In the previous sections, hypotheses were presented to explain how each tip geometry acted to decrease the tip vortex strength. However, flow visualization must be completed to examine the interaction of the freestream flow with the wingtip in order to confirm these theories. Once the flow around the wingtip is well-understood, a tip geometry that is both practical to manufacture as well as efficient can be designed and applied to functioning MAVs and propeller blades.

Although this work describes the effects of wing tip geometry on tip vortex strength, tip geometry is not the only wing characteristic that could be used to reduce tip vortices. It is also possible that surface roughness may have the ability to make improvements in circulation. Preliminary tests using a variety of tip materials in addition to the plastic feathers used in this work would provide insight into the need for future testing in this area.



Finally, the experimental procedure can be improved for future tests. The most time consuming element of the test procedure was the act of setting the feather angles to match the configuration dictated by the genetic algorithm before recording circulation data. In order to decrease the time spent performing this task, the potentiometers used to measure the feather angles should be permanently wired to one data acquisition card instead of changing the connections before reading each feather angle. The virtual instrument could then be modified to read the appropriate channel when the user selects a feather angle to modify.

## REFERENCES

1. U.S. Centennial of Flight Commission (Civil Air Patrol), 2009, "Theories of Flight : Wing Vortices," [http://www.centennialofflight.gov/essay/Theories\\_of\\_Flight/Vortex/TH15.htm](http://www.centennialofflight.gov/essay/Theories_of_Flight/Vortex/TH15.htm)
2. Anderson, J., 2007, *Fundamentals of Aerodynamics 4<sup>th</sup> Edition*, McGraw-Hill, New York, NY, Chap. 5.
3. Bertin, J. & Smith, M., 1989, *Aerodynamics for Engineers 2<sup>nd</sup> Edition*, Prentice Hall, Englewood Cliffs, NJ, Chap. 7.
4. Kinnas, S.A., 1996, "Photographs of Different Types of Cavitation," <http://cavity.ce.utexas.edu/kinnas/cavphotos.html>.
5. Lunin, S.V., 2005, "Increasing Propeller Efficiency with Tip Fins," [http://www.zakpro.com/Tip\\_fins.html](http://www.zakpro.com/Tip_fins.html)
6. Davenport, W.J., Rife, M.C., Liapis, S.I. & Follin, G.J., 1996, "The Structure and Development of a Wing Tip Vortex," *Journal of Fluid Mechanics*, 312, pp. 67-106.
7. Tucker, V.A., 1993, "Gliding Birds: Reduction of Induced Drag by Wing Tip Slots Between the Primary Feathers," *J. exp. Biol.*, pp. 285-310.
8. Rao, P. R., 2003, "Biomimetics," *Sādhanā*, 28, (3-4), pp.657-676.
9. Vincent, J. F. V., 2005, "Stealing Ideas from Nature" Chap. 3 of *Deployable Structures*, Springer-Verlag, Vienna, pp. 51-58.
10. Morris, S. J. & Holden, M., 2003, "Design of Micro Air vehicles and Flight Test Data Validation," [http://www.spyplanes.com/pdf\\_new/notredame0600.pdf](http://www.spyplanes.com/pdf_new/notredame0600.pdf).
11. Oyama, A., Okabe, Y., Fujii, K. & Shimoyama, K., 2007, "A Study on Flapping Motion for MAV Design Using Design Exploration," *AIAA 2007 Conference and Exhibit*, American Institute of Aeronautics and Astronautics.
12. Abdulrahim, M., Garcia, H. & Lind, R., 2005, "Flight Characteristics of Shaping the Membrane Wing of a Micro Air Vehicle," *Journal of Aircraft*, 42, (1), pp. 131-137.
13. Day, A., 2007, "Optimization of a Micro Air Vehicle Planform Using Genetic Algorithms," M.S. Thesis, Worcester Polytechnic Institute.
14. Taylor, S., 2009, "Biologically Inspired Wing Planform Optimization," M.S. Thesis, Worcester Polytechnic Institute.
15. Darwin, C., 2001, *On the Origin of Species by Means of Natural Selection*, Elecbook, London.
16. Fogel, D.B., 2006, *Evolutionary Computation: Toward a New Philosophy of Machine Design*, John Wiley & Sons, Hoboken, New Jersey, pp. 59-84.
17. Spall, J.C., 2003, *Introduction to Stochastic Search and Optimization: Estimation, Simulation, and Control*, John Wiley & Sons, pp.231-255.
18. Oyama, A., Obayashi, S., Nakahashi, K. & Nakamura, T., 2000, "Aerodynamic Optimization of Transonic Wing Design Based on Evolutionary Algorithm," *Third International Conference On Nonlinear Problems in Aviation and Aerospace*, Embry-Riddle Aeronautical University Daytona Beach, FL.
19. Livnat, A., Papadimitriou, C., Dushoff, J. & Feldman, M.W., 2008, "A Mixability Theory of the Role of Sex in Evolution," *Proceedings of the National Academy of Sciences in the United States of America*, 105, (50), pp. 19803-19808.
20. Kibler, D.F., 2005, "Genetic Algorithms," *U.C. Irvine: Introduction to Artificial Intelligence*.
21. Beasley, D., Bull, D. & Martin, R., 1993, "An Overview of Genetic Algorithms: Part 1, Fundamentals," *University Computing, Inter-University Committee on Computing*.
22. Galante, M., 1996, "Genetic Algorithms as an Approach to Optimize Real-World Trusses," *International Journal for Numerical Methods in Engineering*, 39, pp. 361-382.

23. Chipperfield, A. J., Flemming, P.J. & Fonseca, C.M., 1994, "Genetic Algorithm Tools for Control Systems Engineering," *Adaptive Computing in Engineering Design and Control*, Plymouth, UK.
24. Unger, R. & Moulton, J., 1993, "Genetic Algorithms for Protein Folding Simulations," *J. Mol. Biol.*, 231, pp. 75-81.
25. Liebe, W., 1979, "Der Auftrieb am Tragflügel: Entstehung und Zusammenbruch," *Aerokurier* 12, pp. 1520-1523.
26. Maughmer, M. D. & Kunz, P. J., 1997, "Sailplane Winglet Design," *XXV OSTIV Congress*, Saint Auban, France.
27. Kroo, I., 2005, "Nonplanar Wing Concepts for Increased Aircraft Efficiency," *VKI lecture series on Innovative Configurations and Advanced Concepts for Future Civil Aircraft*.
28. Bannasch, R., "From Soaring and Flapping Bird Flight to Innovative Wing and Propeller Constructions," *Progress in Astronautics and Aeronautics*, Vol. 194, pp. 453-471.
29. Berchert, D. W., Bruse, M., Hage, W., and Meyer, R., 1997, "Biological Surfaces and Their Application – Laboratory and Flight Experiments on Drag Reduction and Separation Control," AIAA Paper.
30. Wallace, J.M., 1986, "Methods of Measuring Vorticity in Turbulent Flow," *Experiments in Fluids*, 4, pp. 61-71.
31. Johari, H. and Durgin, W.W., 1998, "Direct Measurement of Circulation Using Ultrasound," *Experiments in Fluids*, 25, (5-6), pp. 445-454.
32. Purutyán, H., 1990, "Ultrasonic measurement of circulation around a plunging airfoil", M.S. Thesis, Worcester Polytechnic Institute.
33. Desabrais, K., 1997, "Direct measurement of wing tip vortex circulation using ultrasound", M.S. Thesis, Worcester Polytechnic Institute.
34. *Slater Museum of Natural History* [online database], 2005, <http://digitalcollections.ups.edu/slater/>.
35. Willits, S. M. - M&H Soaring, "Standard Cirrus: Winglets," <http://www.standardcirrus.org/Winglets.php>.
36. Mõnttinen, J.T., Reed, H. L., Squires, K. D. & Saric, W. S., 2003, "On the Effect of Winglets on the Performance of Micro-Aerial-Vehicles," *The 1<sup>st</sup> Annual REAS Conference*, Arizona State University.
37. Maughmer, M. D., Swan, T. S. & Willits S. M., 2001, "The Design and Testing of a Winglet Airfoil for Low-Speed Aircraft," AIAA.
38. Stache, M., "Bionik at the Technical University of Berlin," <http://www.biokon.net/biokon/profil/BerlinBionik.pdf.en>.

## APPENDICES

### Appendix A: Angle Sensor Calibration

Rotary potentiometers were used as angle sensors. In order to calibrate the potentiometers, an experiment using laser reflection properties was designed. For this test, the fact that lasers reflect off of a surface at the same angle that they approach it with to calculate the angle of the feather.

A laser pointer was hung from the underside of a level table. Aluminum foil was applied to the top surface of each feather on the test wing. The distance from the feather surface to the underside of the table (distance Y) was measured. A tape measure was taped to the underside of the table to provide a scale to measure distance X. The test set-up can be seen in Figure 60.

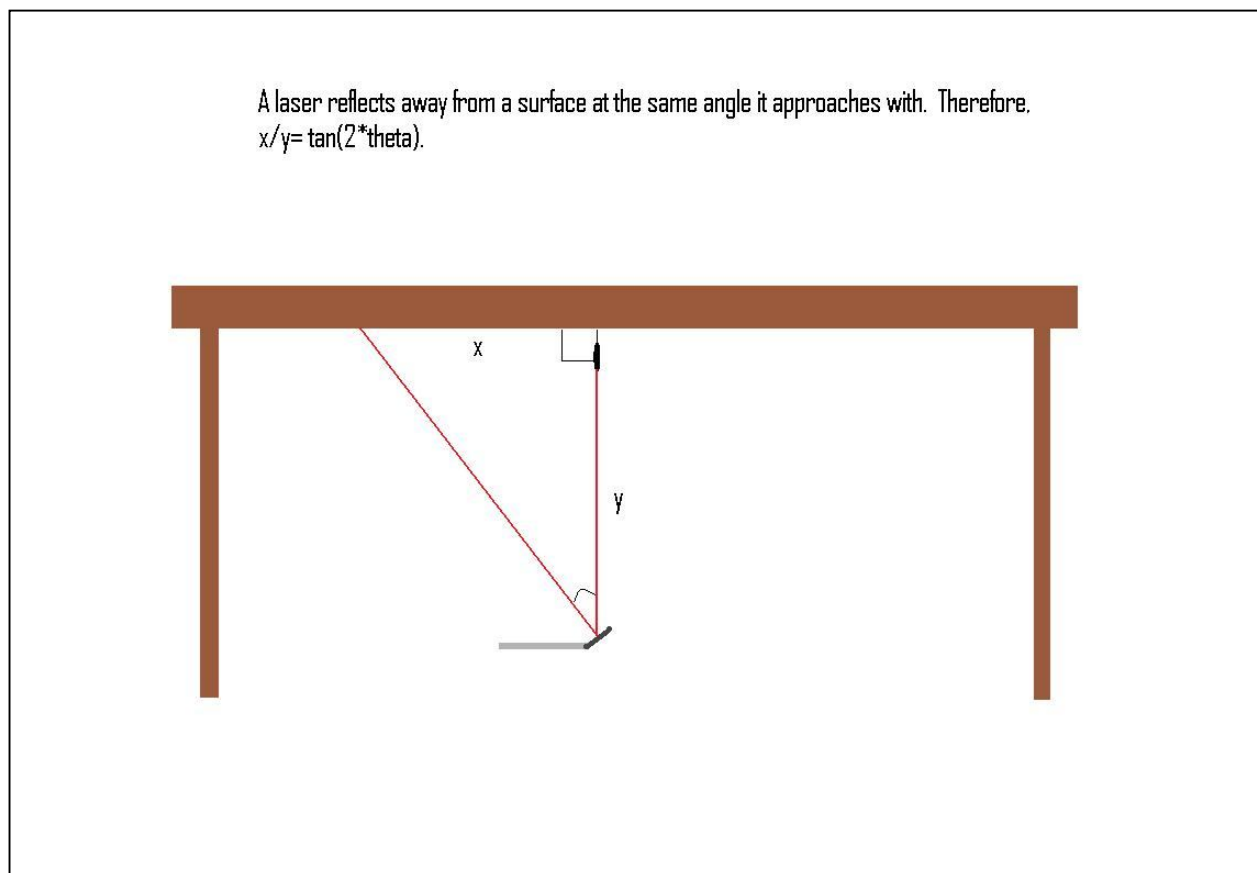


Figure 60: Angle Sensor Calibration Set-Up

A virtual instrument was created in LabView to measure the source and output voltage of the potentiometers. The relative voltage was then calculated. The user input x, y, and offset angle values to the front panel (see Figure 61), where the offset angle was the taper angle of the feather surface relative to the centerline of the feather. The VI would then calculate the angle of the feather as shown below in Figure 62.

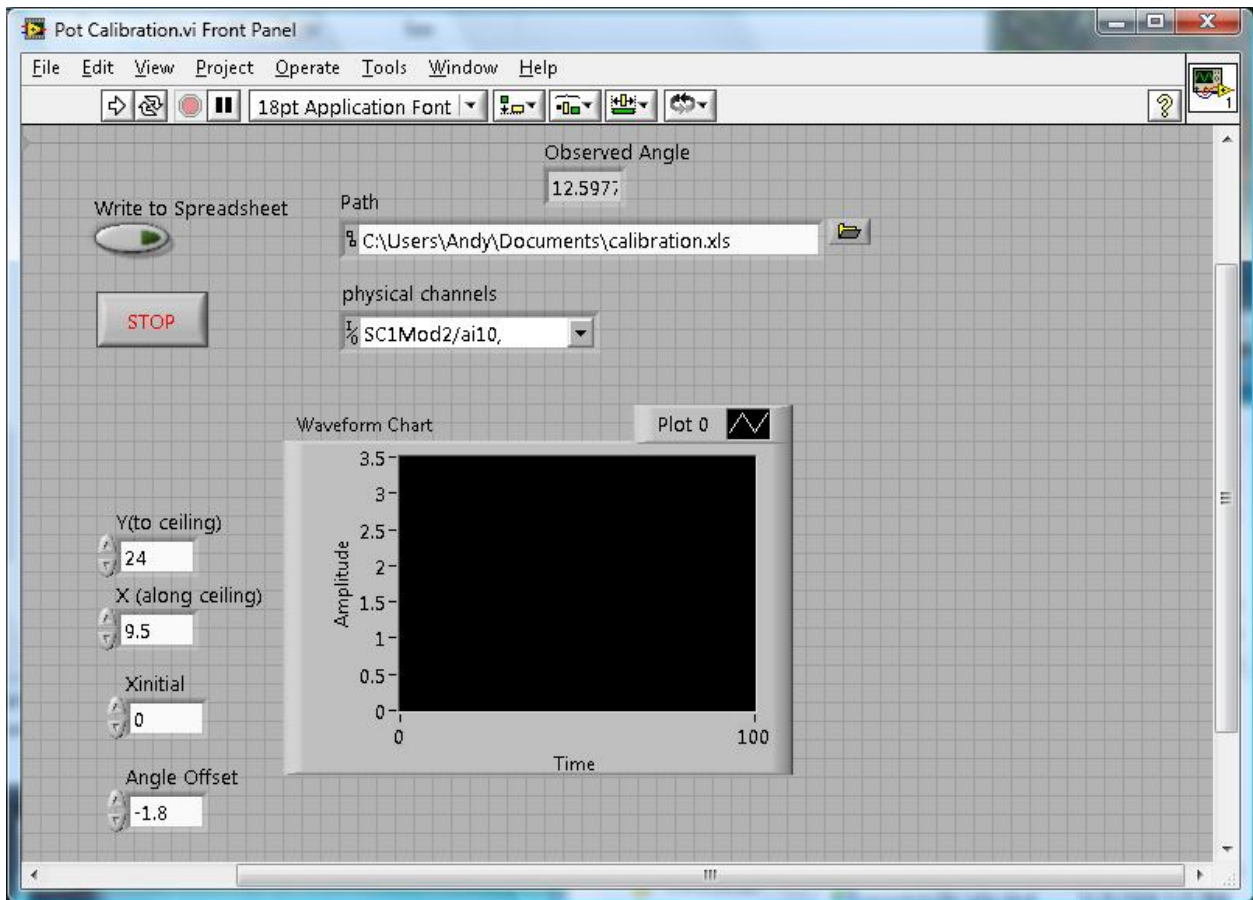


Figure 61: Potentiometer Calibration Front Panel

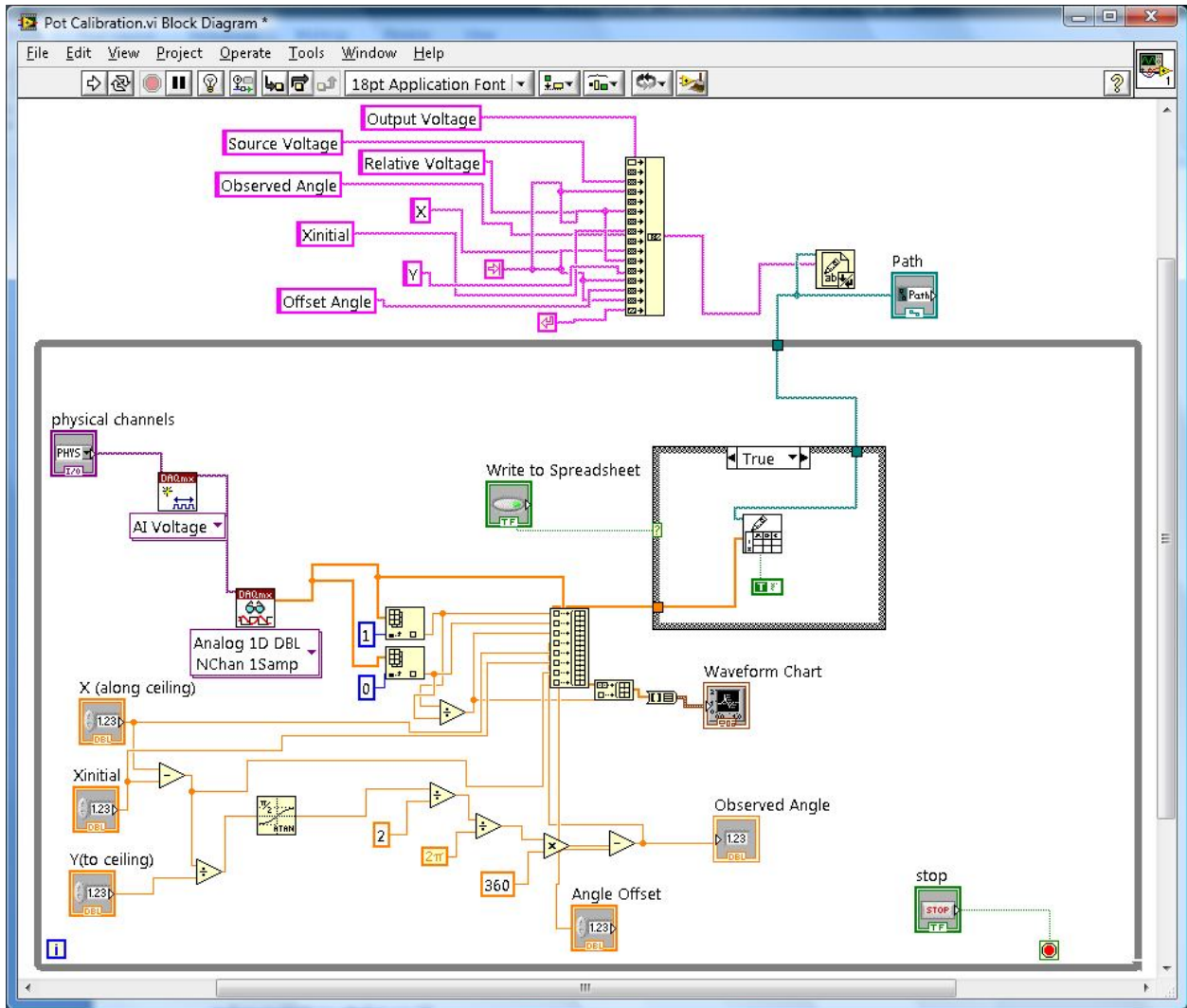


Figure 62: Potentiometer Calibration Block Diagram

When all of the parameters were entered into the front panel, the record to disk button on the front panel was used to write the relative voltage and calculated feather angle to an excel spreadsheet. These data points were then displayed in a scatter plot. As the potentiometers being used have a linear taper, a linear trendline was added to the data plot. From this trendline, a slope and intercept relating the relative voltage measured to the feather angle were calculated. This process was repeated to obtain a slope and intercept for each of the eight feathers on the test wing. The plotted data sets can be seen in Figure 63 through Figure 70.

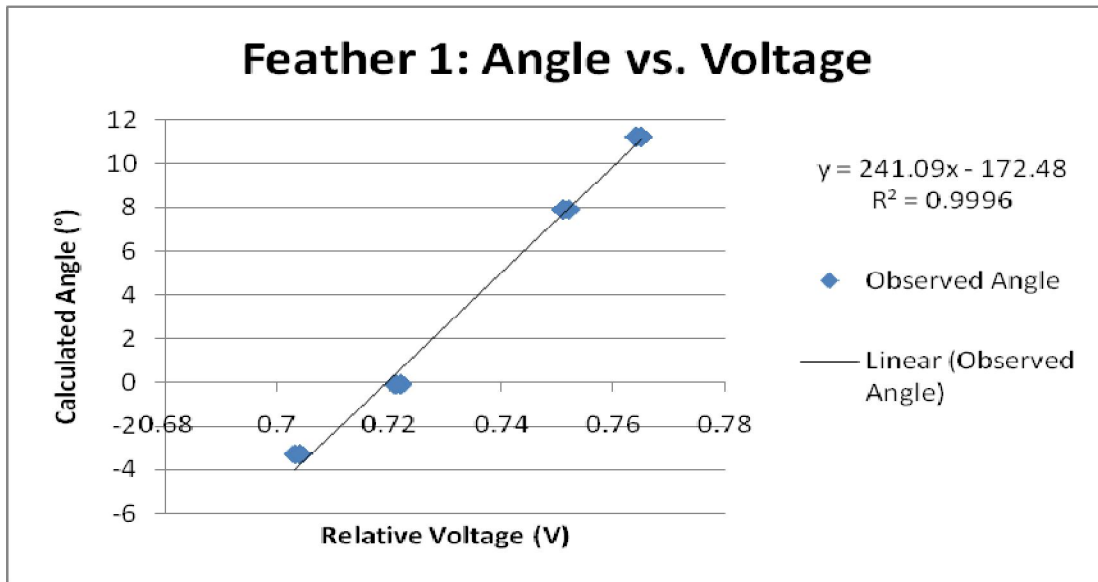


Figure 63: Feather 1 Angle Sensor Calibration Data

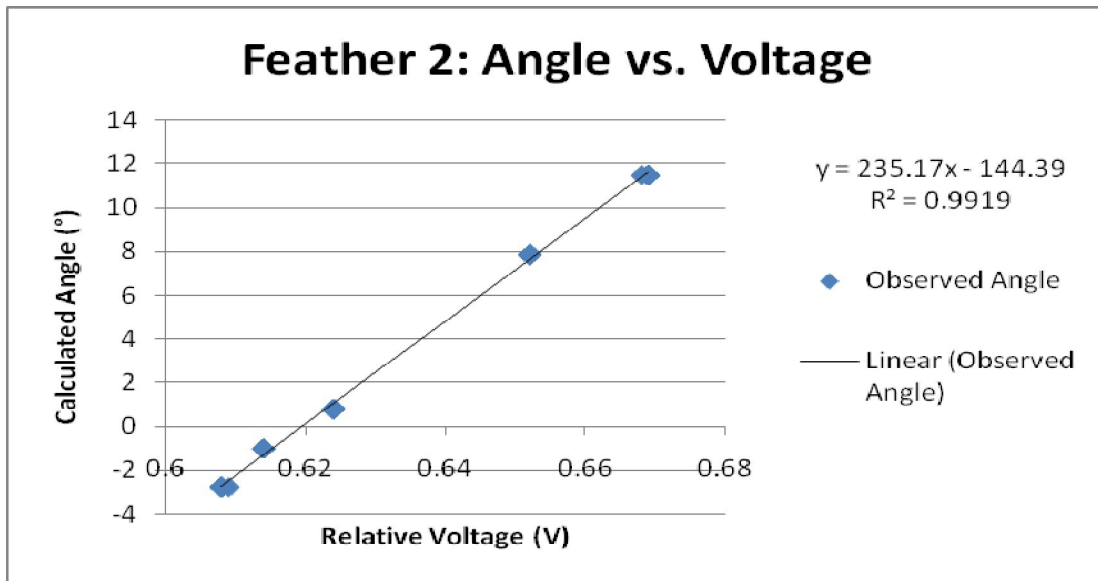


Figure 64: Feather 2 Angle Sensor Calibration

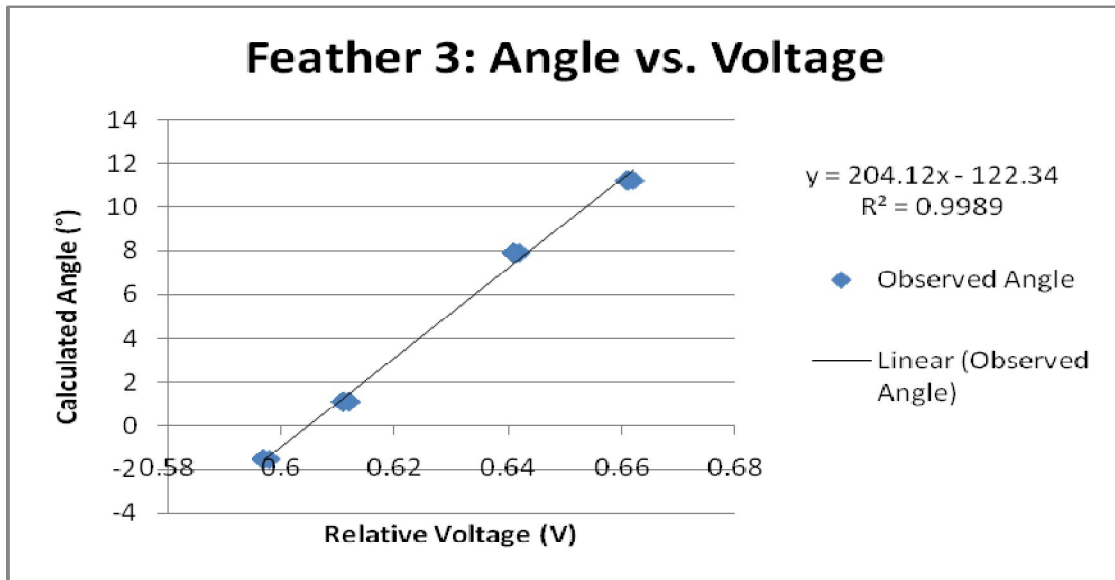


Figure 65: Feather 3 Angle Sensor Calibration

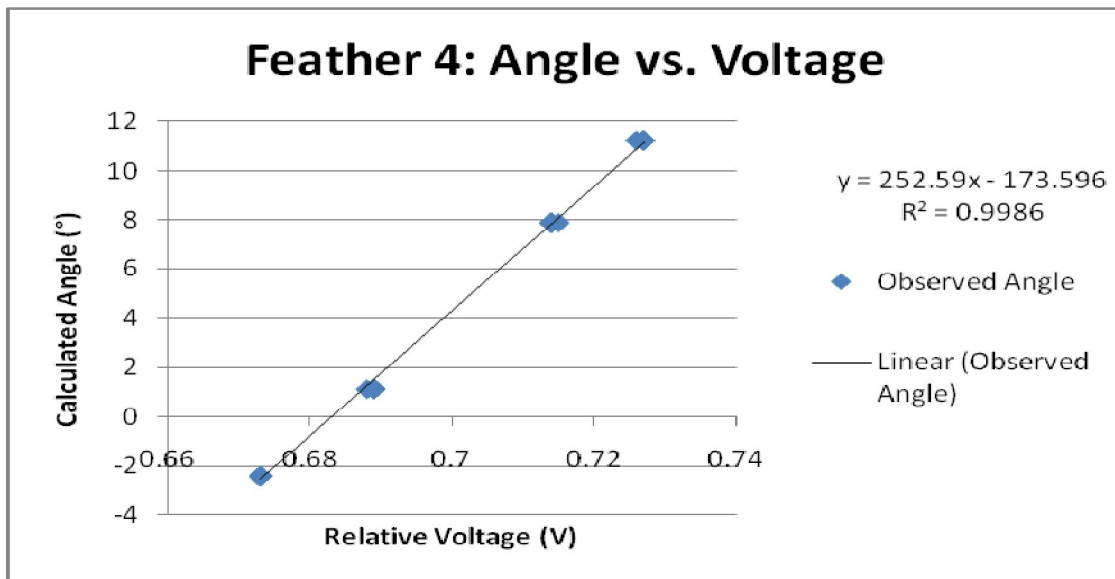


Figure 66: Feather 4 Angle Sensor Calibration



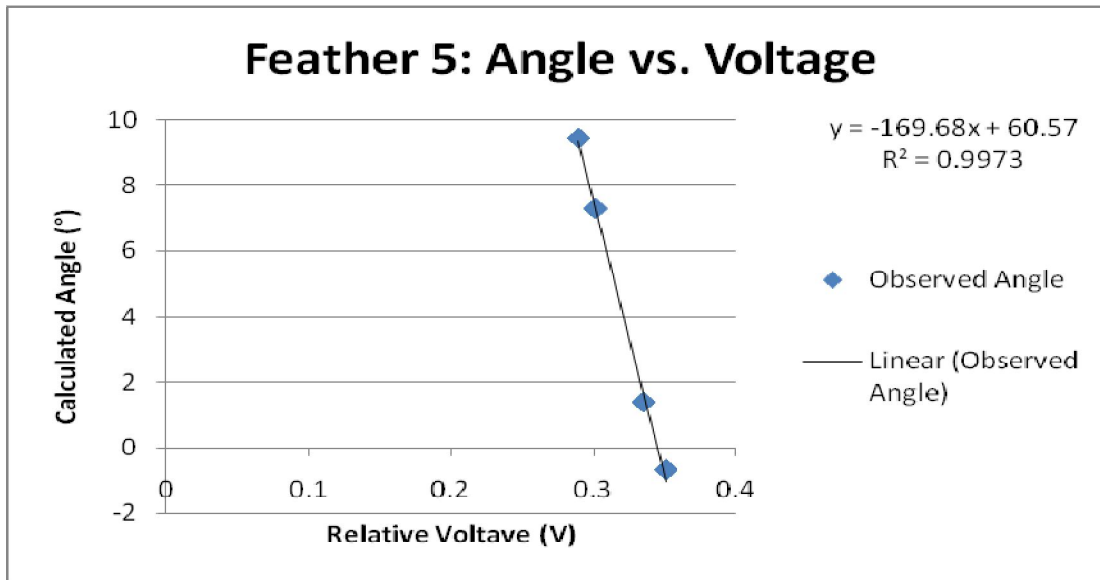


Figure 67: Feather 5 Calibration Data

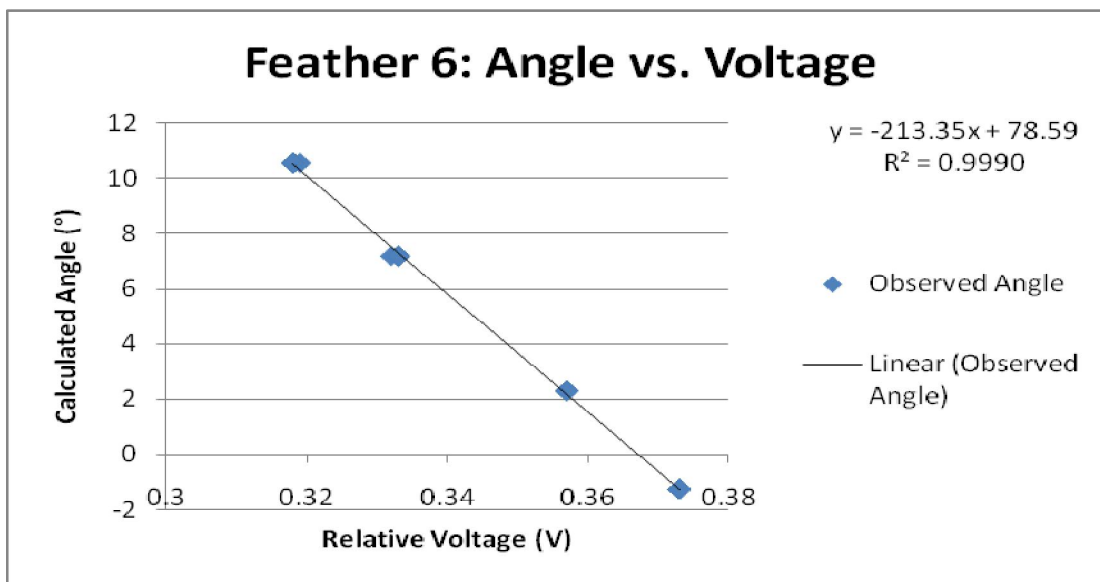


Figure 68: Feather 6 Calibration Data

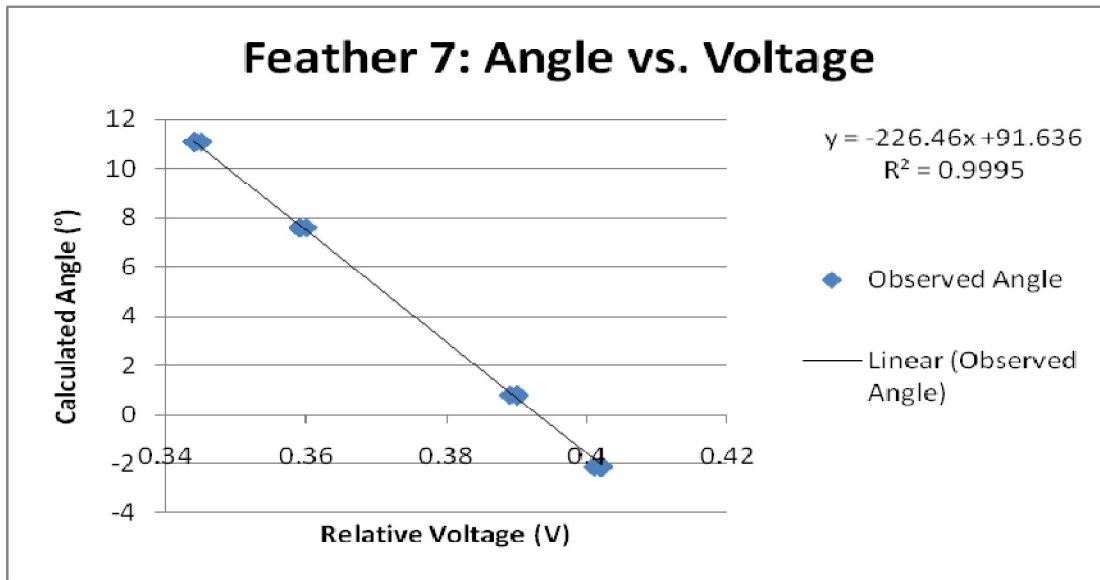


Figure 69: Feather 7 Calibration Data

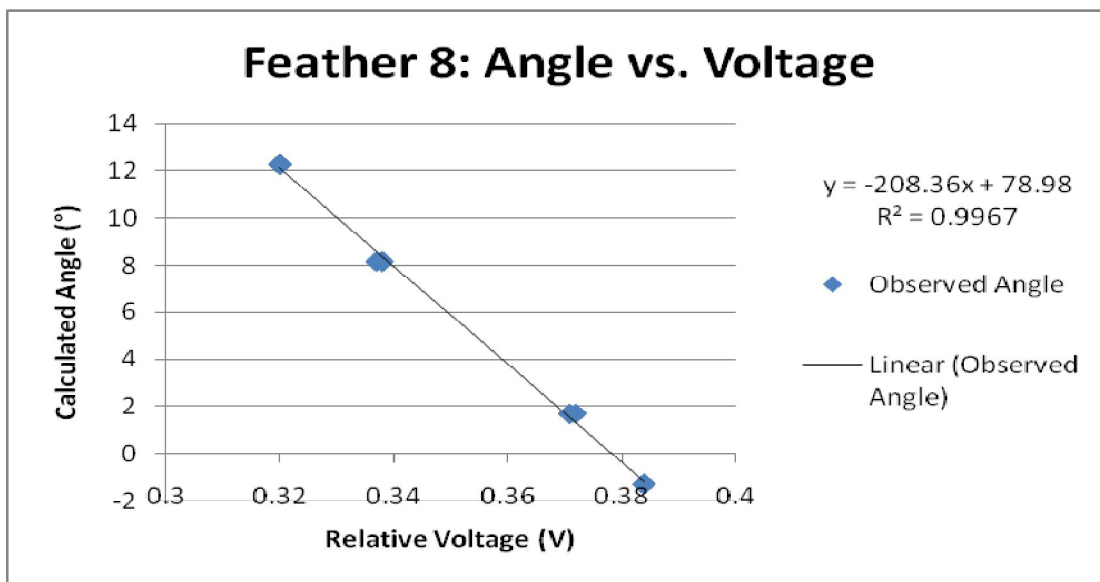


Figure 70: Feather 8 Calibration Data

Each data set had an  $R^2$  value of at least .99. In order to increase accuracy, the X values recorded were kept in the range of  $\pm 11$  in. As the distance increased outside of this range, the beam

diffracted causing less accurate X values. Table 4 shows the calibration data collected for each feather potentiometer.

**Table 4: Potentiometer Calibration Data**

Feather #	Slope	Intercept	R <sup>2</sup>
1	241.09	-172.48	.9996
2	235.17	-144.39	.9919
3	204.12	-122.34	.9989
4	252.59	-173.59	.9986
5	-169.68	60.57	.9973
6	-213.35	78.98	.9990
7	-226.46	91.636	.9995
8	-208.36	78.98	.9967

## Appendix B: Angle Sensor Virtual Instrument

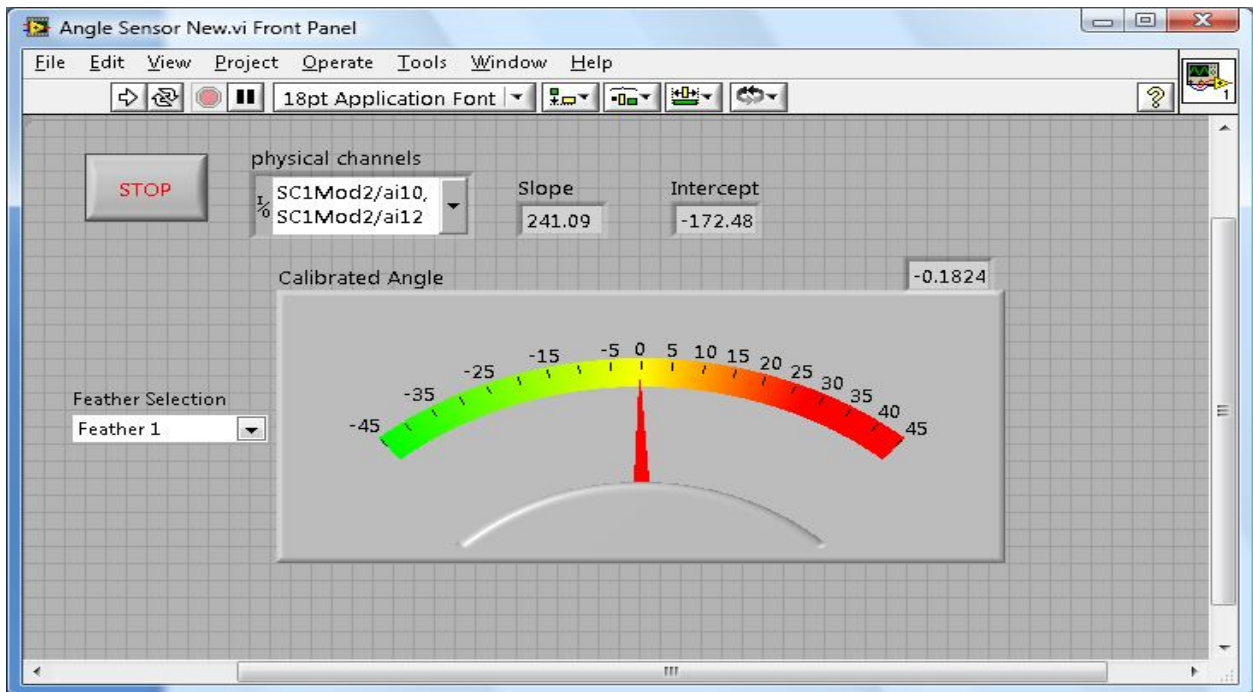


Figure 71: Angle Sensor Front Panel

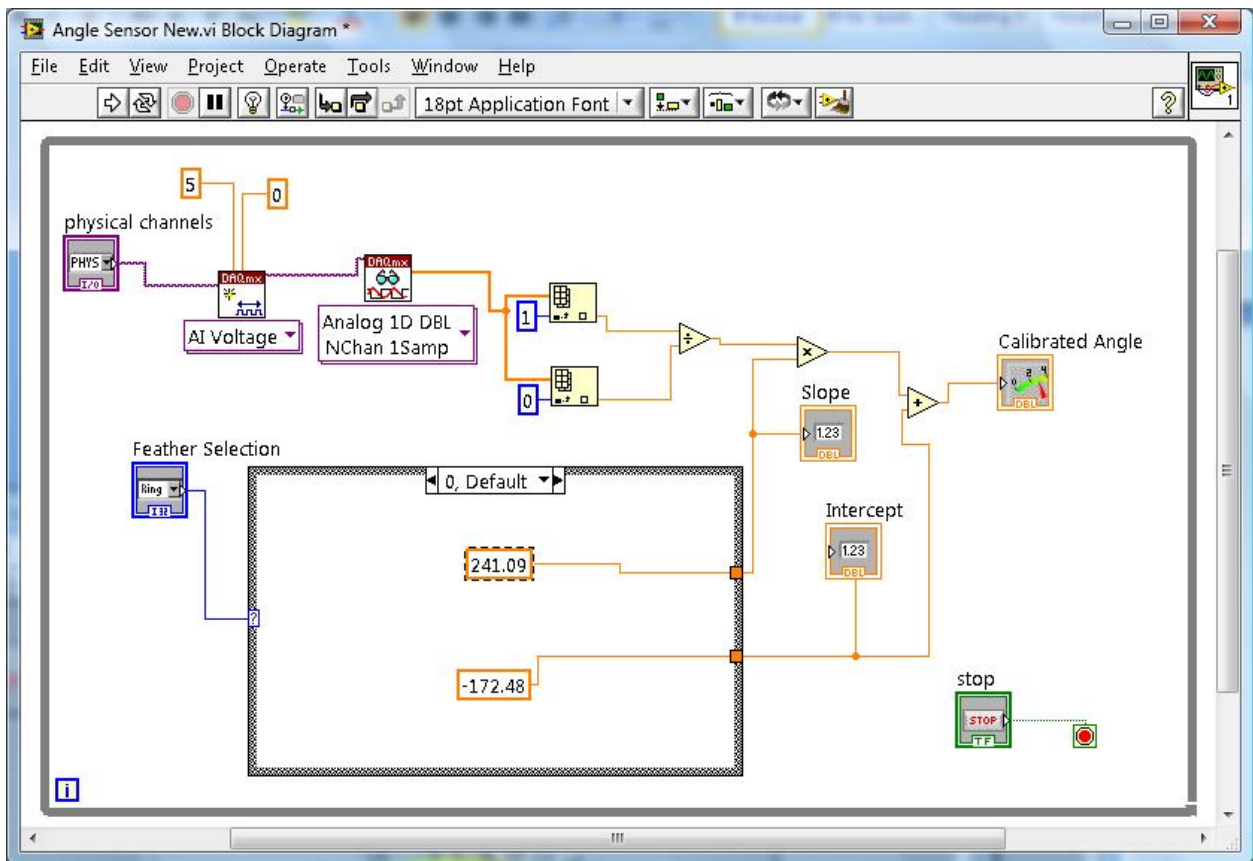


Figure 72: Angle Sensor Block Diagram

## Appendix C: Preliminary Velocity Test

In order to test the functionality of the ultrasonic flowmeter, measurements of the freestream velocity of a wind tunnel a variety of known velocities were taken. For this test, the transducer signal path was directed diagonally across the wind tunnel test section as shown in Figure 73. The difference between upstream and downstream signal transit time can be used to calculate the freestream velocity in the test section using equations (12) through (14).

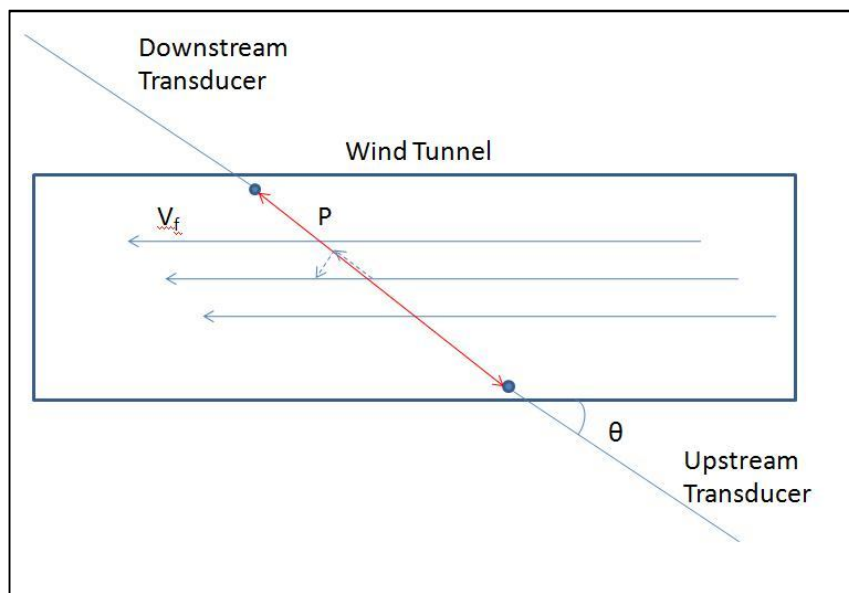


Figure 73: Velocity Test Schematic

$$t_1 = \frac{P}{c + v_f \cos \theta} \quad (12)$$

$$t_2 = \frac{P}{c - v_f \cos \theta} \quad (13)$$

$$v_f = \frac{P}{2 \cos \theta} \cdot \left( \frac{1}{t_1} - \frac{1}{t_2} \right) \quad (14)$$

The velocity through the wind tunnel was set using a fan frequency control. The velocity calculated using the ultrasonic flowmeter data and the velocity calculated using the tunnel frequency

known calibration data are shown in Figure 74. The data in Figure 74 shows that the velocity calculated in the flowmeter is in very good agreement with the velocity calculated using the known wind tunnel calibration data. As this was a preliminary test, there was some airflow access through the tunnel wall where the transducers were inserted. This would account for discrepancies in the measurements.

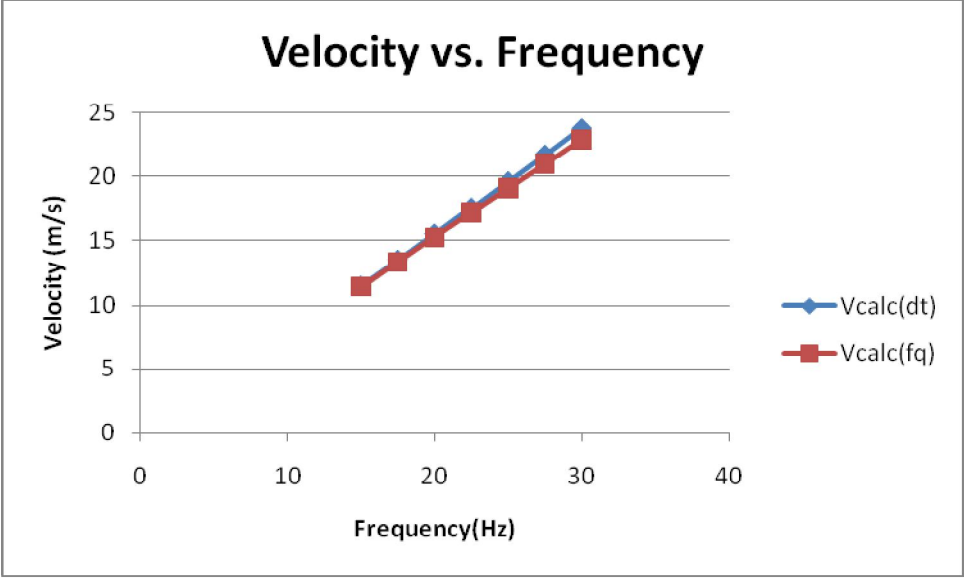


Figure 74: Velocity Test Data

## Appendix D: Circulation Formula Derivation

For discussion of the following equations see the previous Section 2.3.2 and H. Purutyan [32].

For a vortex,

$$w = \frac{\Gamma}{2\pi r(y)} \quad (2)$$

$$v = w \cos \Phi \quad (3)$$

$$v(a, y) = w(r(y)) \frac{a}{\sqrt{a^2 + y^2}} \quad (4)$$

$$v = \frac{\Gamma a}{2\pi(a^2 + y^2)} \quad (5)$$

For the upstream transducer signal,

$$\frac{dy}{dt_{up}} = c + v \quad (7)$$

$$t_{up} = \int_{-P/2}^{P/2} \frac{1}{c + \frac{\Gamma a}{2\pi(a^2 + y^2)}} dy \quad (8)$$

$$t_{up} = \int_{-P/2}^{P/2} \frac{1}{\left(\frac{2\pi(a^2 + y^2)c - \Gamma a}{2\pi(a^2 + y^2)}\right)} dy \quad (15)$$

$$t_{up} = \int_{-P/2}^{P/2} \frac{2\pi(a^2 + y^2)}{2\pi(a^2 + y^2)c - \Gamma a} dy \quad (16)$$

$$t_{up} = \frac{1}{c} \int_{-P/2}^{P/2} \frac{(a^2 + y^2)}{(a^2 + y^2) - \frac{\Gamma a}{2\pi c}} dy \quad (17)$$

Let  $k = \frac{\Gamma a}{2\pi c}$ ,

$$t_{up} = \frac{1}{c} \int_{-P/2}^{P/2} \frac{(a^2 + y^2)}{(a^2 + y^2) - k} dy \quad (18)$$

$$t_{up} = \frac{1}{c} \int_{-P/2}^{P/2} \frac{a^2}{(a^2 + y^2) - k} dy + \frac{1}{c} \int_{-P/2}^{P/2} \frac{y^2}{(a^2 + y^2) - k} dy \quad (19)$$

Let  $\alpha^2 = a^2 - k$

$$t_{up} = \frac{1}{c} \left( \int_{-P/2}^{P/2} \frac{a^2}{y^2 + \alpha^2} dy + \int_{-P/2}^{P/2} \frac{y^2}{y^2 + \alpha^2} dy \right) \quad (20)$$

Note the following relationships:

$$\int \frac{dx}{l^2 + x^2} = \frac{1}{l} \tan^{-1} \frac{x}{l} \quad (21)$$

$$\int \frac{x^2 dx}{m + nx^2} = \frac{x}{n} - \frac{m}{n} \int \frac{dx}{m + nx^2} \quad (22)$$

$$\int \frac{dx}{m + nx^2} = \frac{1}{\sqrt{mn}} \tan^{-1} \frac{x\sqrt{mn}}{m} \quad (23)$$

Using relationship (21) in equation (20),

$$t_{up} = \frac{1}{c} \left( \left[ \frac{a^2}{\alpha} \tan^{-1} \frac{y}{\alpha} \right]_{y=-P/2}^{P/2} + \int_{-P/2}^{P/2} \frac{y^2}{\alpha^2 + y^2} dy \right) \quad (24)$$

Using relationship (22) in equation (24),

$$t_{up} = \frac{1}{c} \left( \left[ \frac{a^2}{\alpha} \tan^{-1} \frac{y}{\alpha} \right]_{y=-P/2}^{P/2} + y - \alpha^2 \int_{-P/2}^{P/2} \frac{1}{\alpha^2 + y^2} dy \right) \quad (25)$$

Using relationship (23) in equation (25),



$$t_{up} = \frac{1}{c} \left[ \left( \frac{a^2}{\alpha} \tan^{-1} \frac{y}{\alpha} \right) + y - \alpha^2 \left( \frac{1}{\sqrt{\alpha^2}} \tan^{-1} y \frac{\sqrt{\alpha^2}}{\alpha^2} \right) \right]_{y=-P/2}^{P/2} \quad (26)$$

$$t_{up} = \frac{1}{c} \left[ \left( \frac{a^2}{\alpha} \tan^{-1} \frac{y}{\alpha} \right) + y - \alpha \tan^{-1} \frac{y}{\alpha} \right]_{y=-P/2}^{P/2} \quad (27)$$

$$t_{up} = \frac{1}{c} \left[ y + \left( \frac{a^2}{\alpha} - \alpha \right) \tan^{-1} \frac{y}{\alpha} \right]_{y=-P/2}^{P/2} \quad (28)$$

$$t_{up} = \frac{1}{c} \left[ y + \left( \frac{a^2}{\alpha} - \alpha \right) \tan^{-1} \frac{y}{\alpha} \right]_{y=-P/2}^{P/2} \quad (29)$$

$$t_{up} = \frac{1}{c} \left[ \frac{P}{2} - \frac{-P}{2} + \left( \frac{a^2}{\alpha} - \alpha \right) \left( \tan^{-1} \frac{P}{2\alpha} - \tan^{-1} \frac{-P}{2\alpha} \right) \right] \quad (30)$$

$$t_{up} = \frac{1}{c} \left[ P + 2 \left( \frac{a^2}{\alpha} - \alpha \right) \tan^{-1} \frac{P}{2\alpha} \right] \quad (31)$$

For downstream transducer signal, the same method can be used to integrate equation (9) from Section 2.3.2 to get equation (32) where,  $\beta^2 = a^2 + k$ .

$$t_{down} = \frac{2}{c} \left[ \frac{P}{2} + \left( \frac{a^2}{\beta} - \beta \right) \tan^{-1} \frac{P}{2\beta} \right] \quad (32)$$

Assuming  $k = \frac{\Gamma a}{2\pi c} \ll a$ ,  $a \sim \alpha \sim \beta$ . Then re-substituting  $k = \frac{\Gamma a}{2\pi c}$ ,

$$\Delta t = \frac{2\Gamma}{\pi c^2} \tan^{-1} \left( \frac{P}{2a} \right) \quad (33)$$

$$\Gamma = \frac{\Delta t \pi c^2}{2 \tan^{-1} \left( \frac{P}{2a} \right)} \quad (10)$$

## Appendix E: Genetic Algorithm Codes

### Initial Population Code

```
popsize=84;
rand('twister',sum(100*clock))
POP=rand(popsize,8);
A=[9, 9, 9, 9, 9, 9, 9, 9];
B=[-4,-4,-4,-4,-4,-4,-4,-4];
for i=1:8
    POP(:,i)=A(i)*POP(:,i)+B(i);
end
InitPopulation=floor(POP);
xlswrite('InitialPopulation.xls', InitPopulation)
```

## Selection Roulette Code

```
function parents = selectionroulette(expectation,nParents)
rand('twister',sum(100*clock))
wheel = cumsum(expectation)/sum(expectation);
parents = zeros(1,nParents);
for i = 1:nParents
    r = rand;
    for j = 1:length(wheel)
        if(r < wheel(j))
            parents(i) = j;
            break;
        end
    end
end
end
```

## Genetic Algorithm Code

```
close all
clear all
clc
PopNum=28;
rand('twister',sum(100*clock))
nParents=PopNum/2;
A=[9,9, 9, 9, 9, 9, 9, 9];
B=[-4,-4,-4,-4,-4,-4,-4,-4];
numgen=input('Enter the generation worksheet number for your current
population\n')
expectation = xlsread('Population.xls', numgen, 'J3:J86'); %reads fitness
values
parents = selectionroulette(expectation,nParents) %function determines
which %individuals are chosen
%to become parents

OldPop=xlsread('Population.xls', numgen, 'B3:I86')
NewPop=zeros(PopNum,8);
for i = 1:nParents %this for loop places the
n=parents(i); %parents into the next
NewPop(i,:)=OldPop(n,:); %generation of
individuals
end

for k = 1:nParents/2 %loop for each pair of
parents
for i = 1:2 %each parent set makes
two children
for j = 1:8
r=rand;
if(r < .5) %if statement
decideds which parent
NewPop(nParents+2*(k-1)+i,j) = NewPop(2*(k-1)+1,j);
%contributes each gene
else
NewPop(nParents+2*(k-1)+i,j) = NewPop(2*(k-1)+2,j);
end
%Below is the mutation function, if the random value is less than the
mutation fraction,the value is mutated to a new random number.
r=rand;
if(r<.2)
r=floor(rand*A(j))-4;
NewPop(nParents+2*(k-1)+i,j) =r;
end

end
end
end
numnewgen=numgen+1
xlswrite('Population.xls', NewPop, numnewgen, 'B3:I30');
```

## Elitist Roulette Code

```
function parents = elitestroulette(expectation,nParents)
rand('twister',sum(100*clock));
wheel = cumsum(expectation)/sum(expectation); %Creates Parent Roulette Wheel
parents = zeros(1,nParents);
emax=max(expectation); %Selects best fitness function
ind=find(expectation/emax < 1); %Eliminates best fitness function
expectation2=expectation(ind);
emax2=max(expectation2); %Selects second best fitness function

%Selects parents based on roulette wheel
for i = 1:nParents;
    r = rand;
    for j = 1:length(wheel)
        if(r < wheel(j))
            parents(i) = j;
            break;
        end
    end
end

%Replaces random parent with best performing species
R=rand*nParents;
R1=ceil(R)
for i = 1:length(expectation)
    if expectation(i) == emax
        parents(R1) = i;
    end
end

%Replaces random parent with second best performing species
R=rand*nParents;
R2=ceil(R)

if R2==R1 %Ensures that best performing species replace different parents
    R=rand*nParents;
    R2=ceil(R)
end
```

## Elitist Genetic Algorithm Code

```
close all
clear all
clc
PopNum=28;
rand('twister',sum(100*clock))
nParents=PopNum/2;
A=[9,9, 9, 9, 9, 9, 9, 9];
B=[-4,-4,-4,-4,-4,-4,-4,-4];
numgen=input('Enter the generation worksheet number for your current
population\n')
expectation = xlsread('Population.xls', numgen, 'J3:J86'); %reads fitness
values
parents = elitestroulette(expectation,nParents) %function determines which
%individuals are chosen
%to become parents

OldPop=xlsread('Population.xls', numgen, 'B3:I86')
NewPop=zeros(PopNum,8);
for i = 1:nParents %this for loop places the
n=parents(i); %parents into the next
NewPop(i,:)=OldPop(n,:); %generation of
individuals
end

for k = 1:nParents/2 %loop for each pair of
parents
for i = 1:2 %each parent set makes
two children
for j = 1:8
r=rand;
if(r < .5) %if statement
decides which parent
NewPop(nParents+2*(k-1)+i,j) = NewPop(2*(k-1)+1,j);
%contributes each gene
else
NewPop(nParents+2*(k-1)+i,j) = NewPop(2*(k-1)+2,j);
end
%Below is the mutation function, if the random value is less than the
mutation fraction, the value is mutated to a new random number.
r=rand;
if(r<.2)
r=floor(rand*A(j))-4;
NewPop(nParents+2*(k-1)+i,j) =r;
end
end
end
end
numnewgen=numgen+1
xlswrite('Population.xls', NewPop, numnewgen, 'B3:I30');
```

## Appendix F: Low AoA Generation Data

### Generation #1

Table 5: Generation #1 Data

Chromosome #	Configuration Number								Fitness Function	$\Gamma$ m <sup>2</sup> /s	1/ $\Gamma$ s/m <sup>2</sup>	Min 1/ $\Gamma$
	1	2	3	4	5	6	7	8				
1	-2	-1	0	3	-3	1	3	-4	0.6976	0.118167	8.4626	7.765
2	-1	1	0	-3	-4	3	-1	0	1.454054	0.108471	9.219054	
3	3	3	4	2	1	0	4	1	1.446835	0.108556	9.211835	
4	4	4	-1	-1	-4	0	4	4	1.603822	0.106737	9.368822	
5	-1	-2	2	4	-2	2	0	0	1.405946	0.10904	9.170946	
6	-3	4	1	-4	-2	4	-4	-2	1.244415	0.110995	9.009415	
7	4	4	1	-4	3	0	-2	-4	0	0.128783	7.765	
8	1	-3	2	-4	0	-4	-3	1	1.654211	0.106166	9.419211	
9	-1	4	-4	2	3	2	2	-4	0.857994	0.115969	8.622994	
10	0	-4	4	-1	3	2	-2	-1	0.814272	0.11656	8.579272	
11	-3	-2	-4	2	2	0	3	1	0.919551	0.115147	8.684551	
12	2	2	4	4	2	1	4	0	0.944436	0.114818	8.709436	
13	0	3	-3	-4	4	-2	-2	1	1.766344	0.104917	9.531344	
14	0	2	2	-4	4	3	4	-1	0.929065	0.115021	8.694065	
15	3	4	0	4	-2	2	0	-3	0.417569	0.122211	8.182569	
16	3	0	4	-1	1	-2	-2	0	0.95256	0.114711	8.71756	
17	-1	1	0	1	-4	-3	1	1	1.420604	0.108866	9.185604	
18	-2	3	-4	-1	-3	4	2	4	1.806943	0.104472	9.571943	
19	-2	-2	3	-4	2	3	2	-1	1.306118	0.11024	9.071118	
20	1	-3	4	0	1	2	-2	-4	0.169367	0.126034	7.934367	
21	2	3	-3	-3	2	1	-1	3	1.292561	0.110405	9.057561	
22	-1	-4	4	0	2	-4	-1	-4	0.555921	0.120179	8.320921	
23	1	1	-4	-1	3	-4	1	2	1.537239	0.107501	9.302239	
24	2	-2	-4	-1	-2	1	-1	-3	0.678307	0.118437	8.443307	
25	0	-1	3	0	-3	2	-4	-4	0.505272	0.120915	8.270273	
26	-1	-1	-3	-1	4	4	-3	0	1.144242	0.112243	8.909242	
27	-1	-4	1	2	4	4	2	3	1.56745	0.107153	9.33245	
28	-4	-4	4	4	3	-4	-3	-4	0.44161	0.121853	8.20661	
29	2	-4	0	2	-4	-3	1	2	1.513848	0.107772	9.278848	
30	1	4	1	-1	1	4	1	-1	0.857251	0.115979	8.622251	
31	3	0	4	2	-1	-2	-1	-4	0.272422	0.124418	8.037422	
32	1	-1	3	-4	2	-1	0	-3	0.891959	0.115514	8.656959	
33	3	0	-1	0	-4	2	-2	0	1.069547	0.113192	8.834547	
34	3	3	-1	2	1	0	-4	0	0.95697	0.114653	8.72197	

35	2	-1	-1	1	1	-2	3	3	1.653413	0.106175	9.418413	
36	-3	4	-3	3	-2	-1	0	3	1.199831	0.111547	8.964831	
37	3	4	2	1	3	2	3	3	1.227967	0.111198	8.992967	
38	-4	4	0	0	-2	3	0	-3	0.507941	0.120876	8.272941	
39	1	-4	-1	0	-4	-3	1	1	1.487234	0.108082	9.252234	
40	-2	3	2	4	4	0	-4	4	1.253108	0.110888	9.018108	
41	-3	-1	3	-3	0	-1	-2	4	1.562401	0.107211	9.327401	
42	4	0	-4	2	-1	-2	-3	3	1.330043	0.10995	9.095043	
43	2	1	-1	2	3	-3	-4	0	1.224006	0.111247	8.989006	
44	4	0	0	2	-2	2	-1	3	1.958276	0.102846	9.723276	
45	3	-2	-1	-4	-2	0	-1	-4	0.310718	0.123828	8.075718	
46	0	4	2	2	3	-3	-4	-2	0.696955	0.118176	8.461955	
47	4	2	-3	-2	4	3	1	3	1.450146	0.108517	9.215146	
48	-2	-2	-2	-4	4	2	4	-4	0.483511	0.121234	8.248511	
49	2	0	-2	3	4	1	-2	1	1.405105	0.10905	9.170105	
50	0	-1	2	-3	0	1	2	3	1.781266	0.104753	9.546266	
51	4	-4	4	4	-4	0	0	0	0.868044	0.115834	8.633044	
52	-1	0	4	-3	0	3	-4	-4	0.500009	0.120992	8.265009	
53	4	2	0	-3	4	0	0	-4	0.289318	0.124157	8.054318	
54	-3	-3	3	-4	2	1	-3	0	1.202243	0.111517	8.967243	
55	-3	-4	-4	-4	1	0	0	-1	0.467079	0.121476	8.232079	
56	1	-2	-2	-4	-4	-3	2	-2	1.017716	0.11386	8.782716	
57	0	-2	-3	4	1	2	0	-4	0.289318	0.124157	8.054318	
58	2	2	-4	4	-4	-2	2	-2	0.98651	0.114266	8.75151	
59	-4	2	-4	1	-2	1	-1	-2	0.31829	0.123712	8.08329	
60	-4	2	4	1	4	0	4	4	2.366302	0.098704	10.1313	
61	3	-3	2	-4	-4	4	1	2	1.019259	0.11384	8.784259	
62	-2	1	2	1	2	4	2	3	1.349358	0.109717	9.114358	
63	-1	-4	-3	-1	-2	-4	0	-3	0.81361	0.116569	8.57861	
64	-4	3	2	-2	2	1	0	-2	0.27365	0.124399	8.03865	
65	0	-4	4	0	-3	3	0	-1	0.825032	0.116414	8.590032	
66	3	2	3	-4	4	-4	-3	0	1.007315	0.113995	8.772315	
67	-1	0	4	-2	1	-2	1	-4	0.695595	0.118195	8.460595	
68	0	4	-1	0	0	-3	-3	-1	0.858663	0.11596	8.623663	
69	-4	2	2	-3	1	1	4	3	1.094593	0.112872	8.859593	
70	3	2	4	3	-4	-3	2	-4	0.698387	0.118156	8.463387	
71	0	0	-2	-4	1	-4	0	3	1.639683	0.10633	9.404684	
72	1	-4	-2	3	0	1	2	-2	0.175478	0.125937	7.940478	
73	-4	1	1	1	-2	-2	2	-1	0.492706	0.121099	8.257707	
74	-4	2	-4	-4	-1	4	4	-2	0.029901	0.128289	7.794901	
75	-3	-3	0	4	-2	3	-2	-1	0.618705	0.119279	8.383705	



<b>76</b>	-3	1	0	-2	-2	-4	-1	-4	0.350697	0.123218	8.115697	
<b>77</b>	-1	3	1	2	-2	-3	4	1	0.873861	0.115756	8.638861	
<b>78</b>	-2	3	3	4	-1	-1	1	3	1.123494	0.112505	8.888494	
<b>79</b>	4	-4	-3	3	-2	0	0	1	1.025204	0.113763	8.790204	
<b>80</b>	1	-1	1	1	-4	-1	4	3	1.517982	0.107724	9.282982	
<b>81</b>	-3	-2	1	-3	-4	2	0	-3	0.183999	0.125802	7.948999	
<b>82</b>	-1	-3	1	4	-1	-3	0	-4	0.551216	0.120247	8.316216	
<b>83</b>	2	-4	-4	4	-4	-4	-2	4	1.684384	0.105827	9.449384	
<b>84</b>	3	-1	-1	4	-3	2	0	-4	0.451994	0.121699	8.216994	

## Generation #2

Table 6: Generation #2 Data

Chromosome #	Configuration Number								Fitness Function	$\Gamma$	$1/\Gamma$	Min $1/\Gamma$
	1	2	3	4	5	6	7	8		m/s	s/m	
1	2	2	-4	4	-4	-2	2	-2	0.229683	0.120431	8.30351	8.073827
2	4	0	0	2	-2	2	-1	3	1.388522	0.105682	9.462349	
3	-1	1	0	-3	-4	3	-1	0	0.802438	0.11266	8.876265	
4	1	-1	1	1	-4	-1	4	3	1.127329	0.108682	9.201156	
5	-4	2	4	1	4	0	4	4	1.669628	0.102633	9.743455	
6	0	3	-3	-4	4	-2	-2	1	1.012456	0.110056	9.086283	
7	0	4	-1	0	0	-3	-3	-1	0.487011	0.116811	8.560838	
8	1	1	-4	-1	3	-4	1	2	0.840021	0.112185	8.913848	
9	-1	1	0	-3	-4	3	-1	0	0.765249	0.113134	8.839076	
10	4	4	-1	-1	-4	0	4	4	0.855701	0.111988	8.929528	
11	-3	4	1	-4	-2	4	-4	-2	0.541218	0.116076	8.615045	
12	4	2	-3	-2	4	3	1	3	1.070368	0.109359	9.144195	
13	0	3	-3	-4	4	-2	-2	1	1.245143	0.107308	9.31897	
14	2	-2	-4	-1	-2	1	-1	-3	0.198429	0.120886	8.272257	
15	2	0	0	-3	0	2	-1	-2	0.322126	0.119105	8.395953	
16	4	2	-4	2	-4	2	1	-2	0.134736	0.121824	8.208563	
17	1	1	1	1	0	3	-1	3	0.933234	0.111024	9.007062	
18	-1	-1	1	-3	-1	-1	3	3	1.091404	0.109108	9.165231	
19	-4	2	4	1	4	3	4	4	1.703733	0.102275	9.77756	
20	0	3	4	1	4	0	-2	1	0.747938	0.113356	8.821765	
21	-1	2	-1	-1	3	-4	-3	2	0.810876	0.112553	8.884703	
22	1	1	-4	-1	0	-3	-3	-1	0.67026	0.114363	8.744087	
23	4	-4	4	-1	0	0	-1	0	0.255827	0.120053	8.329654	
24	-4	1	-1	-3	-4	-1	4	4	1.030822	0.109834	9.104649	
25	4	2	-2	-1	-3	3	-4	3	0.756195	0.11325	8.830022	
26	-4	2	-3	-4	4	4	1	3	0.565706	0.115747	8.639533	
27	0	3	-3	-4	-2	-3	-2	-3	0	0.123857	8.073827	
28	0	3	1	-4	3	-2	-2	1	0.822337	0.112408	8.896164	

### Generation #3

Table 7: Generation #3 Data

Chromosome #	Configuration Number								Fitness Function	$\Gamma$	$1/\Gamma$	Min $1/\Gamma$
	1	2	3	4	5	6	7	8		m/s	s/m	
1	4	0	0	2	-2	2	-1	3	1.321952	0.104869	9.535706	8.213755
2	-4	1	-1	-3	-4	-1	4	4	0.633689	0.113027	8.847444	
3	1	1	-4	-1	3	-4	1	2	0.784716	0.111113	8.99847	
4	-1	-1	1	-3	-1	-1	3	3	0.526664	0.114411	8.740418	
5	1	-1	1	1	-4	-1	4	3	0.890894	0.109834	9.104649	
6	-1	1	0	-3	-4	3	-1	0	0.700093	0.112185	8.913848	
7	0	3	-3	-4	4	-2	-2	1	1.031038	0.108169	9.244793	
8	4	0	0	2	-2	2	-1	3	1.307063	0.105033	9.520817	
9	1	1	-4	-1	0	-3	-3	-1	0.438785	0.115573	8.65254	
10	0	3	-3	-4	4	-2	-2	1	0.942581	0.109214	9.156335	
11	-4	1	-1	-3	-4	-1	4	4	0.467178	0.115195	8.680932	
12	-4	2	4	1	4	3	4	4	1.544437	0.102478	9.758192	
13	4	0	0	2	-2	2	-1	3	1.227868	0.105914	9.441622	
14	0	3	4	1	4	0	-2	1	0.592938	0.11355	8.806693	
15	-4	0	-2	-2	-2	2	0	4	0.860573	0.110201	9.074328	
16	-4	1	-1	-3	-2	-1	-1	3	1.142358	0.106882	9.356112	
17	1	-1	1	-1	3	-1	3	2	1.435029	0.10364	9.648784	
18	1	-1	-2	-1	-2	-4	3	3	1.079235	0.107608	9.292989	
19	-1	-1	1	1	-4	-1	-1	3	0.758154	0.111459	8.971909	
20	0	1	1	-3	-4	3	-1	3	0.776868	0.111227	8.990623	
21	3	0	-3	2	4	-2	-2	3	1.007935	0.10844	9.221689	
22	4	0	0	2	-2	-2	-1	1	0.603499	0.113414	8.817254	
23	0	3	-3	-4	0	-2	-1	-1	0.491284	0.114876	8.705038	
24	4	1	-4	-1	4	-2	-2	1	0.873354	0.110046	9.087109	
25	-4	4	-1	1	-1	3	4	2	0.452583	0.115389	8.666337	
26	-4	2	4	-3	-4	3	4	4	0.857363	0.11024	9.071118	
27	4	3	4	1	-4	2	-2	1	0	0.121747	8.213755	
28	4	3	0	1	4	0	-2	3	0.704704	0.112127	8.918459	

## Generation #4

Table 8: Generation #4 Data

Chromosome #	Configuration Number								Fitness Function	$\Gamma$	$1/\Gamma$	Min $1/\Gamma$
	1	2	3	4	5	6	7	8		m/s	s/m	
1	4	1	-4	-1	4	-2	-2	1	0.933322	0.112833	8.862655	7.929334
2	1	-1	1	1	-4	-1	4	3	1.212771	0.109384	9.142105	
3	-4	4	-1	1	-1	3	4	2	0.605638	0.117165	8.534972	
4	1	-1	1	1	-4	-1	4	3	1.151339	0.110124	9.080673	
5	-4	0	-2	-2	-2	2	0	4	0.716025	0.115669	8.645359	
6	3	0	-3	2	4	-2	-2	3	1.16141	0.110002	9.090744	
7	4	0	0	2	-2	2	-1	3	1.307347	0.108264	9.236681	
8	1	-1	-2	-1	-2	-4	3	3	1.306579	0.108273	9.235913	
9	4	0	0	2	-2	2	-1	3	1.307347	0.108264	9.236681	
10	-1	1	0	-3	-4	3	-1	0	0.658412	0.116445	8.587745	
11	0	3	-3	-4	0	-2	-1	-1	0.698496	0.115904	8.62783	
12	4	0	0	2	-2	2	-1	3	1.298312	0.10837	9.227646	
13	3	0	-3	2	4	-2	-2	3	1.152576	0.110109	9.08191	
14	0	3	4	1	4	0	-2	1	0.774644	0.11489	8.703978	
15	4	-2	-4	-1	4	-1	-2	3	1.100338	0.110746	9.029672	
16	4	1	1	3	-4	-1	-2	3	1.409827	0.107076	9.339161	
17	4	-3	-2	1	-1	-1	4	-3	0.348058	0.120811	8.277392	
18	1	4	-1	1	-1	-1	-4	2	0.757858	0.115112	8.687192	
19	3	-2	-2	-2	3	2	-2	4	0.643466	0.116648	8.5728	
20	3	-1	-2	-1	4	-2	0	4	1.520676	0.10582	9.450009	
21	4	-4	-2	-1	-2	3	2	3	0.897103	0.113296	8.826437	
22	1	-1	1	-1	-2	-4	-1	-3	0.368595	0.120512	8.297929	
23	4	0	0	2	-2	3	-1	-1	0.305253	0.121439	8.234587	
24	-1	0	0	-3	-2	2	-1	3	0.93788	0.112775	8.867213	
25	4	3	0	-4	-2	2	1	-4	0	0.126114	7.929334	
26	0	0	0	2	-2	2	-1	3	1.146229	0.110186	9.075563	
27	0	0	-3	2	4	0	-2	1	1.040885	0.11148	8.970219	
28	0	0	4	1	2	0	-2	3	0.523752	0.1183	8.453085	

## Generation #5

Table 9: Generation #5 Data

Chromosome #	Configuration Number								Fitness Function	$\Gamma$	$1/\Gamma$	Min $1/\Gamma$
	1	2	3	4	5	6	7	8		m/s	s/m	
1	4	1	1	3	-4	-1	-2	3	1.579291	0.108293	9.234207	7.654916
2	4	0	0	2	-2	2	-1	3	1.584239	0.108235	9.239156	
3	4	0	0	2	-2	2	-1	3	1.565328	0.108457	9.220244	
4	3	-1	-2	-1	4	-2	0	4	1.893628	0.104728	9.548545	
5	0	0	-3	2	4	0	-2	1	1.531785	0.108853	9.186701	
6	-1	1	0	-3	-4	3	-1	0	1.201695	0.11291	8.856611	
7	4	-4	-2	-1	-2	3	2	3	1.163192	0.113403	8.818109	
8	1	4	-1	1	-1	-1	-4	2	1.148211	0.113596	8.803127	
9	4	-2	-4	-1	4	-1	-2	3	1.380221	0.110679	9.035138	
10	1	-1	1	1	-4	-1	4	3	1.562863	0.108486	9.217779	
11	3	-1	-2	-1	4	-2	0	4	1.863726	0.105057	9.518642	
12	-1	0	0	-3	-2	2	-1	3	1.157986	0.11347	8.812902	
13	4	0	0	2	-2	2	-1	3	1.404778	0.110379	9.059694	
14	3	-1	-2	-1	4	-2	0	4	1.822768	0.105511	9.477685	
15	4	-3	2	3	-4	-1	-2	3	1.463846	0.109664	9.118763	
16	4	0	1	1	-4	2	-1	0	0.419758	0.123844	8.074675	
17	3	0	0	-1	4	2	1	4	1.649833	0.107472	9.304749	
18	4	0	-2	2	4	2	-1	3	1.628152	0.107723	9.283069	
19	0	1	0	2	4	3	-2	0	0.773376	0.118648	8.428292	
20	-1	0	-4	-3	-4	-2	-1	0	1.02353	0.115228	8.678446	
21	4	4	3	-1	-2	-1	-4	2	0.517222	0.122367	8.172138	
22	4	3	-2	-1	-1	3	2	0	0.825841	0.117914	8.480757	
23	4	-2	-4	-1	-4	-4	-2	-2	0.703981	0.119633	8.358898	
24	4	-2	-4	-1	-2	-1	-2	-2	0.766562	0.118744	8.421478	
25	-1	0	2	-3	-2	2	0	-4	0	0.130635	7.654916	
26	-1	0	-2	-1	-2	2	0	3	1.490366	0.109346	9.145282	
27	3	-1	0	4	4	-2	0	4	1.498485	0.109249	9.153402	
28	3	-1	0	-2	4	-2	0	3	1.648188	0.107491	9.303104	

## Generation #6

Table 10: Generation #6 Data

Chromosome #	Configuration Number								Fitness Function	$\Gamma$	$1/\Gamma$	Min $1/\Gamma$
	1	2	3	4	5	6	7	8		m/s	s/m	
1	4	0	0	2	-2	2	-1	3	0.893182	0.109336	9.146118	8.252936
2	0	1	0	2	4	3	-2	0	0.033716	0.120676	8.286652	
3	4	-2	-4	-1	-2	-1	-2	-2	0.043685	0.120531	8.296621	
4	3	-1	-2	-1	4	-2	0	4	1.252587	0.105202	9.505523	
5	4	1	1	3	-4	-1	-2	3	0.983745	0.108264	9.236681	
6	4	0	-2	2	4	2	-1	3	0.897199	0.109288	9.150135	
7	4	-4	-2	-1	-2	3	2	3	0.757859	0.110978	9.010795	
8	3	-1	-2	-1	4	-2	0	4	1.444034	0.103125	9.69697	
9	3	-1	-2	-1	4	-2	0	4	1.346941	0.104168	9.599877	
10	3	-1	0	4	4	-2	0	4	1.061867	0.107356	9.314803	
11	3	-1	-2	-1	4	-2	0	4	1.415065	0.103434	9.668001	
12	1	-1	1	1	-4	-1	4	3	0.955846	0.108592	9.208781	
13	4	-3	2	3	-4	-1	-2	3	0.44007	0.115035	8.693006	
14	4	3	-2	-1	-1	3	2	0	0.155513	0.118928	8.408449	
15	4	-4	0	0	-2	2	-1	3	0.926429	0.10894	9.179365	
16	4	0	0	2	-2	3	-2	3	0.865827	0.109664	9.118763	
17	4	-2	0	-1	4	-2	0	-2	0	0.121169	8.252936	
18	3	-2	-4	-1	3	-1	-1	4	1.002724	0.108042	9.25566	
19	4	0	-3	2	-4	-1	2	1	0.789309	0.110592	9.042245	
20	4	0	-2	0	-4	2	-1	3	1.21694	0.105598	9.469876	
21	-2	-4	-2	-1	-2	3	2	2	0.547944	0.113625	8.80088	
22	3	-1	-2	-1	-2	3	0	4	1.453163	0.103028	9.706099	
23	4	-1	0	-1	4	-2	0	4	1.013531	0.107916	9.266467	
24	3	-1	1	4	4	-2	0	4	0.868239	0.109635	9.121175	
25	3	-1	1	4	4	-1	4	3	0.436445	0.115083	8.689381	
26	1	-1	1	-1	-4	-2	-2	4	1.044287	0.107559	9.297223	
27	4	3	-2	3	0	3	-2	3	0.612784	0.112794	8.86572	
28	4	0	-1	-1	-4	-1	-2	0	0.345516	0.1163	8.598452	

## Generation #7

Table 11: Generation #7 Data

Chromosome #	Configuration Number								Fitness Function	$\Gamma$	1/ $\Gamma$	Min 1/ $\Gamma$
	1	2	3	4	5	6	7	8		m/s	s/m	
1	4	0	-3	2	-4	-1	2	1	0.691296	0.11353	8.808245	8.116949
2	4	0	0	2	-2	2	-1	3	0.949399	0.110298	9.066348	
3	1	-1	1	1	-4	-1	4	3	0.89482	0.110966	9.011769	
4	4	-4	-2	-1	-2	3	2	3	0.513934	0.115863	8.630883	
5	3	-2	-4	-1	3	-1	-1	4	0.989358	0.109814	9.106307	
6	4	0	-2	2	4	2	-1	3	0.982894	0.109892	9.099843	
7	3	-1	-2	-1	4	-2	0	4	0.959932	0.11017	9.076881	
8	1	-1	1	-1	-4	-2	-2	4	0.691994	0.113521	8.808943	
9	3	-1	-2	-1	4	-2	0	4	1.270607	0.106524	9.387556	
10	4	0	-3	2	-4	-1	2	1	0.591046	0.114837	8.707995	
11	4	0	0	2	-2	2	-1	3	0.861162	0.111382	8.978111	
12	3	-2	-4	-1	3	-1	-1	4	0.923253	0.110617	9.040202	
13	4	0	-3	2	-4	-1	2	1	0.580821	0.114972	8.69777	
14	4	0	-3	2	-4	-1	2	1	0.67032	0.113801	8.787269	
15	0	0	1	2	-4	-1	2	1	0	0.123199	8.116949	
16	4	0	-3	2	-4	2	2	3	0.939874	0.110414	9.056823	
17	1	-4	-2	1	-2	3	4	3	0.606542	0.114633	8.723491	
18	4	-1	2	-1	-2	-1	0	2	0.635327	0.114256	8.752276	
19	4	-2	-2	2	3	2	-1	4	0.57568	0.11504	8.692629	
20	4	-2	-2	-1	4	0	1	4	0.540685	0.115505	8.657634	
21	1	-1	1	-1	4	-2	0	4	1.297119	0.106224	9.414068	
22	3	-1	-2	4	-4	0	0	4	0.968509	0.110066	9.085458	
23	3	0	-2	-1	-4	-2	2	1	0.76168	0.11263	8.878629	
24	3	1	-3	4	4	-1	0	4	0.974952	0.109988	9.091901	
25	2	0	-4	-1	-2	-1	-1	3	0.568356	0.115137	8.685305	
26	3	-3	0	2	3	-1	0	3	0.635327	0.114256	8.752276	
27	2	0	-3	2	-4	-3	-1	1	0.566169	0.115166	8.683118	
28	4	0	-3	2	-4	-1	4	3	0.731199	0.113018	8.848148	

## Generation #8

Table 12: Generation #8 Data

Chromosome #	Configuration Number								Fitness Function	$\Gamma$	$1/\Gamma$	Min $1/\Gamma$
	1	2	3	4	5	6	7	8		m/s	s/m	
1	3	-1	-2	-1	4	-2	0	4	1.039303	0.103272	9.683167	8.643864
2	4	0	-2	2	4	2	-1	3	0.95924	0.104133	9.603104	
3	3	-1	-2	4	-4	0	0	4	1.022081	0.103456	9.665945	
4	4	0	0	2	-2	2	-1	3	0.893661	0.104849	9.537525	
5	1	-1	1	1	-4	-1	4	3	0.724168	0.106746	9.368033	
6	1	-4	-2	1	-2	3	4	3	0.567971	0.108556	9.211835	
7	3	-1	-2	-1	4	-2	0	4	1.067514	0.102972	9.711378	
8	3	-2	-4	-1	3	-1	-1	4	0.677625	0.107279	9.321489	
9	4	0	-2	2	4	2	-1	3	0.855067	0.105275	9.498931	
10	1	-1	1	-1	4	-2	0	4	1.253598	0.101036	9.897462	
11	3	1	-3	4	4	-1	0	4	0.964591	0.104075	9.608455	
12	1	-4	-2	1	-2	3	4	3	0.725836	0.106727	9.3697	
13	3	-2	-4	-1	3	-1	-1	4	0.780496	0.106108	9.42436	
14	2	0	-4	-1	-2	-1	-1	3	0.737791	0.106591	9.381655	
15	4	0	-2	2	4	-2	-1	3	0.73436	0.10663	9.378224	
16	3	0	-2	-1	4	3	-1	4	0.440768	0.110076	9.084632	
17	3	-1	0	2	-4	0	0	4	0.687802	0.107162	9.331666	
18	3	0	-2	2	-2	2	-1	4	1.363842	0.099923	10.00771	
19	1	-1	1	1	-2	2	4	3	0.713124	0.106872	9.356988	
20	1	-4	-2	1	2	2	4	-1	0	0.115689	8.643864	
21	3	3	-4	-1	4	-2	-1	1	0.382058	0.110792	9.025922	
22	-1	-1	-2	0	3	-1	-3	4	0.58276	0.108382	9.226624	
23	1	-1	1	2	4	-2	-3	3	0.26149	0.112292	8.905354	
24	4	0	-2	-1	4	0	-2	3	0.389152	0.110705	9.033016	
25	3	1	-2	3	-2	-1	0	3	0.956566	0.104162	9.60043	
26	3	1	0	4	4	-1	0	4	0.941382	0.104327	9.585246	
27	3	-2	-4	-1	3	4	-1	3	0.769407	0.106233	9.413271	
28	3	-2	-4	-4	1	-1	-1	4	0.639118	0.107724	9.282982	



## Generation #9

Table 13: Generation #9 Data

Chromosome #	Configuration Number								Fitness Function	$\Gamma$	$1/\Gamma$	Min $1/\Gamma$
	1	2	3	4	5	6	7	8		m/s	s/m	
1	1	-1	1	-1	4	-2	0	4	1.702909	0.103698	9.643388	7.940478
2	3	-1	-2	-1	4	-2	0	4	1.406364	0.106988	9.346843	
3	4	0	-2	2	4	2	-1	3	1.239476	0.108933	9.179955	
4	-1	-1	-2	0	3	-1	-3	4	0.833376	0.113975	8.773854	
5	3	-1	-2	4	-4	0	0	4	1.335013	0.107811	9.275491	
6	3	-2	-4	-1	3	-1	-1	4	1.363405	0.107482	9.303883	
7	3	-2	-4	-1	3	-1	-1	4	1.278746	0.108469	9.219224	
8	3	3	-4	-1	4	-2	-1	1	0.852045	0.113733	8.792523	
9	3	1	-2	3	-2	-1	0	3	1.289467	0.108343	9.229946	
10	3	1	0	4	4	-1	0	4	1.396241	0.107104	9.336719	
11	4	0	-2	2	4	-2	-1	3	1.169811	0.109766	9.110289	
12	3	0	-2	-1	4	3	-1	4	0.801392	0.114392	8.74187	
13	3	3	-4	-1	4	-2	-1	1	0.725934	0.115388	8.666412	
14	3	-1	-2	4	-4	0	0	4	1.647433	0.104298	9.587912	
15	1	3	-2	-1	4	-2	0	4	1.533166	0.105556	9.473644	
16	2	-1	1	-1	4	3	0	4	1.313469	0.108062	9.253947	
17	-1	-1	-2	0	1	-1	-3	2	1.085526	0.110791	9.026004	
18	-1	-1	-2	2	4	2	-1	3	1.361761	0.107501	9.302239	
19	3	-2	-2	4	3	-1	0	4	1.290319	0.108333	9.230798	
20	3	-1	-2	4	-4	-1	0	4	1.716506	0.103552	9.656984	
21	3	-2	-4	-1	4	-1	-1	4	1.414846	0.106891	9.355325	
22	3	3	-4	-1	3	-2	-1	4	1.446285	0.106533	9.386763	
23	3	1	-2	0	1	-1	0	-4	0	0.125937	7.940478	
24	3	1	0	3	-2	-1	0	4	1.756303	0.103127	9.696782	
25	4	0	-2	-1	-4	-2	-1	4	1.330885	0.107859	9.271364	
26	4	0	-2	-1	4	3	-1	3	0.736838	0.115243	8.677317	
27	1	3	3	4	-4	0	-1	4	0.991124	0.111962	8.931602	
28	-2	3	-2	2	-4	0	-1	4	1.15862	0.109901	9.099098	

## Generation #10

Table 14: Generation #10 Data

Chromosome #	Configuration Number								Fitness Function	$\Gamma$	$1/\Gamma$	Min $1/\Gamma$
	1	2	3	4	5	6	7	8		m/s	s/m	
1	3	1	0	3	-2	-1	0	4	0.66255	0.107269	9.322358	8.659808
2	3	0	-2	-1	4	3	-1	4	0	0.115476	8.659808	
3	3	-1	-2	4	-4	0	0	4	0.527484	0.108846	9.187292	
4	3	1	0	4	4	-1	0	4	0.315161	0.111421	8.974969	
5	1	-1	1	-1	4	-2	0	4	0.910394	0.104491	9.570202	
6	1	-1	1	-1	4	-2	0	4	0.965665	0.103891	9.625473	
7	3	3	-4	-1	3	-2	-1	4	0.227185	0.112524	8.886993	
8	1	-1	1	-1	4	-2	0	4	0.78788	0.105846	9.447688	
9	-1	-1	-2	2	4	2	-1	3	0.331623	0.111217	8.991431	
10	3	3	-4	-1	3	-2	-1	4	0.369293	0.110753	9.029101	
11	3	-1	-2	4	-4	0	0	4	0.615683	0.107811	9.275491	
12	-1	-1	-2	2	4	2	-1	3	0.34174	0.111092	9.001548	
13	4	0	-2	-1	-4	-2	-1	4	0.696304	0.106882	9.356112	
14	3	1	0	3	-2	-1	0	4	0.85657	0.105082	9.516378	
15	1	1	0	-1	4	-3	-1	4	0.435235	0.10995	9.095043	
16	3	1	0	-1	-2	-1	0	4	0.47954	0.109417	9.139348	
17	3	-1	-2	4	4	0	1	4	0.571756	0.108324	9.231565	
18	3	-1	2	4	4	3	2	4	0.645807	0.107462	9.305615	
19	3	-1	1	-1	-1	-2	0	4	0.649099	0.107424	9.308907	
20	1	-3	1	-1	3	-2	0	4	0.746556	0.106311	9.406364	
21	1	-1	-4	-1	3	-2	-1	4	0.563497	0.108421	9.223305	
22	3	-1	4	-1	4	-2	-1	4	0.561881	0.10844	9.221689	
23	3	3	-3	-1	3	-2	-1	4	0.291862	0.111711	8.95167	
24	3	-1	-4	2	3	2	-1	4	0.7844	0.105885	9.444208	
25	-4	-1	-2	4	-4	0	0	3	0.326856	0.111276	8.986664	
26	3	-1	2	4	4	0	0	4	0.227185	0.112524	8.886993	
27	3	0	-2	-1	-4	-2	0	2	0.42004	0.110134	9.079848	
28	3	0	-3	4	-2	-2	-1	4	0.349607	0.110995	9.009415	

## Generation #11

Table 15: Generation #11 Data

Chromosome #	Configuration Number								Fitness Function	$\Gamma$	$1/\Gamma$	Min $1/\Gamma$
	1	2	3	4	5	6	7	8		m/s	s/m	
1	3	-1	-4	2	3	2	-1	4	0.888123	0.102788	9.728762	8.840639
2	3	1	0	3	-2	-1	0	4	1.182515	0.099769	10.02315	
3	4	0	-2	-1	-4	-2	-1	4	0.816252	0.103553	9.656891	
4	1	-1	1	-1	4	-2	0	4	1.496454	0.096739	10.33709	
5	1	-1	1	-1	4	-2	0	4	1.533774	0.096391	10.37441	
6	3	0	-2	-1	-4	-2	0	2	0.97965	0.10183	9.820289	
7	3	1	0	3	-2	-1	0	4	1.153465	0.100059	9.994103	
8	3	-1	-2	4	-4	0	0	4	0.900064	0.102662	9.740702	
9	-1	-1	-2	2	4	2	-1	3	0.519765	0.106833	9.360404	
10	-1	-1	-2	2	4	2	-1	3	0.508738	0.106959	9.349377	
11	3	1	0	4	4	-1	0	4	0.774931	0.103998	9.61557	
12	1	-1	1	-1	4	-2	0	4	1.251095	0.099091	10.09173	
13	3	-1	4	-1	4	-2	-1	4	0.722425	0.104569	9.563064	
14	3	-1	-2	4	-4	0	0	4	1.062509	0.100978	9.903147	
15	3	1	0	3	-2	1	0	4	1.271096	0.098895	10.11173	
16	3	-1	-4	4	3	2	2	4	1.158261	0.100011	9.9989	
17	3	0	1	-1	-4	-2	0	4	0.719774	0.104598	9.560412	
18	4	0	-2	-1	-4	-2	-1	4	1.090045	0.100698	9.930684	
19	3	-1	-2	-1	-4	2	0	4	1.142889	0.100165	9.983527	
20	3	-1	-2	-1	4	-2	0	4	0.989013	0.101733	9.829652	
21	3	2	-1	3	-2	0	0	4	0.762465	0.104133	9.603104	
22	3	-4	-2	4	-2	-3	1	4	0.702985	0.104782	9.543624	
23	-1	-1	-2	2	4	2	-1	3	0.432358	0.10784	9.272997	
24	-1	-1	2	2	4	-1	-1	3	0.31159	0.109263	9.152229	
25	1	1	0	-1	4	4	0	4	0.81448	0.103572	9.655119	
26	3	4	0	0	4	-1	0	4	0.28978	0.109524	9.130419	
27	3	4	4	0	-4	-2	0	4	0	0.113114	8.840639	
28	0	-1	-2	4	4	-1	-2	4	0.759791	0.104162	9.60043	

## Generation #12

Table 16: Generation #12 Data

Chromosome #	Configuration Number								Fitness Function	$\Gamma$	$1/\Gamma$	Min $1/\Gamma$
	1	2	3	4	5	6	7	8		m/s	s/m	
1	1	-1	1	-1	4	-2	0	4	1.703336	0.104133	9.603104	7.899768
2	-1	-1	-2	2	4	2	-1	3	1.091663	0.111217	8.991431	
3	-1	-1	-2	2	4	2	-1	3	1.078344	0.111382	8.978111	
4	-1	-1	-2	2	4	2	-1	3	0.981858	0.112592	8.881626	
5	3	-4	-2	4	-2	-3	1	4	0.926513	0.113298	8.826281	
6	1	-1	1	-1	4	-2	0	4	1.662381	0.104579	9.562149	
7	1	-1	1	-1	4	-2	0	4	1.629759	0.104937	9.529527	
8	-1	-1	-2	2	4	2	-1	3	1.118341	0.110888	9.018108	
9	1	-1	1	-1	4	-2	0	4	1.798895	0.103107	9.698663	
10	3	1	0	3	-2	1	0	4	1.706011	0.104104	9.605779	
11	1	-1	1	-1	4	-2	0	4	1.766177	0.103456	9.665945	
12	1	-1	1	-1	4	-2	0	4	1.779744	0.103311	9.679511	
13	4	0	-2	-1	-4	-2	-1	4	1.546136	0.105866	9.445903	
14	3	-1	-2	-1	4	-2	0	4	1.402471	0.107501	9.302239	
15	-1	-1	1	2	4	2	0	2	0.78916	0.115089	8.688928	
16	1	-1	1	-1	4	-2	4	3	1.496344	0.106427	9.396112	
17	-1	-1	2	2	4	2	-2	3	0.850517	0.114282	8.750284	
18	-1	-1	-2	2	-4	2	1	3	1.394085	0.107598	9.293853	
19	3	-4	-2	4	-2	-3	0	-4	0	0.126586	7.899768	
20	3	-2	-2	-1	4	-3	0	4	1.374863	0.107821	9.274631	
21	1	-1	-2	2	4	-2	-1	4	1.419202	0.107308	9.31897	
22	1	0	-2	2	4	-2	0	4	1.900023	0.102043	9.79979	
23	3	1	1	-1	4	1	0	4	1.196103	0.10994	9.09587	
24	2	-1	0	3	-2	-2	1	4	1.61317	0.10512	9.512938	
25	1	-1	1	-1	4	-2	0	4	1.725705	0.103891	9.625473	
26	1	-1	1	4	4	-4	0	4	1.368245	0.107898	9.268012	
27	3	2	-2	-1	4	-2	-1	4	1.161815	0.110356	9.061583	
28	4	0	2	-1	-4	-2	-1	4	1.047257	0.111769	8.947025	

## Generation #13

Table 17: Generation #13 Data

Chromosome #	Configuration Number								Fitness Function	$\Gamma$	$1/\Gamma$	Min $1/\Gamma$
	1	2	3	4	5	6	7	8		m/s	s/m	
1	1	-1	1	-1	4	-2	4	3	1.561291	0.10784	9.272997	7.711706
2	1	0	-2	2	4	-2	0	4	2.00609	0.102904	9.717795	
3	1	-1	1	-1	4	-2	0	4	1.966963	0.10332	9.678668	
4	1	0	-2	2	4	-2	0	4	1.867297	0.104395	9.579003	
5	3	-1	-2	-1	4	-2	0	4	1.597201	0.107424	9.308907	
6	1	-1	1	-1	4	-2	0	4	1.93531	0.103659	9.647016	
7	-1	-1	1	2	4	2	0	2	0.809593	0.117353	8.521299	
8	1	-1	1	4	4	-4	0	4	1.288303	0.111111	9.000009	
9	-1	-1	-2	2	4	2	-1	3	1.149379	0.112853	8.861085	
10	-1	-1	-2	2	4	2	-1	3	1.153936	0.112795	8.865641	
11	3	-1	-2	-1	4	-2	0	4	1.455962	0.109079	9.167667	
12	-1	-1	-2	2	-4	2	1	3	1.608133	0.107298	9.319838	
13	1	0	-2	2	4	-2	0	4	1.749838	0.105691	9.461544	
14	1	-1	1	-1	4	-2	0	4	1.873541	0.104327	9.585246	
15	1	3	-2	2	4	-2	4	-3	0.735025	0.118389	8.446731	
16	1	1	-2	3	4	-2	0	4	1.412299	0.109601	9.124004	
17	1	0	-2	-1	4	-2	0	1	1.333975	0.11055	9.045681	
18	1	0	-2	-1	4	-2	0	2	1.501742	0.108537	9.213448	
19	-2	2	-1	-1	4	-2	0	4	1.039804	0.114266	8.75151	
20	3	-2	-2	-1	-2	-2	0	4	1.324493	0.110666	9.036199	
21	-4	-1	1	4	-3	-4	0	2	1.395348	0.109805	9.107053	
22	-1	-1	1	4	4	2	-2	-2	0	0.129673	7.711706	
23	-1	-1	3	2	4	2	-1	3	1.005094	0.114721	8.7168	
24	-1	-1	-2	2	4	0	-1	3	1.23684	0.11175	8.948546	
25	3	-2	-2	-1	4	2	0	4	1.051691	0.114111	8.763397	
26	3	-1	-2	-1	-4	-2	0	3	1.637671	0.106959	9.349377	
27	1	-1	-2	2	4	-2	0	-1	1.041259	0.114247	8.752965	
28	1	-3	1	2	4	-2	1	4	1.681847	0.106456	9.393552	

## Generation #14

Table 18: Generation #14 Data

Chromosome #	Configuration Number								Fitness Function	$\Gamma$	$1/\Gamma$	Min $1/\Gamma$
	1	2	3	4	5	6	7	8		m/s	s/m	
1	1	0	-2	2	4	-2	0	4	1.452848	0.106272	9.409816	7.956969
2	-1	-1	-2	2	-4	2	1	3	1.166203	0.109611	9.123172	
3	3	-1	-2	-1	-4	-2	0	3	1.308553	0.107927	9.265522	
4	1	-3	1	2	4	-2	1	4	1.120489	0.110163	9.077458	
5	3	-1	-2	-1	4	-2	0	4	1.004809	0.111585	8.961778	
6	3	-1	-2	-1	4	-2	0	4	1.114972	0.11023	9.07194	
7	1	-1	1	-1	4	-2	0	4	1.574375	0.104917	9.531344	
8	1	1	-2	3	4	-2	0	4	1.457986	0.106214	9.414955	
9	-1	-1	-2	2	4	2	-1	3	1.122879	0.110134	9.079848	
10	1	-1	1	-1	4	-2	0	4	1.871717	0.101743	9.828686	
11	-1	-1	-2	2	4	2	-1	3	1.003203	0.111605	8.960172	
12	1	3	-2	2	4	-2	4	-3	0.36326	0.120189	8.320229	
13	1	0	-2	2	4	-2	0	4	1.663966	0.10394	9.620935	
14	1	-3	1	2	4	-2	1	4	1.29364	0.108101	9.250608	
15	-3	0	-2	-2	-2	-2	0	3	0.818348	0.113956	8.775317	
16	0	-1	-2	2	-4	2	1	4	1.508874	0.105643	9.465843	
17	-1	-1	1	-1	3	0	0	4	1.039882	0.11115	8.996851	
18	3	-3	-2	2	-4	-2	-3	4	1.025013	0.111334	8.981982	
19	3	-3	-2	-1	4	-2	0	4	0.882888	0.113124	8.839857	
20	3	-1	0	-1	4	-2	0	4	1.091904	0.110511	9.048873	
21	1	1	-2	3	4	-2	0	4	1.281248	0.108246	9.238217	
22	1	-1	-2	-1	4	-2	0	4	1.218858	0.108982	9.175827	
23	-1	-1	1	-1	4	-2	-3	-3	0	0.125676	7.956969	
24	1	0	-2	-1	4	-2	0	3	1.433143	0.106495	9.390112	
25	1	-1	-2	-3	4	-2	4	3	1.206666	0.109127	9.163635	
26	-1	-2	-2	2	4	2	4	-2	0.184961	0.122821	8.14193	
27	-2	0	-2	2	3	-2	0	4	1.138902	0.10994	9.09587	
28	1	0	1	2	-1	-2	0	4	0.861762	0.113395	8.818731	

## Generation #15

Table 19: Generation #15 Data

Chromosome #	Configuration Number								Fitness Function	$\Gamma$	$1/\Gamma$	Min $1/\Gamma$
	1	2	3	4	5	6	7	8		m/s	s/m	
1	1	0	-2	2	4	-2	0	4	1.64459	0.103398	9.671367	8.026777
2	-1	-1	-2	2	4	2	-1	3	0.880163	0.112272	8.90694	
3	1	-1	1	-1	4	-2	0	4	1.754513	0.102236	9.78129	
4	3	-1	0	-1	4	-2	0	4	1.165413	0.108788	9.19219	
5	1	0	1	2	-1	-2	0	4	0.857137	0.112563	8.883914	
6	1	-1	1	-1	4	-2	0	4	1.70653	0.10274	9.733307	
7	1	1	-2	3	4	-2	0	4	1.232911	0.107995	9.259688	
8	1	-1	1	-1	4	-2	0	4	1.675461	0.103069	9.702238	
9	1	-1	-2	-1	4	-2	0	4	1.377022	0.10634	9.403799	
10	-1	-1	-2	2	4	2	-1	3	0.971693	0.11113	8.99847	
11	3	-1	-2	-1	-4	-2	0	3	1.214684	0.108208	9.241461	
12	1	-1	1	-1	4	-2	0	4	1.766487	0.102111	9.793264	
13	-2	0	-2	2	3	-2	0	4	1.127127	0.109243	9.153905	
14	0	-1	-2	2	-4	2	1	4	1.403626	0.10604	9.430404	
15	-1	0	0	-3	4	-2	0	1	0.367837	0.119124	8.394614	
16	-1	-1	-2	2	4	2	-1	4	0.95214	0.111372	8.978918	
17	3	-1	1	-1	4	-2	0	4	1.318318	0.107008	9.345096	
18	3	-1	0	-1	2	-3	0	4	1.306544	0.107143	9.333321	
19	1	-1	4	-4	-1	-2	0	4	1.712028	0.102682	9.738805	
20	1	0	1	2	4	-2	0	4	1.307415	0.107133	9.334192	
21	1	-1	1	-1	4	-2	0	4	1.859237	0.101153	9.886014	
22	1	-1	-2	-1	4	-2	0	4	1.475584	0.105237	9.502361	
23	-1	1	-2	2	4	3	0	2	0.885481	0.112205	8.912259	
24	1	3	-2	1	4	-2	-1	3	1.031604	0.110395	9.058381	
25	1	2	1	-1	4	-2	0	4	1.383039	0.106272	9.409816	
26	3	-1	1	-1	-4	-2	0	-4	0	0.124583	8.026777	
27	-2	0	-2	2	3	-2	2	4	1.546082	0.104462	9.572859	
28	-2	0	-2	2	3	-2	1	-3	0.058408	0.123683	8.085186	

## Generation #16

Table 20: Generation #16 Data

Chromosome #	Configuration Number								Fitness Function	$\Gamma$	$1/\Gamma$	Min $1/\Gamma$
	1	2	3	4	5	6	7	8		m/s	s/m	
1	1	-1	1	-1	4	-2	0	4	1.054924	0.103766	9.637068	8.582144
2	3	-1	1	-1	4	-2	0	4	0.852619	0.105991	9.434763	
3	1	2	1	-1	4	-2	0	4	0.711709	0.107598	9.293853	
4	1	-1	1	-1	4	-2	0	4	1.033426	0.103998	9.61557	
5	-2	0	-2	2	3	-2	2	4	0.71923	0.107511	9.301374	
6	1	-1	-2	-1	4	-2	0	4	0.857785	0.105933	9.439929	
7	1	-1	1	-1	4	-2	0	4	0.99154	0.104453	9.573684	
8	1	-1	1	-1	4	-2	0	4	1.006687	0.104288	9.588831	
9	1	0	-2	2	4	-2	0	4	0.927266	0.105159	9.50941	
10	1	-1	1	-1	4	-2	0	4	1.129234	0.102972	9.711378	
11	1	-1	-2	-1	4	-2	0	4	0.888898	0.105585	9.471042	
12	3	-1	0	-1	2	-3	0	4	0.68922	0.107859	9.271364	
13	1	2	1	-1	4	-2	0	4	0.616557	0.108711	9.198701	
14	-2	0	-2	2	3	-2	2	4	0.722605	0.107472	9.304749	
15	1	1	1	-1	4	-2	0	4	0.797751	0.106611	9.379895	
16	3	-1	1	-1	4	-2	0	4	0.805412	0.106524	9.387556	
17	-2	2	1	-1	4	-2	0	4	0.357922	0.111856	8.940066	
18	1	-1	1	-1	4	-2	0	4	1.033426	0.103998	9.61557	
19	-2	0	-4	-1	3	-2	0	4	0.71923	0.107511	9.301374	
20	4	-4	-2	-1	3	-2	0	4	0.50893	0.109998	9.091074	
21	1	-1	1	-1	-1	-2	0	4	0.736044	0.107317	9.318188	
22	1	1	1	-1	4	-2	4	3	0.478617	0.110366	9.060761	
23	1	0	-2	-1	4	-2	0	4	0.862064	0.105885	9.444208	
24	1	1	-2	-1	4	-4	0	4	0.537035	0.109659	9.119179	
25	1	-1	0	-1	4	-3	0	4	0.560379	0.109379	9.142523	
26	1	-1	-2	-1	-2	-4	-4	4	0	0.116521	8.582144	
27	-1	0	-2	2	3	-2	0	4	0.410824	0.111198	8.992967	
28	4	-4	-2	2	4	-2	2	4	0.318613	0.11235	8.900757	



## Generation #17

Table 21: Generation #17 Data

Chromosome #	Configuration Number								Fitness Function	$\Gamma$	$1/\Gamma$	Min $1/\Gamma$
	1	2	3	4	5	6	7	8		m/s	s/m	
1	3	-1	1	-1	4	-2	0	4	1.045617	0.106572	9.383328	8.337711
2	3	-1	0	-1	2	-3	0	4	0.906228	0.108179	9.243938	
3	-2	0	-2	2	3	-2	2	4	0.893854	0.108324	9.231565	
4	1	1	-2	-1	4	-4	0	4	0.756588	0.109959	9.094299	
5	1	-1	0	-1	4	-3	0	4	0.841401	0.108943	9.179112	
6	1	-1	1	-1	4	-2	0	4	1.331879	0.103417	9.66959	
7	1	-1	1	-1	4	-2	0	4	1.300286	0.103756	9.637997	
8	3	-1	1	-1	4	-2	0	4	1.154188	0.105353	9.491899	
9	1	-1	1	-1	4	-2	0	4	1.499968	0.10165	9.837678	
10	1	0	-2	2	4	-2	0	4	0.959512	0.107559	9.297223	
11	3	-1	0	-1	2	-3	0	4	0.900506	0.108246	9.238217	
12	3	-1	1	-1	4	-2	0	4	1.261798	0.104172	9.599509	
13	1	-1	1	-1	4	-2	0	4	1.573976	0.100891	9.911687	
14	3	-1	0	-1	2	-3	0	4	1.025235	0.106804	9.362945	
15	3	-1	2	-1	2	-3	0	4	1.273423	0.104046	9.611134	
16	2	3	1	-1	2	-2	-4	4	0	0.119937	8.337711	
17	1	0	-2	3	-1	-2	2	4	1.349114	0.103233	9.686825	
18	1	-4	2	2	-4	0	2	4	0.898032	0.108275	9.235742	
19	-2	-1	1	-1	4	-1	0	4	0.381293	0.114692	8.719004	
20	1	-1	-4	-1	4	-2	0	4	1.133332	0.105585	9.471042	
21	1	-3	4	-1	4	-2	0	4	1.335527	0.103378	9.673238	
22	1	-1	1	-1	0	3	0	-1	0.267327	0.116211	8.605037	
23	-3	0	1	-1	4	-2	0	-1	0.08909	0.118669	8.426801	
24	1	-3	1	-1	4	-2	0	-1	0.303987	0.115718	8.641698	
25	3	3	1	-1	4	-2	0	4	0.874973	0.108546	9.212684	
26	3	-1	0	-1	4	-2	0	-2	0.017485	0.119686	8.355196	
27	-1	-1	0	-1	4	-3	0	4	0.436836	0.113966	8.774547	
28	1	-1	1	-1	4	-2	0	0	0.412344	0.114285	8.750055	

## Appendix G: High AoA Generation Data

### Generation #1

Table 22: Generation #1 Data

Chromosome #	Configuration Number								Fitness Function	$\Gamma$	$1/\Gamma$	Min $1/\Gamma$
	1	2	3	4	5	6	7	8		m/s	s/m	
1	4	-4	-4	-3	-3	2	3	-4	0.608723	0.150984	6.623218	6.014495
2	3	-3	1	0	1	2	2	2	0.68473	0.149271	6.699225	
3	4	-1	2	-4	2	3	0	-2	0.662231	0.149774	6.676726	
4	3	-4	-2	0	-4	1	-3	-4	0.415836	0.155513	6.430331	
5	3	4	-2	3	0	-2	0	-2	0.218792	0.160429	6.233287	
6	1	-1	-4	-2	-2	2	3	0	0.897167	0.144683	6.911662	
7	-2	1	-4	0	-3	2	0	0	1.170136	0.139186	7.184631	
8	-2	-2	1	-3	-4	4	1	-3	0.82213	0.146271	6.836625	
9	-2	-2	3	3	-2	4	-3	-1	0.81494	0.146425	6.829435	
10	-3	3	-3	-4	3	-3	4	-3	1.020921	0.142138	7.035416	
11	4	3	3	-4	1	2	-4	0	0.703452	0.148855	6.717947	
12	-3	1	2	2	-3	-2	0	-4	0.591398	0.15138	6.605892	
13	-4	2	3	4	-4	3	2	-4	0.743906	0.147964	6.758401	
14	3	4	1	-4	-4	1	0	4	0.962509	0.143328	6.977004	
15	0	-3	0	4	-3	4	2	3	1.477489	0.133476	7.491984	
16	1	-3	-4	1	1	-3	-1	1	1.10031	0.140552	7.114804	
17	2	2	1	-3	1	-2	0	-2	0.321195	0.157836	6.33569	
18	0	2	-3	4	3	4	-3	-1	0.708285	0.148748	6.722779	
19	-3	-1	-4	-3	-4	-2	-1	2	1.245349	0.137744	7.259844	
20	-4	4	1	1	2	-2	-2	2	0.848028	0.145719	6.862523	
21	4	4	-1	-2	-4	-4	2	4	0.969087	0.143193	6.983582	
22	0	3	-2	0	2	2	0	0	0.548994	0.152358	6.563489	
23	-4	0	-4	1	3	0	0	1	1.04835	0.141586	7.062845	
24	-1	-1	1	-1	1	1	-2	-4	0.10688	0.163362	6.121375	
25	-2	-4	-1	3	-4	1	-3	-1	0.950749	0.14357	6.965243	
26	0	-2	-1	-4	3	2	-2	1	1.114105	0.14028	7.1286	
27	2	-4	-3	-2	-4	3	-4	-3	0.469496	0.154226	6.483991	
28	-4	-4	-1	0	3	0	-1	-3	0.20155	0.160874	6.216045	
29	-2	4	1	-1	-3	-2	3	-3	0.81494	0.146425	6.829435	
30	4	-2	-2	2	1	-3	-4	3	0.767833	0.147442	6.782328	
31	-2	-4	-4	0	1	2	0	1	0.868149	0.145293	6.882644	
32	4	-3	1	1	1	-2	1	1	0.692998	0.149087	6.707493	
33	-1	-2	4	-4	3	0	-1	1	1.156637	0.139448	7.171132	

34	3	3	-4	-4	-2	2	-2	1	0.710048	0.148709	6.724543
35	4	3	-2	2	-3	-3	-4	-4	0	0.166265	6.014495
36	0	-3	-2	3	-2	4	-2	-2	0.905968	0.144499	6.920463
37	4	-4	3	0	-4	1	1	3	1.176128	0.13907	7.190623
38	-3	1	-1	-2	-4	-1	-2	-4	0.46584	0.154313	6.480335
39	-2	1	2	-2	-2	-2	-1	-2	0.432709	0.155106	6.447204
40	3	-4	3	0	-2	4	1	-1	0.68994	0.149155	6.704435
41	2	4	1	4	3	-4	0	3	0.835759	0.14598	6.850253
42	2	-3	0	0	1	-1	2	4	1.1457	0.139661	7.160195
43	3	-4	3	-3	4	0	2	2	1.08178	0.140919	7.096275
44	0	0	3	3	4	1	-3	-2	0.349703	0.157129	6.364198
45	-1	3	-4	4	-4	3	3	-3	0.921761	0.14417	6.936256
46	-1	0	-4	-2	-4	0	-4	4	1.062345	0.141306	7.07684
47	2	1	0	1	-2	-3	1	2	0.84257	0.145835	6.857064
48	2	3	-3	3	2	-3	0	4	1.166627	0.139254	7.181122
49	0	4	0	2	0	-2	-2	0	0.576637	0.151719	6.591132
50	4	-3	-3	-2	-2	-4	-3	-4	0.194063	0.161068	6.208558
51	3	-2	-3	4	-4	3	4	4	1.48997	0.133254	7.504465
52	-1	-4	0	-1	2	1	-4	1	0.882865	0.144983	6.89736
53	2	3	-2	2	3	-3	-2	-3	0.14815	0.162268	6.162645
54	3	-2	4	-2	3	2	-2	3	1.16065	0.13937	7.175145
55	2	-4	4	-1	1	4	-2	3	1.044461	0.141664	7.058956
56	2	4	-1	2	1	-4	-3	4	0.740345	0.148042	6.75484
57	3	-1	3	4	-2	-2	2	-4	0.545248	0.152445	6.559743
58	1	0	2	4	-1	-1	-2	2	0.767419	0.147451	6.781914
59	2	-4	1	-1	-2	-4	0	4	1.34933	0.135799	7.363824
60	-3	-2	1	-4	1	1	3	-2	0.68473	0.149271	6.699225
61	-4	4	0	4	-2	-2	1	-1	0.833929	0.146019	6.848424
62	1	4	-1	-1	4	-4	-3	0	0.858074	0.145506	6.872569
63	-2	-2	4	4	-4	1	2	-2	0.83346	0.146029	6.847955
64	1	-1	-2	2	0	-1	4	-3	0.962947	0.143319	6.977442
65	-1	-2	2	2	-3	-3	0	0	0.953563	0.143512	6.968058
66	-2	-2	-2	3	-1	-4	0	0	1.190168	0.138799	7.204663
67	-3	-1	4	-1	1	2	2	-2	0.519531	0.153045	6.534026
68	3	4	0	3	-4	-3	-1	-3	0.338745	0.1574	6.35324
69	4	2	0	1	1	4	4	1	0.690839	0.149135	6.705334
70	4	2	-1	2	0	-4	-2	0	0.465463	0.154322	6.479957
71	-2	-4	2	2	3	-2	4	0	0.79332	0.14689	6.807815
72	2	-2	3	2	4	1	0	3	1.015184	0.142254	7.029679
73	-1	-2	-4	4	-1	3	3	2	1.244822	0.137754	7.259317
74	2	0	-4	-2	1	4	1	-3	0.739022	0.148071	6.753517

<b>75</b>	-1	0	4	-3	-2	0	-4	1	1.08178	0.140919	7.096275	
<b>76</b>	3	-1	-4	3	-1	-4	1	3	1.35405	0.135712	7.368545	
<b>77</b>	3	0	1	-2	2	-4	0	4	1.188663	0.138828	7.203158	
<b>78</b>	-2	-1	1	2	1	2	-4	4	0.843933	0.145806	6.858428	
<b>79</b>	-1	3	-1	-1	-2	1	-1	1	1.002753	0.142506	7.017248	
<b>80</b>	-4	2	-1	3	-1	0	4	2	1.313284	0.136467	7.327779	
<b>81</b>	-1	-1	1	-4	-2	-4	-3	-4	0.368959	0.156655	6.383454	
<b>82</b>	3	1	0	-2	-4	-4	2	3	1.094493	0.140667	7.108988	
<b>83</b>	1	3	2	3	0	0	4	0	0.526968	0.152871	6.541463	
<b>84</b>	-2	3	4	1	4	-4	-2	4	1.401647	0.134841	7.416142	

## Generation #2

Table 23: Generation #2 Data

Chromosome #	Configuration Number								Fitness Function	$\Gamma$	$1/\Gamma$	Min $1/\Gamma$
	1	2	3	4	5	6	7	8		m/s	s/m	
1	-1	-4	0	-1	2	1	-4	1	0.256575	0.145864	6.855707	6.599132
2	0	-3	0	4	-3	4	2	3	0.909168	0.133186	7.5083	
3	3	-2	-3	4	-4	3	4	4	1.118916	0.129566	7.718048	
4	4	-1	2	-4	2	3	0	-2	0.127154	0.14867	6.726286	
5	2	0	-4	-2	1	4	1	-3	0.128906	0.148632	6.728038	
6	-1	0	-4	-2	-4	0	-4	4	0.499118	0.14088	7.098249	
7	-1	3	-1	-1	-2	1	-1	1	0.454538	0.14177	7.05367	
8	1	-1	-4	-2	-2	2	3	0	0.633769	0.138257	7.2329	
9	2	-4	4	-1	1	4	-2	3	0.455983	0.141741	7.055115	
10	-2	-2	1	-3	-4	4	1	-3	0.448765	0.141886	7.047897	
11	4	-4	3	0	-4	1	1	3	0.665296	0.137657	7.264428	
12	4	-3	1	1	1	-2	1	1	0.190802	0.147277	6.789934	
13	-2	-1	1	2	1	2	-4	4	0.232552	0.146377	6.831683	
14	-4	4	1	1	2	-2	-2	2	0.47482	0.141364	7.073952	
15	-1	-4	0	-1	2	4	-4	3	0.658153	0.137793	7.257285	
16	0	2	0	4	-3	0	2	1	0.443481	0.141993	7.042613	
17	3	0	2	2	-4	3	4	-2	0.012668	0.151245	6.6118	
18	4	-2	-3	4	-4	3	4	4	0.947554	0.132508	7.546686	
19	2	0	-4	-2	-4	4	-4	-4	0.074588	0.149841	6.67372	
20	3	0	2	-1	1	4	1	4	0.763121	0.135828	7.362253	
21	1	3	-1	-1	-2	1	-1	0	0	0.151535	6.599132	
22	1	0	-4	-1	-2	2	3	1	0.652041	0.137909	7.251173	
23	-2	-2	1	-1	1	4	0	3	0.934898	0.132731	7.53403	
24	-2	-4	1	-3	-4	4	1	3	1.054885	0.13065	7.654017	
25	4	-3	3	1	1	1	-1	1	0.203766	0.146996	6.802897	
26	4	-4	4	4	-4	1	1	3	0.869551	0.133892	7.468682	
27	-4	4	1	2	1	2	-4	4	0.512308	0.140619	7.111439	
28	-4	4	1	2	1	1	-4	0	0.249759	0.146009	6.84889	

### Generation #3

Table 24: Generation #3 Data

Chromosome #	Configuration Number								Fitness Function	$\Gamma$	$1/\Gamma$	Min $1/\Gamma$
	1	2	3	4	5	6	7	8		m/s	s/m	
1	2	-4	4	-1	1	4	-2	3	0.709694	0.14178	7.053181	6.343487
2	-2	-1	1	2	1	2	-4	4	0.304477	0.150422	6.647964	
3	1	0	-4	-1	-2	2	3	1	0.794985	0.140086	7.138472	
4	-2	-2	1	-1	1	4	0	3	0.923479	0.137609	7.266967	
5	-1	3	-1	-1	-2	1	-1	1	0.609552	0.143822	6.953039	
6	-2	-2	1	-1	1	4	0	3	0.971855	0.136699	7.315342	
7	1	-1	-4	-2	-2	2	3	0	0.61749	0.143658	6.960977	
8	3	-2	-3	4	-4	3	4	4	1.328107	0.130351	7.671594	
9	-2	-4	1	-3	-4	4	1	3	1.328696	0.130341	7.672183	
10	-2	-4	1	-3	-4	4	1	3	1.349294	0.129992	7.692781	
11	-1	-4	0	-1	2	1	-4	1	0.489541	0.146348	6.833028	
12	-2	-4	1	-3	-4	4	1	3	1.38204	0.129441	7.725527	
13	1	-1	-4	-2	-2	2	3	0	0.61938	0.143619	6.962867	
14	3	0	2	-1	1	4	1	4	0.836655	0.139273	7.180143	
15	-2	-1	1	-1	1	2	-2	4	0.402558	0.148235	6.746045	
16	-2	-4	1	2	1	4	-2	3	1.051431	0.135228	7.394918	
17	-2	0	-4	-1	1	2	0	3	0.958928	0.136941	7.302415	
18	0	0	1	-1	-3	2	0	0	0.232129	0.152077	6.575616	
19	-2	3	1	-1	1	3	-1	-4	0	0.157642	6.343487	
20	4	3	2	-1	1	-2	3	1	0.176948	0.153364	6.520435	
21	3	-1	-3	-2	-2	2	4	2	0.80136	0.139961	7.144847	
22	3	-2	-4	4	-2	3	4	0	0.731901	0.141335	7.075388	
23	-2	-4	-4	1	-4	4	1	3	1.463767	0.128086	7.807255	
24	-2	-4	1	0	-4	4	1	2	1.040347	0.135431	7.383834	
25	2	-4	1	-3	-4	1	3	1	0.965653	0.136815	7.30914	
26	-2	-4	1	-1	-4	1	3	1	1.045093	0.135344	7.38858	
27	3	-1	2	-2	-2	2	3	4	0.877251	0.13849	7.220738	
28	3	-1	2	-1	-2	2	-3	0	0.483663	0.146474	6.82715	

## Generation #4

Table 25: Generation #4 Data

Chromosome #	Configuration Number								Fitness Function	$\Gamma$	$1/\Gamma$	Min $1/\Gamma$
	1	2	3	4	5	6	7	8		m/s	s/m	
1	2	-4	1	-3	-4	1	3	1	0.561749	0.136651	7.317912	6.756163
2	-2	-4	1	-3	-4	4	1	3	0.856678	0.131357	7.612841	
3	3	-1	2	-2	-2	2	3	4	0.582532	0.136264	7.338695	
4	3	-2	-3	4	-4	3	4	4	0.944615	0.129857	7.700779	
5	-2	-4	1	-1	-4	1	3	1	0.612382	0.135712	7.368545	
6	-2	-4	-4	1	-4	4	1	3	0.938334	0.129963	7.694498	
7	3	-1	2	-2	-2	2	3	4	0.558109	0.136719	7.314272	
8	-2	-1	1	-1	1	2	-2	4	0.181007	0.144151	6.93717	
9	-2	-4	1	-3	-4	4	1	3	0.941177	0.129915	7.697341	
10	-2	-4	1	-3	-4	4	1	3	0.927456	0.130147	7.683619	
11	3	-2	-3	4	-4	3	4	4	0.948056	0.129799	7.70422	
12	-2	-4	-4	1	-4	4	1	3	1.084268	0.127544	7.840432	
13	3	-2	-4	4	-2	3	4	0	0.270651	0.142312	7.026814	
14	-1	-4	0	-1	2	1	-4	1	0.038654	0.147171	6.794817	
15	-2	-4	1	4	-4	1	1	1	0.810423	0.13216	7.566586	
16	1	-3	1	-3	1	4	3	3	0.72713	0.133631	7.483294	
17	3	-1	2	4	-2	2	3	4	0.523605	0.137367	7.279769	
18	3	-1	-3	4	-2	3	4	-2	0.368526	0.140357	7.124689	
19	-2	-4	1	1	4	1	1	1	0.188474	0.143996	6.944637	
20	4	-4	-4	1	-4	1	1	1	0.608692	0.13578	7.364855	
21	-4	-1	0	-1	-2	2	1	4	0.814261	0.132093	7.570424	
22	3	1	1	2	1	-4	3	4	0.063351	0.146638	6.819515	
23	-2	2	1	-3	-4	-1	3	3	0.647241	0.135073	7.403404	
24	-2	1	1	-3	-4	4	1	3	0.717902	0.133796	7.474065	
25	3	-4	-4	1	-4	3	4	3	0.727634	0.133622	7.483798	
26	-2	-4	-4	4	4	2	1	3	0.594022	0.136051	7.350185	
27	-4	-2	4	4	-2	1	-4	-1	0	0.148013	6.756163	
28	3	-2	1	4	-2	-3	-4	0	0.055687	0.146803	6.81185	

Generation #5

Chromosome #	Configuration Number								Fitness Function	$\Gamma$	$1/\Gamma$	Min $1/\Gamma$
	1	2	3	4	5	6	7	8		m/s	s/m	
1	1	-3	1	-3	1	4	3	3	1.108819	0.131357	7.612841	6.504023
2	4	-4	-4	1	-4	1	1	1	0.911074	0.13486	7.415097	
3	3	-2	-3	4	-4	3	4	4	1.192725	0.129925	7.696748	
4	2	-4	1	-3	-4	1	3	1	0.880302	0.135422	7.384325	
5	-2	-4	1	-3	-4	4	1	3	1.169868	0.130312	7.67389	
6	-2	-4	-4	1	-4	4	1	3	1.31208	0.127941	7.816103	
7	-2	-4	1	4	-4	1	1	1	1.096494	0.13157	7.600517	
8	3	-1	-3	4	-2	3	4	-2	0.640365	0.13997	7.144388	
9	2	-4	1	-3	-4	1	3	1	0.880847	0.135412	7.38487	
10	3	-2	-4	4	-2	3	4	0	0.744613	0.137957	7.248635	
11	-2	-4	-4	1	-4	4	1	3	1.339976	0.127486	7.843999	
12	3	-2	-3	4	-4	3	4	4	1.249358	0.128976	7.75338	
13	3	-2	-3	4	-4	3	4	4	1.246413	0.129025	7.750436	
14	-2	-4	1	-3	-4	4	1	3	1.113864	0.13127	7.617887	
15	4	-4	-4	-3	-4	4	3	-4	0	0.153751	6.504023	
16	1	3	-3	-3	-4	4	1	4	0.620159	0.140367	7.124182	
17	3	-4	1	4	-4	1	4	4	1.188758	0.129992	7.692781	
18	3	-4	1	4	-4	3	3	4	1.042634	0.132509	7.546657	
19	-2	-3	1	-3	-4	4	1	3	1.161926	0.130447	7.665949	
20	-2	-4	1	-3	-4	4	1	3	1.229032	0.129315	7.733055	
21	3	-2	1	4	-2	3	1	1	0.544833	0.141867	7.048856	
22	-2	-4	1	0	-2	1	3	-2	0.595678	0.140851	7.099701	
23	2	-2	1	2	-4	1	1	3	0.707654	0.138664	7.211677	
24	-3	-4	1	1	-3	3	4	-2	0.617724	0.140415	7.121746	
25	3	-4	-3	4	-2	-1	2	1	0.659147	0.139603	7.16317	
26	2	-4	-3	4	-4	3	4	4	0.956047	0.134047	7.46007	
27	4	-4	1	-3	-1	3	1	4	0.698098	0.138848	7.20212	
28	3	-4	-3	4	-4	-3	2	-3	0.402055	0.1448	6.906077	



## Generation #6

Table 26: Generation #6 Data

Chromosome #	Configuration Number								Fitness Function	$\Gamma$	$1/\Gamma$	Min $1/\Gamma$
	1	2	3	4	5	6	7	8		m/s	s/m	
1	-3	-4	1	1	-3	3	4	-2	0.501027	0.14298	6.993985	6.492958
2	2	-4	-3	4	-4	3	4	4	1.059798	0.132402	7.552756	
3	1	-3	1	-3	1	4	3	3	0.93972	0.134541	7.432679	
4	-2	-3	1	-3	-4	4	1	3	1.184349	0.130254	7.677307	
5	2	-4	-3	4	-4	3	4	4	1.061966	0.132364	7.554924	
6	3	-4	1	4	-4	3	3	4	1.077465	0.132093	7.570424	
7	3	-2	-3	4	-4	3	4	4	1.100863	0.131686	7.593822	
8	-2	-4	-4	1	-4	4	1	3	1.276144	0.128715	7.769102	
9	-3	-4	1	1	-3	3	4	-2	0.611131	0.140764	7.104089	
10	-2	-4	-4	1	-4	4	1	3	1.277895	0.128686	7.770853	
11	-2	-4	-4	1	-4	4	1	3	1.35461	0.127428	7.847569	
12	-2	-4	-4	1	-4	4	1	3	1.284361	0.128579	7.77732	
13	-2	-4	-4	1	-4	4	1	3	1.292536	0.128444	7.785494	
14	-2	-4	-4	1	-4	4	1	3	1.269751	0.128821	7.762709	
15	-3	-4	0	4	-2	3	-2	-2	0.591653	0.141151	7.084612	
16	-3	-4	-3	4	-4	3	-3	4	0.946687	0.134415	7.439646	
17	1	-3	1	-3	4	4	4	3	0.895076	0.135354	7.388034	
18	-2	-3	1	-3	2	4	3	3	1.238363	0.129344	7.731321	
19	-1	-4	-3	-2	0	3	3	-2	0	0.154013	6.492958	
20	3	-1	1	4	-4	3	1	4	0.900374	0.135257	7.393333	
21	-2	-2	-4	4	-4	4	4	3	1.069164	0.132238	7.562123	
22	2	-4	-3	1	-4	4	4	4	1.150315	0.130834	7.643273	
23	-3	-4	-3	1	-4	2	4	-1	0.924229	0.134822	7.417187	
24	-3	-4	4	1	-4	4	1	3	0.962217	0.134135	7.455176	
25	-2	-4	-4	1	-4	4	1	-1	1.001159	0.133438	7.494117	
26	-2	-4	-4	1	-4	4	1	3	1.358184	0.12737	7.851142	
27	4	-4	-4	1	-4	4	1	3	0.99521	0.133544	7.488169	
28	-2	-4	-2	-2	-4	4	1	3	0.811003	0.136912	7.303962	

## Generation #7

Table 27: Generation #7 Data

Chromosome #	Configuration Number								Fitness Function	$\Gamma$	$1/\Gamma$	Min $1/\Gamma$
	1	2	3	4	5	6	7	8		m/s	s/m	
1	-2	-2	-4	4	-4	4	4	3	0.575771	0.130641	7.654565	7.078794
2	-3	-4	-3	4	-4	3	-3	4	0.649659	0.129392	7.728453	
3	-2	-4	-4	1	-4	4	1	3	0.8501	0.126121	7.928894	
4	-2	-4	-4	1	-4	4	1	3	0.833099	0.126392	7.911893	
5	-2	-4	-4	1	-4	4	1	3	0.8501	0.126121	7.928894	
6	-2	-4	-4	1	-4	4	1	3	0.853118	0.126073	7.931912	
7	-2	-4	-4	1	-4	4	1	3	0.830659	0.126431	7.909453	
8	2	-4	-3	1	-4	4	4	4	0.588859	0.130418	7.667653	
9	-2	-4	-4	1	-4	4	1	3	0.840994	0.126266	7.919788	
10	-2	-4	-2	-2	-4	4	1	3	0.231361	0.136796	7.310155	
11	-2	-4	-4	1	-4	4	1	3	0.7933	0.127031	7.872094	
12	-2	-4	-4	1	-4	4	1	3	0.799874	0.126925	7.878669	
13	1	-3	1	-3	1	4	3	3	0.472308	0.132431	7.551102	
14	-3	-4	-3	1	-4	2	4	-1	0.270364	0.13607	7.349159	
15	1	-2	-3	4	-4	2	4	4	0.788531	0.127108	7.867325	
16	-3	-4	-3	4	-4	4	-3	4	0.492776	0.132073	7.57157	
17	1	-4	-4	1	-4	-1	1	3	0.603114	0.130176	7.681908	
18	-2	-4	-4	-1	-4	0	1	3	0.796276	0.126983	7.87507	
19	-2	-4	-4	1	-4	4	1	3	0.789088	0.127099	7.867883	
20	-2	-4	-4	-3	-4	4	1	3	0.46513	0.132557	7.543925	
21	-2	-2	-4	1	-4	4	-3	3	0.812558	0.126721	7.891352	
22	2	-4	-4	1	1	4	4	4	0.255219	0.136351	7.334013	
23	3	2	-4	-2	4	4	1	3	0.042952	0.140415	7.121746	
24	-2	0	-4	0	-4	4	1	3	0.316671	0.135218	7.395465	
25	-2	-4	-4	1	-4	4	1	-1	0.34853	0.134638	7.427324	
26	-2	-4	-4	1	-4	-2	-1	3	0.817979	0.126634	7.896773	
27	4	-4	1	1	-4	2	3	3	0.156101	0.138219	7.234895	
28	1	-4	1	1	-4	2	4	-1	0	0.141267	7.078794	

## Generation #8

Table 28: Generation #8 Data

Chromosome #	Configuration Number								Fitness Function	$\Gamma$	$1/\Gamma$	Min $1/\Gamma$
	1	2	3	4	5	6	7	8		m/s	s/m	
1	-2	-4	-4	1	-4	4	1	3	0.840166	0.126867	7.88227	7.042105
2	-2	-4	-4	1	-4	4	1	3	0.734005	0.128599	7.77611	
3	-2	-4	-4	1	-4	4	1	3	0.849808	0.126712	7.891912	
4	-2	-4	-4	1	-4	4	1	3	0.762225	0.128134	7.80433	
5	-2	-4	-4	1	-4	4	1	3	0.862534	0.126508	7.904638	
6	-2	-4	-4	1	-4	4	1	3	0.856477	0.126605	7.898582	
7	-2	-4	-2	-2	-4	4	1	3	0.434139	0.133757	7.476244	
8	2	-4	-4	1	1	4	4	4	0.332744	0.135596	7.374849	
9	-2	-4	-4	1	-4	4	1	3	0.811442	0.127331	7.853547	
10	-2	-4	-4	1	-4	4	1	3	0.826397	0.127089	7.868502	
11	-2	-4	-4	1	-4	4	1	3	0.763383	0.128115	7.805487	
12	-2	-4	-4	1	-4	4	1	3	0.836564	0.126925	7.878669	
13	-2	-4	-4	1	-4	4	1	3	0.834764	0.126954	7.876869	
14	-2	-4	-4	1	-4	4	1	3	0.846197	0.12677	7.888302	
15	3	3	-4	1	-4	4	1	3	0.300794	0.136186	7.342899	
16	-2	-4	-4	1	-4	4	-4	3	0.752188	0.128299	7.794293	
17	-2	-4	3	1	-4	4	1	3	0.506204	0.13248	7.548309	
18	-2	-4	-4	-4	3	4	1	3	0.239201	0.137338	7.281306	
19	-2	-4	0	1	-4	4	1	3	0.344347	0.135383	7.386452	
20	-2	-4	-4	1	-4	4	1	3	0.807127	0.127401	7.849232	
21	2	-4	-1	2	-4	3	-1	4	0.440629	0.133641	7.482734	
22	2	-4	-2	3	-4	4	4	4	0.520018	0.132238	7.562123	
23	1	-4	-4	1	-4	4	1	3	0.581997	0.131163	7.624101	
24	1	-4	-4	1	-4	4	1	0	0.294007	0.136312	7.336111	
25	1	4	4	1	-4	4	1	3	0	0.142003	7.042105	
26	-2	-4	-4	1	1	4	1	3	0.522249	0.132199	7.564354	
27	-2	-4	-4	1	-4	4	2	3	0.834764	0.126954	7.876869	
28	-2	-4	-4	1	-4	4	1	-1	0.404522	0.134289	7.446626	

## Generation #9

Table 29: Generation # Data

Chromosome #	Configuration Number								Fitness Function	$\Gamma$	$1/\Gamma$	Min $1/\Gamma$
	1	2	3	4	5	6	7	8		m/s	s/m	
1	-2	-4	-4	1	-4	4	1	3	0.941575	0.127554	7.839839	6.898264
2	-2	-4	-4	1	-4	4	2	3	0.975027	0.127012	7.873292	
3	-2	-4	-4	1	-4	4	1	3	0.988849	0.126789	7.887114	
4	-2	-4	-4	1	-4	4	1	3	0.989451	0.126779	7.887716	
5	-2	-4	-4	1	-4	4	1	3	0.904279	0.128163	7.802543	
6	-2	-4	-4	1	-4	4	1	3	0.924955	0.127825	7.823219	
7	-2	-4	-4	1	-4	4	1	-1	0.48133	0.135509	7.379594	
8	-2	-4	-4	1	-4	4	1	3	0.963047	0.127205	7.861311	
9	-2	-4	-4	1	-4	4	1	3	0.979829	0.126934	7.878094	
10	3	3	-4	1	-4	4	1	3	0.42277	0.136593	7.321034	
11	-2	-4	-4	1	-4	4	1	3	0.946336	0.127476	7.844601	
12	-2	-4	-4	1	-4	4	1	3	0.984637	0.126857	7.882902	
13	-2	-4	-4	1	-4	4	1	3	0.966637	0.127147	7.864902	
14	-2	-4	-4	1	-4	4	-4	3	0.824964	0.12948	7.723229	
15	-2	-4	-4	1	-4	4	1	3	0.935656	0.12765	7.833921	
16	-2	-4	2	1	-4	4	2	3	0.608961	0.133205	7.507226	
17	-2	-4	2	1	2	4	-4	3	0.297378	0.138973	7.195642	
18	-2	-4	-3	1	-4	4	1	3	0.564478	0.133999	7.462742	
19	-2	-2	-4	1	2	-2	1	3	0.740455	0.130912	7.638719	
20	-2	-4	-4	-2	-4	4	1	0	0.366168	0.137657	7.264433	
21	-2	-4	-4	-4	-4	4	1	-1	0.260957	0.13968	7.159221	
22	-2	-4	-4	1	-4	4	1	-4	0.390259	0.137202	7.288523	
23	2	-4	-4	1	-4	4	1	3	0.641792	0.132625	7.540057	
24	-2	3	-4	1	-4	-3	-3	3	0.303389	0.138857	7.201653	
25	-3	-1	-4	-1	-4	4	-4	3	0.339668	0.138161	7.237933	
26	-2	3	-4	1	3	1	1	-4	0	0.144964	6.898264	
27	-2	-4	-4	1	-4	4	1	3	0.940999	0.127563	7.839264	
28	-2	-4	-4	1	-4	4	-1	3	0.901926	0.128202	7.80019	

## Generation #10

Table 30: Generation #10 Data

Chromosome #	Configuration Number								Fitness Function	$\Gamma$	$1/\Gamma$	Min $1/\Gamma$
	1	2	3	4	5	6	7	8		m/s	s/m	
1	-2	-4	-4	1	-4	4	1	3	1.059051	0.126818	7.885316	6.826265
2	-2	-4	-4	1	-4	4	2	3	0.981599	0.128076	7.807864	
3	-2	-4	-4	1	-4	4	1	3	1.009436	0.127621	7.835701	
4	-2	-4	-4	1	-4	4	1	-1	0.593069	0.134783	7.419333	
5	-2	-4	-4	1	-4	4	1	3	1.092269	0.126286	7.918534	
6	-2	-4	-4	1	-4	4	1	3	1.067454	0.126683	7.893719	
7	-2	-4	-4	1	-4	4	1	3	1.028454	0.127312	7.854719	
8	-2	-2	-4	1	2	-2	1	3	0.920149	0.129092	7.746413	
9	-2	-4	-4	1	-4	4	1	3	1.069262	0.126654	7.895526	
10	-2	-4	-4	1	-4	4	1	3	1.095343	0.126237	7.921608	
11	-2	-4	-4	1	-4	4	1	3	1.077749	0.126518	7.904014	
12	-2	-4	-4	1	-4	4	1	3	1.090451	0.126315	7.916716	
13	-2	-4	-4	1	-4	4	1	3	1.074127	0.126576	7.900392	
14	-2	-4	-4	1	-4	4	-4	3	0.942838	0.128715	7.769102	
15	-2	-4	-4	1	-4	4	2	3	1.092269	0.126286	7.918534	
16	-2	-4	0	1	-4	4	1	3	0.598412	0.134686	7.424677	
17	-2	-4	-4	1	-4	4	1	-1	0.589877	0.134841	7.416142	
18	2	-4	-4	1	1	4	1	3	0.520248	0.136119	7.346513	
19	-2	-1	-4	1	-4	4	1	3	0.657029	0.133631	7.483294	
20	-2	-4	-4	1	-4	4	1	3	1.081999	0.12645	7.908264	
21	-2	-4	-4	-3	2	4	0	3	0.605364	0.13456	7.431629	
22	4	0	-4	1	2	4	1	3	0.647242	0.133806	7.473506	
23	-2	-4	-4	1	2	4	1	-2	0	0.146493	6.826265	
24	-2	-4	-4	1	0	4	1	3	0.66353	0.133515	7.489795	
25	-2	-4	2	3	-4	4	1	-4	0.209647	0.142128	7.035911	
26	-2	-4	-4	1	-4	4	1	3	1.106277	0.126063	7.932542	
27	-2	-4	4	1	-4	4	1	3	0.728146	0.132373	7.554411	
28	-2	-4	-4	1	-4	4	3	3	1.081374	0.12646	7.907639	

## Generation #11

Table 31: Generation #11 Data

Chromosome #	Configuration Number								Fitness Function	$\Gamma$	$1/\Gamma$	Min $1/\Gamma$
	1	2	3	4	5	6	7	8		m/s	s/m	
14	-2	-4	-4	1	-4	4	1	3	0.952597	0.126005	7.936169	6.983573
5	-2	-4	-4	1	-4	4	1	3	0.947723	0.126083	7.931296	
2	-2	-4	-4	1	-4	4	1	3	0.903529	0.126789	7.887102	
28	-2	-4	-4	1	-4	4	1	3	0.890907	0.126993	7.87448	
15	-2	-4	-4	1	-4	4	1	3	0.881916	0.127138	7.865489	
20	-2	-4	-4	1	-4	4	1	3	0.880719	0.127157	7.864292	
19	-2	-4	-4	1	-4	4	1	3	0.868766	0.127351	7.852339	
7	-2	-4	-4	1	-4	4	1	3	0.867573	0.12737	7.851146	
13	-2	-4	-4	1	-4	4	1	3	0.866976	0.12738	7.850549	
27	-2	-4	-4	1	-4	4	1	3	0.86638	0.127389	7.849953	
21	-2	-4	-4	1	-4	-1	3	3	0.863995	0.127428	7.847568	
3	-2	-4	-4	1	-4	4	1	3	0.861016	0.127476	7.844589	
17	-2	-4	-4	1	-4	4	4	3	0.847936	0.127689	7.831509	
6	-2	-4	-4	1	-4	4	2	3	0.819548	0.128154	7.803121	
11	-2	-4	-4	1	-4	4	3	3	0.80191	0.128444	7.785483	
4	-2	-4	-4	1	-4	4	3	3	0.783768	0.128744	7.76734	
9	-2	-4	-4	1	-4	4	2	3	0.77269	0.128928	7.756263	
8	-2	-4	-4	1	-4	4	3	3	0.7408	0.12946	7.724372	
1	-2	-4	-4	1	-4	4	3	3	0.724665	0.129731	7.708238	
22	-2	-4	3	4	-4	4	3	3	0.578003	0.132248	7.561576	
16	-4	1	-4	1	-4	4	3	3	0.553184	0.132683	7.536757	
10	-2	-4	-4	1	0	4	1	3	0.472693	0.134115	7.456266	
26	0	-4	-4	1	0	4	1	3	0.430428	0.13488	7.414001	
18	-2	-4	-4	1	4	4	1	3	0.429365	0.134899	7.412938	
12	-2	-4	-4	1	0	4	1	3	0.381284	0.13578	7.364857	
25	1	-3	1	1	-4	1	1	3	0.360868	0.136157	7.344441	
23	-2	-4	-4	1	0	4	2	3	0.302349	0.137251	7.285921	
24	-2	-4	-4	4	0	4	1	-2	0	0.143193	6.983573	

## Generation #12

Table 32: Generation #12 Data

Chromosome #	Configuration Number								Fitness Function	$\Gamma$	$1/\Gamma$	Min $1/\Gamma$
	1	2	3	4	5	6	7	8		m/s	s/m	
1	-2	-4	-4	1	-4	4	1	3	0.086146	0.126963	7.87631	7.790164
2	-2	-4	-4	1	-4	4	3	3	0.083108	0.127012	7.873272	
3	-2	-4	-4	1	-4	4	1	3	0.057405	0.127428	7.847569	
4	-2	-4	-4	1	-4	4	1	3	0.112038	0.126547	7.902202	
5	-2	-4	-4	1	-4	4	1	3	0.109604	0.126586	7.899768	
6	-2	-4	-4	1	-4	4	1	3	0.105362	0.126654	7.895526	
7	-2	-4	-4	1	-4	-1	3	3	0	0.128367	7.790164	
8	-2	-4	-4	1	-4	4	1	3	0.115662	0.126489	7.905826	
9	-2	-4	-4	1	-4	4	1	3	0.107794	0.126615	7.897958	
10	-2	-4	-4	1	-4	4	1	3	0.13565	0.12617	7.925814	
11	-2	-4	-4	1	-4	4	2	3	0.040751	0.127699	7.830915	
12	-2	-4	-4	1	-4	4	1	3	0.095774	0.126808	7.885938	
13	-2	-4	-4	1	-4	4	1	3	0.102371	0.126702	7.892535	
14	-2	-4	-4	1	-4	4	1	3	0.106609	0.126634	7.896773	
15	4	-4	-4	1	-4	4	-3	3				
16	-3	-4	-4	1	-4	4	3	3				
17	-2	-4	-4	1	4	4	1	3				
18	-3	3	-4	1	4	4	1	3				
19	-2	-4	-4	1	-4	4	1	3				
20	-2	-4	-4	1	-4	4	1	3				
21	-2	-4	-4	1	4	1	3	3				
22	-2	-4	-4	1	4	-1	0	3				
23	-2	-4	-4	1	-4	4	-4	3				
24	-2	3	-4	-1	-4	-1	1	3				
25	-2	-4	-4	1	-4	4	3	3				
26	-2	-4	-4	1	-4	4	1	3				
27	-2	-4	-4	1	-4	4	1	3				
28	-2	-4	-4	1	-4	4	1	3				